Design and Material Characterization of a Hyperelastic Tubular Soft Composite

A thesis submitted
to the Faculty of Graduate and Postdoctoral Studies
in partial fulfilment of the requirements for the degree of

MASTER OF APPLIED SCIENCE

in Mechanical Engineering

by

Robert Shaheen

Spring, 2017

Ottawa-Carleton Institute for
Mechanical and Aerospace Engineering

University of Ottawa
Ottawa, Ontario, Canada, KN1 6N5

Abstract

Research within the field of human motion assistive device development, with the purpose of reducing the metabolic cost of daily activities, is seeing the benefits of the exclusive use of passive actuators to store and release energy during the gait cycle. Designs of novel exoskeletons at the University of Ottawa implement the Pneumatic Artificial Muscle (PAM) as the primary method of nonlinear, passive actuation. The PAM is proven as a superior actuator for these devices when compared to the linear mechanical springs used by other researchers. There are, however, challenges regarding PAM pressure loss and the limitation of PAM elongation that have been identified.

This thesis aims to develop a hyperelastic tubular soft composite that replicates the distinctive mechanical behaviour of the PAM without the need for internal pressurization. The final soft composite solution was achieved by impregnating a prefabricated polyethylene terephthalate braided sleeve, held at a high initial fibre angle, with a silicone prepolymer. A comprehensive experimental evaluation was performed on numerous prototypes for a variety of customizable design parameters including: initial fibre angle, silicone stiffness, and braided sleeve style. Moreover, two separate analytical models were formulated based on incompressible finite elasticity theory using either a structural model of Holzapfel's type, or a phenomenological model of Fung's type. Both models were in good agreement with the experimental data that were collected through a modified extension-inflation test.

This research has successfully developed, tested, and validated an innovative soft composite that can achieve specific mechanical properties, such as contraction distance and nonlinear stiffness, for optimal use in human motion assistive devices.

Acknowledgements

My Master's thesis is a representation of the years education that I have received, and it would have not been possible without the support and encouragement of many individuals. I would first like to express my gratitude to all of the teachers and professors who, through their inspirational teachings, have lead me to begin this degree.

Specifically, I sincerely thank my supervisor, Dr. Marc Doumit, for without whom none of this would have been possible. His excellent guidance has helped me develop the confidence and background that I needed to achieve such a goal.

I greatly extend my gratitude to the University of Ottawa mechanical and biomedical engineering faculty members, administrators, and machine shop staff who shared some of their insight or wisdom with me. I am deeply thankful for those who helped guide me in the right direction when I experienced problems or difficulties in my research.

Finally, I express my love and gratitude to my amazing family who gave me their endless support throughout my education. More specifically I extend my deepest gratitude to: my Mom who with her constant encouragement and support makes me love learning, my Dad who took it upon himself to show me the beauty within numbers from a very young age, Cindy for her stimulating and inspiring late night conversations, Michelle for her great sense of "humour" and constant moral support, and Sarah for her very much needed emotional support which knows no boundaries.

Contents

List of Figures

List of Tables

Chapter 1

Introduction

Recent work within the field of human motion assistive devices [1] illustrates the benefits of using passive actuators to store and release energy during the gait cycle. Designs of novel passive exoskeletons, with the purpose of reducing the metabolic cost of daily activities, have been ongoing endeavours at the University of Ottawa. Leclair *et al.* [2] and Doumit *et al.* [3] implemented the Pneumatic Artificial Muscle (PAM) as the primary method of nonlinear, passive actuation to an ankle exoskeleton. The PAM has ideal nonlinear mechanical stiffness properties (as seen in figure 1.1a) for this application; however, challenges regarding PAM pressure dissipation over prolonged use, and limitations of the PAM's elongation range of 30 % of its contracted length [4] have been identified.

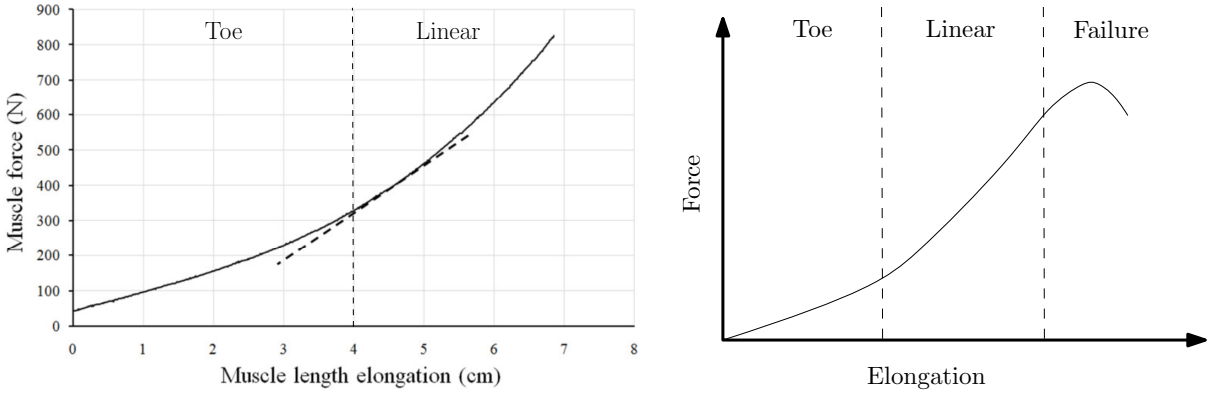

(a) PAM **(b)** Soft biological tissue

Figure 1.1: Tensile response of PAM eccentric loading at an internal pressure of 96 kPa [4] (left), and soft biological tissue adapted from [5] (right).

This motivates the design and development of a novel passive actuation device with mechanical properties similar to the PAM but without the need for internal pressurization. The desired passive elastic behaviour of the PAM, which resembles that of soft biological tissue, is described by the force-elongation response shown in figure 1.1b. This behaviour is comprised of an initial toe response distinguished by minimal force resistance, followed by a linear region with increasing force resistance, and finally ends with a failure region at which the maximum force resistance is achieved and elongation is restrained. This research considers a hyperelastic tubular soft composite as a suitable candidate for replicating the toe and linear regions of the passive mechanical behaviour.

The proposed passive actuator, henceforth referred to as the soft composite (SC), is presented in figure 1.2. It consists of a braided sleeve that is embedded into an elastomeric matrix. The operation of the SC is simple. As tensile forces are on the SC, it elongates, and the fibres begin to align parallel to the applied force. Its resistive tensile force increases as it continues to be axially stretched until it reaches its maximum elongation potential.

Figure 1.2: SC prototype in its resting (top) and stretched (bottom) configuration.

1.1 Objective

The primary objective of this thesis is to design and develop a hyperelastic, tubular soft composite that replicates the distinct mechanical behaviour of the PAM without the need for internal pressurization. Secondly, it is desired to produce a SC so that it can exceed the PAM's elongation range of 30 % of its contracted length. Furthermore, this research aims to both, experimentally and analytically, characterize the mechanical behaviour of the SC to propose a development method that helps designers select specific SCs that meet the actuation requirements of passive exoskeletons.

1.2 Methodology

A multi-step methodology was used to guide the research activities. Firstly, a SC specimen was designed and fabricated. This step considered the fabrication process, the types of materials used for fabrication, and the key input control parameters that dictate the mechanical behaviour of the SC. Next, the mechanical behaviour of the SC was experimentally evaluated through a variety of testing scenarios. The final step to this research project involved the analytical characterization, and validation with experimental results, of the tensile behaviour of the SC using constitutive models that are based on incompressible finite elasticity theory.

1.3 Thesis contributions

This thesis contributes a novel design of a SC to be used as a passive actuator. The fabrication method employs a single step process to impregnate a braided mesh sleeve with a silicone polymer. The SC successfully replicates the PAM mechanical passive behaviour without the need of internal pressurization. Specimens were created with the ability to achieve elongation ranges between 30 % and 110 % of their original length. Some SC specimens were fabricated with an initial fibre angle larger than 54.7°, so that they may achieve greater elongation potentials which, to the knowledge of the author, has not been claimed in literature.

An experimental evaluation was performed to understand the behaviour of the SC. More specifically, its elongation and resistive tensile force was extensively studied for different design parameters, namely, the initial fibre angle, the stiffness of the silicone matrix, and the braided sleeve style. These experimental results characterized the SC behaviour and are essential for developing a SC that meets passive exoskeleton requirements.

Two separate constitutive models, based on incompressible finite elasticity theory, have been developed to analytically characterize the SC. The first model was based on the structural strain energy function of Holzapfel's type and the second model was based on the phenomenological strain energy function of Fung's type. These models both provided predictive insight into the mechanical behaviour of the SC.

1.4 Thesis outline

This thesis is organized into five chapters.

Chapter 1 introduces the SC, the thesis objective, the adopted methodology, and the contributions of this thesis.

Chapter 2 presents the results of a literature survey. The structure of this review is separated into categories, namely, alternative solutions to a SC that achieve similar behaviour, existing SC specimens and their mechanical behaviour, and existing analytical material models that may be used to characterize the nonlinear behaviour of the SC.

Chapter 3 presents the SC experimental evaluation. The SC behaviour and constituent materials are analysed for a variety of different control parameters. These parameters include the initial fibre angle, the stiffness of the silicone matrix, and the type of braided sleeve used in the SC. This chapter also presents many of the experimental setups and SC design, development, and fabrication process.

Chapter 4 exhibits a model of the initial tensile response for the SC based on incompressible finite elasticity theory. This chapter outlines the details of the modified extension-inflation experimental setup that is used to help characterize the mechanical behaviour of the SC. The applied axial force versus the stretch ratio of the SC is characterized through the nonlinear optimization of material constants found within a strain energy function of either Holzapfel's or Fung's type using the Levenberg-Marquardt optimizer. This chapter is concluded with the validation of the theoretical results with experimental data obtained from the modified extension-inflation test.

Chapter 5 presents the conclusions to this thesis as well as future research considerations that are recommended for the SC.

Chapter 2

Literature Review

This chapter presents a comprehensive review of hyperelastic tubular SCs found in literature. Firstly, existing types of hyperelastic tubular braids are introduced along with some of their applications and mechanical behaviour. Next, existing tubular SCs are reviewed along with their applications, design traits, and mechanical behaviour. Finally, a review of some of the analytical models used to characterize the mechanical behaviour of tubular SCs is presented.

2.1 Overview of existing types tubular braids with hyperelastic properties

The purpose of this research, which is to create a nonliear passive actuator, may be accomplished using a number of solutions besides a SC tube. Hyperelastic tubular braids have a wide variety of industrial applications including, but not limited to: hoses, ropes, medical scaffolds, fuel lines, energy absorbing composite reinforcements or preforms, sporting equipment, military equipment, soft robotics, and artificial tendons and ligaments [6]. This literature survey shows that the construction of hyperelastic tubular braids was previously achieved through an elastic core wrapped with a tubular braid, multi-layered tubular braids, or tubular braids using blended/hybrid fabrics. Options involving the use of different types of tubular braids that demonstrate hyperelastic mechanical behaviour, as well as some methods of analysing these tubular braids, are briefly discussed in this section.

2.1.1 Tubular braids with an elastic core

Tubular braids with an elastic core have been used in a number of different applications such as bungee cables and hair elastics. More advanced applications include preforms or support for composite structures. Current literature reviewing the mechanical properties of tubular braids with an elastic core is sparse, but recent studies from Rawal *et al.* [7] examined the tensile behaviour of these braids based on the initial braid geometry, core properties, and tensile properties of the braids monofilaments.

For this study, two sets of tubular braids wound with either four or eight monofilaments were used. Specimens were created with initial fibre angles varying between 10° and 50°. Different initial fibre densities were also used for various experimental tests. The study primarily concluded that increasing the initial fibre angle exhibited greater specimen elongation under tensile loads when compared to other specimens of the same initial length but smaller initial fibre angle. It was also seen that increasing the fibre density applied a radial pressure on the core that, if great enough, could cause the core to "squeeze out" [7] of the braids and, therefore, would significantly influence the mechanical response of the specimen.

The work of Rawal *et al.* [7] was based upon two major studies from the past 30 years. The first was a study conducted by Phoenix *et al.* [8] which developed a linear elastic response model for a diamond tubular braid containing a flexible, but incompressible, elastic core. This research concluded that key parameters affecting the mechanical response were the braid helix angle, the crimp angle at strand crossovers, and the elastic modulus and Poisson's ratio of the elastic core. The model was only valid for small displacements and, therefore, only the initial response was predicted [7]. Nevertheless, [8] helped pave the way for improved experiments achieved by Hopper *et al.* [9].

The model proposed in [9] determined the tensile response of a tubular braid with an elastic core for four modes of operation. Parameters input included initial geometric configuration and material properties of a hybrid braid, and the model output forces, strains, modes of operation, and braid geometry. The results showed that, for two of the modes, the elastic core did most of the work and was not in contact with the braid, whereas, for the other two modes, the core and braid were in contact with each other and displayed a "unique synergism" [7]. This study was able

to incorporate nonlinear yarn tensile response, large deformations, yarn failure, and varying hybrid deformation modes. According to [7], the major drawback of this study was that it did not validate the model with suitable experimental work.

In the biomedical field, tubular, hyperelastic braids were introduced for use as artificial ligaments and tendons. Most recent studies include Bach *et al.* [10, 11], where they wound 12 ultra-high-molecular-weight-polyethelene threads around a core of multiple parallel polyvinyl alcohol cords to emulate and model the natural mechanical properties of a ligament. Two series of designs were constructed with the first varying the number of core yarns between 8, 12, and 16, and the second varying initial fibre angles of 40°, 45°, 50°, and 55°, with a measurement error of ±2°. Other biomedical models were proposed to try to mimic the natural ligament. One study by Cruz *et al.* [12] proposed both circular braids with axially reinforcing yarns and circular braids with axially reinforcing braids.

2.1.2 Multi-layered tubular braids

Multi-layered braided structures are becoming increasingly common in applications relating to composites and medical scaffolds due to their excellent strength to weight ratio and low fabrication costs. These structures may be classified as either two or three dimensional braids. 2-D braid structures have a braided layer, with another layer braided directly on top, allowing both layers to run parallel. 3-D braid structures have the same geometry but the layers interconnect, therefore, creating one resulting braided structure that is thicker than the individual initial layers [13].

The most recent study that examined the mechanical behaviour of multi-layered braided structures, and predicted their tensile response, was performed by Saraswat *et al.* [6]. They embellished upon the tensile model of a tubular braid proposed by [7]. This study provided computations for the toughness of multi-layered braids as well as the effect of the outer layer braid angle on the stress-strain characteristics of the specimen. Single, double, and triple layered braid structures, with combinations of initial fibre angles of 30° and 45°, were tested. They concluded that varying the initial fibre angle had the greatest influence on the mechanical properties of the braids, and that the initial fibre angle of the outer layer affected the overall extension of the specimen. They also found that the radial pressure exerted by the outer layers in a double or triple layer braid on the internal layers is non-negligible.

In the biomedical field, multi-layered tubular braids were used as scaffolds for ligament tissue engineering. The architecture of the scaffold allowed the braid to mimic a natural ligament's deformation while maintaining morphological requirements for tissue growth. In most recent studies, Laurent *et al.* [14] proposed a scaffold that was constructed from concentric circular braided layers, with 16 fibres in each layer, that were deformable at a low strain range to permit low tension in everyday motion. The braid exhibited high stiffness and strength at large strains. Laurent *et al.* [14] illustrated that the number of layers and fibre diameter adjusts the stiffness of the braid, and the initial fibre angle affects properties of the toe region of the braid. A finite element analysis was performed on the braid where each fibre was modelled as a kinematically enriched beam accounting for cross sectional strains within a large deformation framework. The model included contact friction between the fibres, and it was validated by experimental results.

2.1.3 Tubular braids using blended/hybrid fabrics

The tensile properties of a tubular braid can be altered by using different types of fibres for its fabrication [14]. Numerous types of fibres can be used in a single braid. The mechanical behaviour of circular hybrid braids, with two different fibre types, was analysed by Hristov *et al.* [15]. A predictive tensile model of the braid was created based on the constituent fibre characteristics and the structural geometry of the tubular braid. The predictive model was validated experimentally although, for specimens with initial fibre angles greater than 25°, the model underestimates the strength of the braid.

Models for hybrid braids were also proposed by [6] and [7] as expansions of their tensile models for their respective tubular braids. It is concluded, just as with the other braid configurations, that the initial fibre angle, diameter, and fibre characteristics are the major contributors to the tensile mechanics of the braid. It is beneficial to use hybrid fabrics in junction with other design ideas to optimize tensile response.

2.2 Overview of existing hyperelastic, tubular SCs

Tubular braided fabrics are used as preforms or reinforcements for many rigid composites in a wide variety of applications such as scaffolds for either artificial ligaments or vascular grafts, hoses,

energy absorbing tubes, and many others [6]. They are also used as reinforcements for hyperelastic laminates or composites of any shape [16]. This section refers to tubular SCs that exhibit hyperelastic tensile behaviour and are fabricated using tubular braided fibres suspended in an elastomeric matrix. Not only are these composites useful in tensile applications, but their geometry allows for extreme flexibility within the radial direction as well as the ability to withstand internal pressurization. These traits make them extremely popular in vascular scaffold designs, as well.

Given the focus of this thesis, the following literature review will pertain to applications where the main focus is on tensile loading applications as opposed to composite reinforcements or vascular grafts.

2.2.1 Applications within the field of soft tissue prostheses

Tubular SC designs were initially proposed as ligament prostheses using hydrogel polymer matrices reinforced with polyethylene teraphthalate (PET) fibres in the mid to late 1990's [17, 18, 19]. Recent trends, however, regarding the design of ligament prostheses have largely shifted away from the use of SC materials towards biocompatible scaffolds that dissolve and get replaced with biological tissue over time [20]. Studies in this field provide good insight toward the research goals of this work.

In a recent study, Thayer *et al.* [21] proposed a hydrogel SC design for ligament tissue engineering. This study suggested that electrospun poly-lactic-*co*-glycolic acid or poly(ester urethane)urea meshes formed into composites with a polyethylene glycol hydrogel matrix could withstand cyclic loading from gait stimulus. Another example in recent trends, from Lou *et al.* [22], included a study examining open-meshed tubular braided composites consisting of PET fibres in a gelatin matrix. The tensile strength of the composite was tested and it was found that the increase in gelatin concentration resulted in decreased tensile displacement of the composite but did not change the tensile strength. The same studies were carried out on a polylactic acid (PLA)/spandex hybrid braid immersed into a gelatin solution. It was found that an increase in the density of the PLA yarns resulted in an overall increase of tensile strength of the composite, whereas the increase in spandex yarn density did not influence the overall tensile strength.

Early accounts of hyperelastic SCs used as artificial ligament prostheses were seen in the work of Iannace *et al.* [17] where they based their material on a hydrogel polymer matrix reinforced

with bundles of PET fibres. They wound a bundle of PET fibres helically around a polyethylene hose while simultaneously coating it with a matrix material, plasticizer, and a cross-linking agent. Multiple specimens with unique initial fibre angles of 19° and 35° were then separately inserted into a Teflon tube which was filled with the prepolymer matrix composed of 2-hydroxyethyl methacrylate (HEMA or commercially vended as HydroThane^{TM}). The impregnated mold was allowed to cure for 60 min at 90 °C and then demolded to yield the final SC specimen. Figure 2.1 illustrates the final composite ligament.

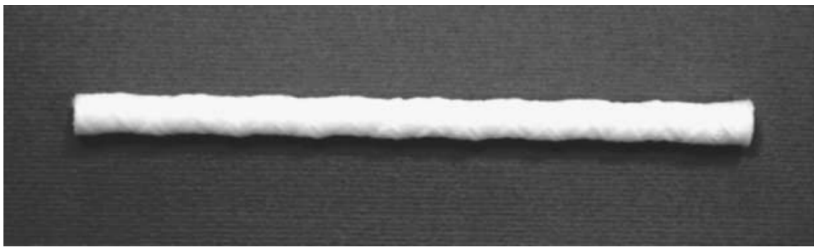

Figure 2.1: HydroThane^{TM} reinforced with PET fibres used as a ligament prosthesis, by Iannace *et al.* [23].

The specimen was tested in tensile mode by an Instron machine at an elongation rate of 0.1 mm min^{-1} at room temperature. The results were compared to those of rabbit anterior cruciate ligaments (ACL) and Achilles tendons. The results seen in figure 2.2, for the composite with an inner diameter of 1.5 mm, show good agreement between the composite, natural ACL, and natural Achilles tendon.

Iannace *et al.* [17] concluded that the increase in the initial fibre angle mainly had an influence on the length of the critical deformation and less so on the slope of the toe region of the SC. They specified that the response of the SC within the toe region was mainly governed by the properties of the matrix while the response within the linear region was attributed mainly to the properties and geometry of the fibres. They stated that an increase in the matrix rigidity resulted in a stiffer toe and linear region response.

Similar work was accomplished by Ambrosio *et al.* [19], in 1998. They used the same SC that was manufactured in [17] for stress-relaxation tests to attempt to further characterize the material properties. Stress-relaxation tests help determine important characteristics of the dimensional stability of the composite. Ambrosio *et al.* [19] applied an instantaneous deformation to the specimen and then recorded the relaxation stress due to structural rearrangements. These tests

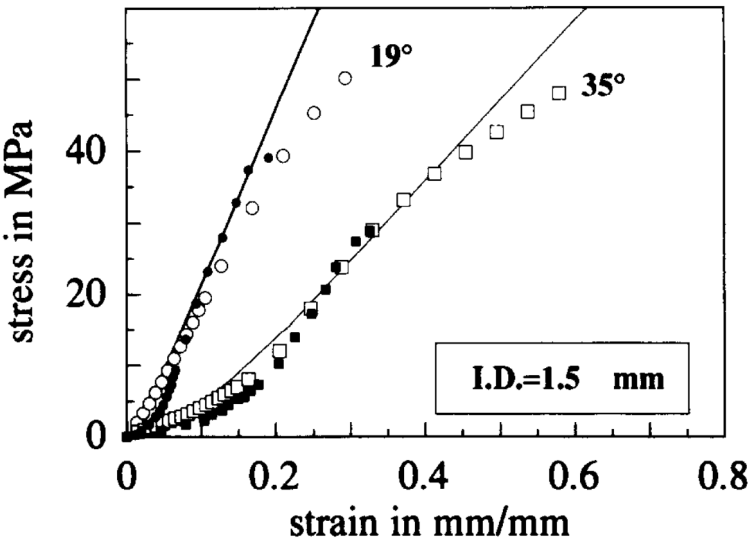

Figure 2.2: Tensile test results for a composite prosthesis. Experimental stress-strain data of the prosthetic, represented by ∘ and □, is compared to a natural rabbit ACL(■) and Achilles tendon (•). Theoretical predictions (−) are provided for each specimen [17].

were performed in a MTS Bionix test system in distilled water. They applied a step deformation to the material so that the imposed strain was achieved in less than 0.08 s. Figure 2.3 shows the stress-relaxation curve for a composite ligament with an initial fibre angle of 35° for over 2 h. It was

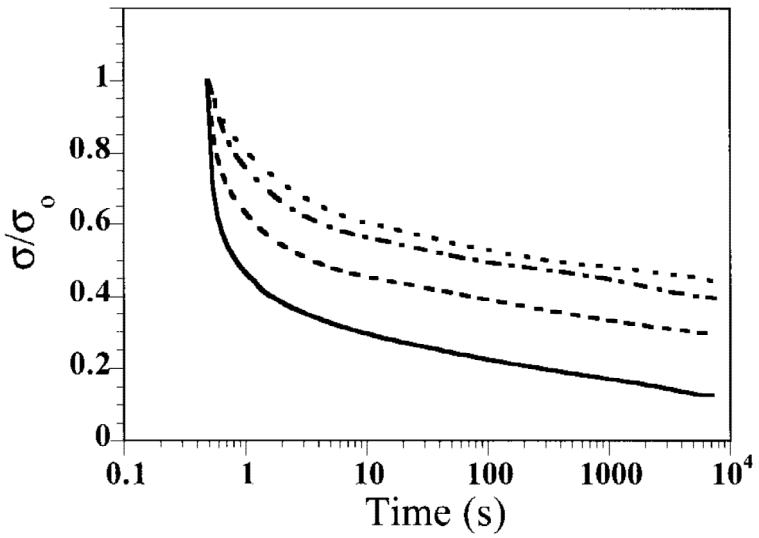

Figure 2.3: Stress-relaxation behavior of a composite ligament with an initial fibre angle of 35° at different levels of strain ($\cdots, \epsilon = 10\,\%; -\cdot, \epsilon = 15\,\%; --, \epsilon = 20\,\%; -, \epsilon = 40\,\%$) [19].

seen that the slopes of the curves were approximately the same for the first 10 s and then the curves began to level out into an asymptomatic settlement over the remaining time. They concluded that

the relaxation rate of the composite was controlled mainly by the matrix properties.

The study was concluded with a discussion regarding the implications of using this SC for ligament prosthetic design. It was determined that the SC was able to mimic the initial tensile properties of a natural ligament, and it was therefore deemed as a successful replacement candidate for short term use. The study did, however, find that a slower relaxation rate was exhibited by the SC when compared to the natural tissue after 500 s.

Another type of prosthetic ligament was created by Mollica *et al.* [24] that used a similar fabrication method illustrated by [17]. They wound a bundle of PET fibres, composed of 192 monofilaments, helically around a steel mandrel with a filament winding machine. Some of the PET fibres were plasma treated prior to winding so that their respective specimens could later be compared to those with the untreated PET fibres. The PET fibres were impregnated with HydroThane^{TM} and dimethylacetamide (DMAC) in a 18/72 %, by weight, prior to the braiding process. Composite specimens were kept under a hood vent for 24 h, to cure, and then placed in a distilled water bath for 24 h, at room temperature. Specimens were created with initial fibre angles of 20° and 40°, as illustrated in figure 2.4, and with different fibre volume fractions. The specimens were then tested in simple tension on an Instron dynamometer at a speed of 3 mm s^{-1} at room temperature.

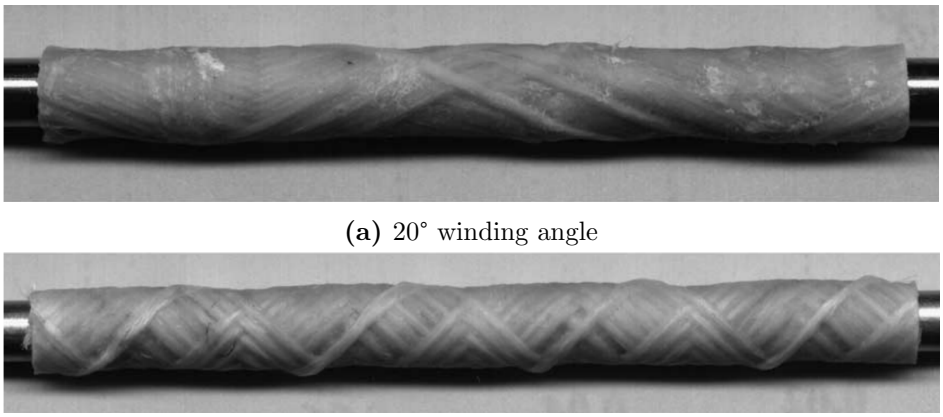

(a) 20° winding angle

(b) 40° winding angle

Figure 2.4: Artificial ligament specimens fabricated by Mollica *et al.* with different initial winding angles [24].

The major contributor to the properties of the SC was the initial fibre angle. Figure 2.5 illustrates the gross difference in the length of the toe region for specimens with initial fibre angles of

20° and 40°. It was determined that the plasma treatments created a better fibre to matrix interface and resulted in a stiffer composite with a shorter toe region in the response curve. Evidence of this behaviour is witnessed in figure 2.5 which shows the plasma treated fibres in groups 2 and 5 against the other non-plasma treated fibres.

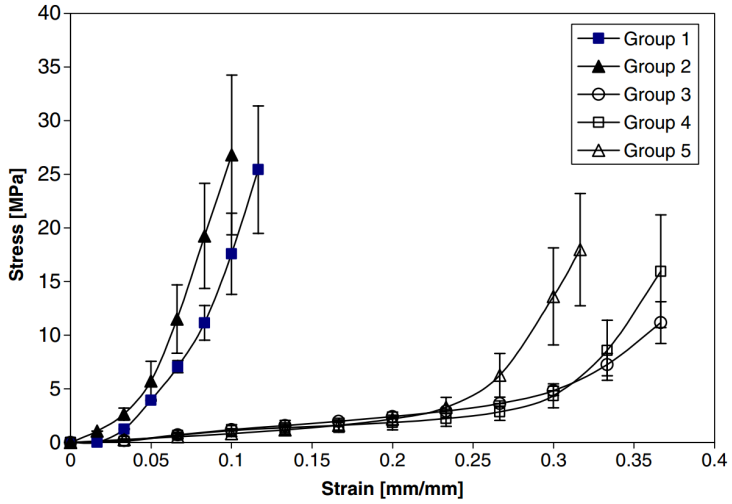

Figure 2.5: Tensile test results of SC specimens. Groups 1 and 2 have an initial fibre angle of 20° and groups $3-5$ have an initial fibre angle of 40° [24].

The effects of the fibre volume fraction on the tensile response, according to [24], were not as significant as the initial fibre angle or plasma treatment. Figure 2.6 illustrates the little variance within the response curves for specimens with fibre volume fractions of 10 %, 20 %, and 60 %.

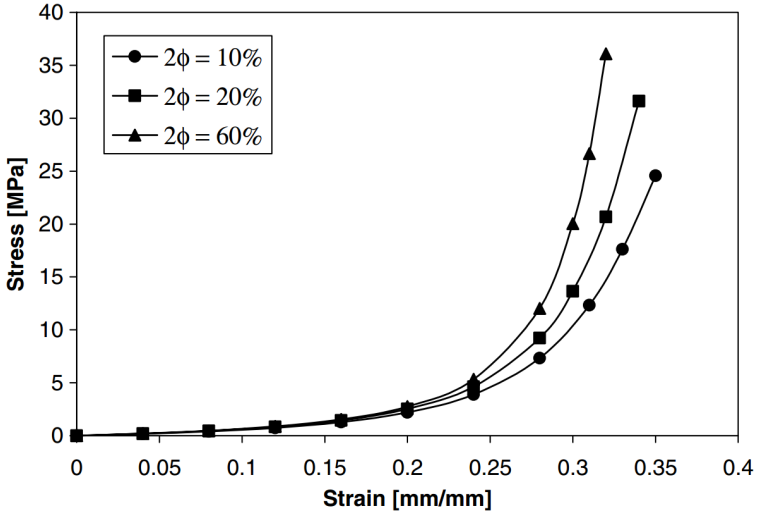

Figure 2.6: Influence of the fibre volume fraction on the tensile behaviour of the SCs [24].

2.2.2 Applications within the field of soft robotics

Researchers are currently experimenting with ways to fabricate soft actuators for a variety of delicate applications [25]. Some initiatives involve wrapping the PAM with an elastomeric layer [26], but more interestingly, recent research has been coating an entire braided actuator with an elastomer to create a SC [25, 27].

A simple method to manufacture hyperelastic tubular braided composites was outlined by Obiajulu *et al.* [27]. They used off-of-the shelf PET tubular braids and a prepolymer mix to fabricate a SC actuator. Two different prepolymers, each with a different stiffness, were used to make separate classes of actuators. The fabrication method involved fitting the PET braid over an inner tube and then coating the entire apparatus with the elastomer to yield a soft actuator.

The inner tubing was created by mixing a prepolymer and pouring it into a plastic mold. The mold was then degassed in a vacuum chamber for 10 min at an absolute pressure of 10 kPa then cured in a pressure chamber heated to 60 °C for 1 h. The inner tube was then demolded and fit into a PET braided sleeve. To complete the SC actuator, the PET sleeve, fitted with the inner tube, was coated with more elastomer and cured using a heat gun. Plugs on either end were created and a stylet was inserted into one end for air to be added or released. The final actuators are demonstrated in figure 2.7.

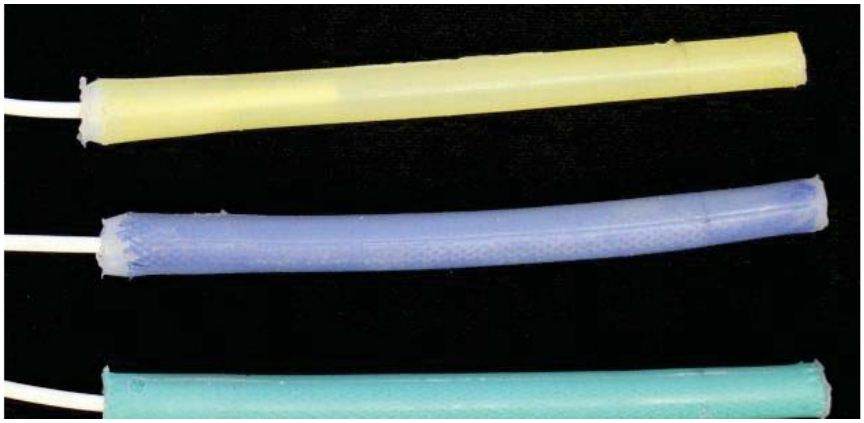

Figure 2.7: The finished SC actuators from Obiajulu *et al.* [27].

The fibre component of the specimens were created using braided sleeves that had initial fibre angles, ranging from 22° to 45°, and elastomers of different stiffness for the matrix. The authors performed two different types of tests on these specimens. The first type was an isometric con-

traction test, which means that the tensile force was measured while the length of the actuator was held constant and its internal pressure was increased. The second type of test was a constant pressure contraction test, where tensile force was measured while the internal pressure of the actuator was held constant and its length was increased. Additional tests were completed, to failure, to investigate the modes of failure for the composite. All tests were completed using a tensile testing apparatus and a 2 kN load cell.

The results of the isometric and constant pressure tests concluded that the SCs fabricated with the stiffer silicone were, overall, less quick at responding to changes in internal pressure or force. SC specimens made from the softer silicone had a larger range of contraction as well. The influence of the initial fibre angle largely affected the response of the composite, just as it did in every other study presented in this review.

Most of the causes of failure for specimens made with the softer elastomer were due to slipping of the air supply line. Specimens made from higher stiffness silicone failed because the opposite end plug failed. Failure occurred at internal pressures as low as 270 kPa or as high as 720 kPa.

An example of where these actuators were applied can be seen in the work of Roche *et al.* [25]. They utilized the same composite actuator that was created in [27] as a soft actuator to assist with contractions of the left ventricle. Figure 2.8 shows the composite actuators being put into a mold and then filled with more of the elastomer and cured to yield the final actuator shown on the right side of the image.

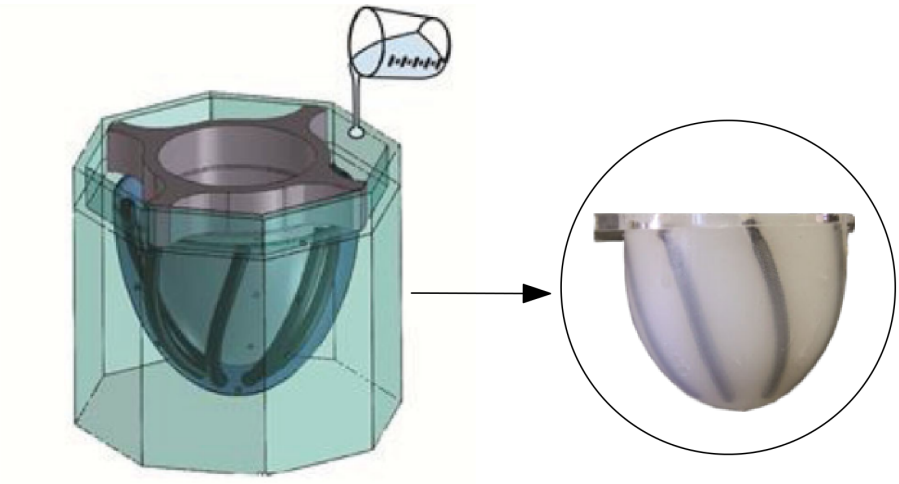

Figure 2.8: Artificical heart actuator made from elastomeric materials by Roche *et al.*. Image adapted from [25].

2.3 Existing material characterization models

It is imperative to analytically characterize a mechanical component in order to understand its mechanical behaviour. Many attempts have been made to characterize a hyperelastic tubular SC. Past research has modelled this type of material using composite laminate theory, nonlinear continuum mechanics, and finite element analysis (FEA). The scope of this research does not include FEA, therefore the review presented in the remainder of this section will focus only on methods regarding geometric aspects of the SC, composite laminate theory, and nonlinear continuum mechanics.

2.3.1 Models based solely upon geometric aspects of the SC

Modeling the geometry of braided tubes was briefly outlined in section 2.1. An indepth review article presented by Rawal *et al.* [28] discusses the most recent models of the tensile response of braided structures. Analytical models, formulated from the geometry of braided structures, were presented for the case of biaxial and triaxial braided cylinders, and for multi-layered tubular braids with and without elastic cores. No models were mentioned in [28] that describe braids surrounded by an elastomeric matrix. Mathematical models of braided structures derived solely from the geometric properties of the braid when they are embedded into a soft matrix are scarce. Researchers tend to use models involving composite laminate theory or nonlinear finite elasticity theory to analyse tubular SC materials.

2.3.2 Models based on composite laminate theory

Early accounts of using composite laminate theory to model tubular SCs were presented by Gershon *et al.* [29] and Iannace *et al.* [17] to characterize their synthetic soft tissues. The basis of composite laminate theory assumes a composite lamina similar to the one shown in figure 2.9.

The compliance $1/E_x$ along the x-axis of the orthotropic lamina is defined by [29] as

$$\frac{1}{E_x} = \frac{\cos^4(\theta)}{E_L} + \frac{\sin^4(\theta)}{E_T} + \frac{1}{4}\left(\frac{1}{G_{LT}} - \frac{2\nu_{LT}}{E_L}\right)\sin^2(2\theta), \tag{2.1}$$

where θ is shown in figure 2.9, E_x, E_L, and E_T are the Young's moduli in the x, longitudinal, and transverse directions, respectively, G_{LT} is the shear modulus, and ν_{LT} is Poisson's ratio. A similar

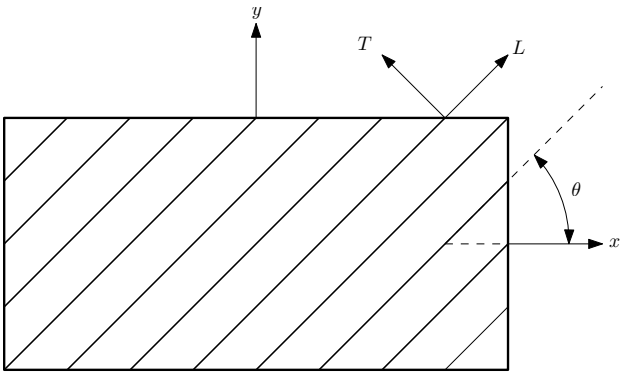

Figure 2.9: An orthotropic lamina showing its longitudinal (L) and transverse (T) axes tilted at an angle θ with respect to the coordinate x, y axes. Adapted from Gershon *et al.* [29].

formula may be developed for the compliance in the y-direction, $1/E_y$.

The longitudinal and transverse moduli of elasticity may be expressed in terms of the volumetric fraction ϕ of each of the fibre and matrix components, as

$$E_L = E_f \phi_f + E_m \phi_m \tag{2.2}$$

and

$$E_T = \frac{E_f E_m}{E_f \phi_m + E_m \phi_f}, \tag{2.3}$$

where the subscripts f and m represent properties relating to the fibre and matrix, respectively. The volumetric fraction was determined through calometric analysis and the elastic moduli of the fibres and the matrix were taken from tabular data relating to the properties of the chosen materials.

Figure 2.10 illustrates the stress-strain results from [29]. It can be seen that the model was unable to predict the non-linearity within the deformation along the x direction. The results in this paper were not substantial enough to develop a more conclusive criticism on the model since only engineering strains up to 50 % were illustrated.

The results obtained by the composite laminate model for the prosthetic designed by [17] are shown in figure 2.2. The curves that show the theoretical results grossly overestimate the experimental data when relating to the tensile response of each specimen. The theoretical results were generally more linear than the experimental data and the model was unable to predict the difference between the toe and linear regions of the response curve.

The current challenge faced while using composite laminate theory to represent the mechanics

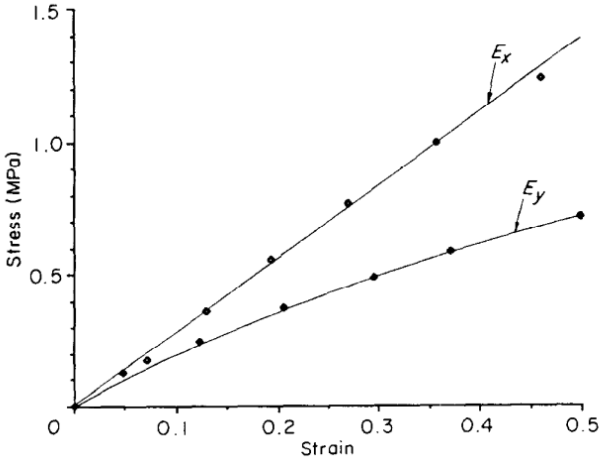

Figure 2.10: Stress-strain results for a SC with an initial fibre angle of $\theta = 33.5°$ from Gershon *et al.* [29]. Experimental data (•) versus predicted results (−).

of a SC is that the elastic behaviour of the matrix is assumed to be linear. In reality, this behaviour is very much nonlinear and thus attributes to the poor results found in the models developed by [17] and [29].

2.3.3 Models formed using a continuum mechanical framework

Another approach to modelling the tensile response of a SC involves the use of hyperelastic theory based upon a continuum mechanical framework. The SC, in this case, is assumed as a single continuum, therefore, there is no differentiation between the matrix and fibre materials used to fabricate the composite. A continuum mechanical model works by employing a constitutive formula to express the stresses of a material as a function of the strain. A strain energy function W is used as a replacement to the more common elastic modulus used in the analysis of linear deformation to relate the stress to the strain of a material. The strain energy function is nonlinear in the case of hyperelastic materials, and it is governed by several material constants that are determined through data fitting the model to experimental results. For a cylindrical tube, these experimental data are typically determined from extension-inflation tests which were orginaly proposed by Boonstra *et al.* [30] but were made popular by Vankergo *et al.* [31]. A detailed explanation about the basis of hyperelastic continuum mechanics is given in section 4.2.

One could derive their own strain energy function for its specified application but many can be found in literature. A continuum model can either be classified as a phenomenological or a

structural model. Phenomenological models purely base their integrity through fitting the theoretical predictions to experimental results while a structural model gives some insight about the anisotropic properties of the material. In the case of SC tubes, structural models tend to acknowledge a preferred direction within the material which is correlated to the direction of the fibres that are embedded within the composite's matrix. Arguments were made in past studies for either model type without a true conclusion of superiority [32].

2.3.3.1 Phenomenological models

Many phenomenological strain energy functions have been created to model a variety of different soft materials. Fung *et al.* [33] proposed a widely used strain energy function W that is most predominantly used to model the mechanical response of arterial walls, and is written as

$$W = \frac{c}{2}\left[\exp(Q) - 1\right]. \tag{2.4}$$

The parameter Q is given by

$$Q = A_{ijkl}E_{ij}E_{kl} \tag{2.5}$$

where repeated indices imply summation according to the Einstein summation convention. The parameters c and A_{ijkl} are material constants that are optimized by fitting Fung's strain energy function to experimental data, and E_{ij}, E_{kl} represent the ij and kl components of the second order Green strain tensor $\mathbf{E}$. **Boldface font** is used to represent first order, second order, and higher order tensors.

The full version of Fung's strain energy function has not been used in practice due to the unavailability of a suitable mechanical testing apparatus that can exert stresses in multiple directions while measuring the corresponding strains. The most complete version of Fung's strain energy model, that has been experminetally used, was a seven parameter version of the model proposed by Sun *et al.* [34]. This model is expressed as

$$W = \frac{c}{2}\left[\exp(Q) - 1\right] \tag{2.6}$$

where

$$Q = A_1 E_{11}^2 + A_2 E_{22}^2 + A_3 E_{11} E_{22} + A_4 E_{12}^2 + 2A_5 E_{12} E_{11} + 2A_6 E_{12} E_{22}, \tag{2.7}$$

and $E_{12} = E_{21}$ due to the assumed symmetry of $\mathbf{E}$.

This seven parameter version of Fung's strain energy model was tested using an experimental protocol developed by Sacks [35] with the hopes of determining the effects of the in-plane shear E_{12}, E_{21}. The protocol used rotating carriages to allow the mounted specimen to rotate its material axis freely about the defined test axes, with negligible friction, throughout the testing procedure. These rotations created shear strains within the material which were measured and used to determine resulting shear stresses within the material. The coupling of the strain energy function in (2.6) and the testing apparatus developed in [35] yielded satisfactory results in the desired material characterization.

For most cases involving planar and isotropic materials, a strain energy function of Fung's type is expressed in a two dimensional formulation [33] as

$$W = \frac{1}{2} c_1 \left(\exp\left(Q\right) - 1 \right) \tag{2.8}$$

where

$$Q = c_2 E_{11}^2 + c_3 E_{22}^2 + 2c_4 E_{11} E_{22} \tag{2.9}$$

and c_i are the material constants determined through data fitting the model to experimental results. This version of Fung's model is widely used in literature and it was shown, in many cases, to provide accurate material characterizations for isotropic materials [36]. Fung's model can also be expressed in terms of cylindrical coordinates by replacing the basis $1, 2, 3$ with the basis R, Θ, Z.

2.3.3.2 Structural models

A structural continuum based model of a material uses a strain energy function that incorporates geometric properties of the specimen, as well as using material constants that are optimized by fitting the predicted values to experimental data. In the case of hyperelastic SC materials, the geometric properties are derived from the properties of the embedded fibres. The strain energy function is assumed as an additive split of an isotropic matrix with anisotropic properties dependant

on fibre orientation, distribution, and relevant density within the SC. Available literature shows that there are a wide variety of examples where a soft material is modelled using a strain energy function of this type. Applications of this method range from inorganic materials like prostheses or SC tubes to biological tissue such as tendons and arteries.

During the late 1990's and early 2000's, researchers were creating artificial ligament prostheses from SC materials. Some of these studies were outlined in section 2.2.1. Some of the researchers have characterized their prosthetics using models created from structural strain energy functions, or FEA, created from these models. Such an example is seen in the work of Vena *et al.* [37].

Vena *et al.* created a SC prosthetic with the geometry shown in figure 2.11. The strain energy

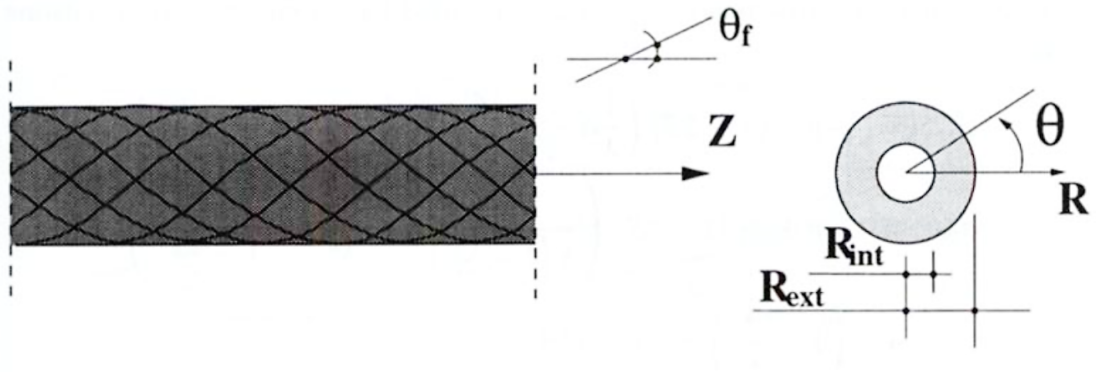

Figure 2.11: Configuration of the SC ligament prosthetic by Vena *et al.* [37].

function used to model this hyperelastic, SC prosthetic is composed of material properties from both the elastomeric matrix material and the embedded fibres. They assumed that the fibres were linearly elastic and therefore did not exhibit a nonlinear flexural response. The compressive stiffness of the fibres was neglected because it was assumed that the fibres would buckle under the smallest compressive loads. The implemented strain energy model W_c was based upon the work of Lanir *et al.* [38] for fibrous connective tissues, and expressed as

$$W_c = \left(1 - \sum_{k=1}^{n} S_k\right) W_m + \sum_{k=1}^{n} S_k W_{kf}. \tag{2.10}$$

The terms W_{kf} and W_m represent the strain energy functions of the k^{th} type of fibres and the matrix, respectively, and S_k is the volume fraction of the k^{th} type of fibres. The elastomeric matrix

is further defined as a Mooney-Rivlin material [39, 40] whose strain energy function is given by

$$W_m = \delta_1 (I_c - 3) + \delta_2 (II_c - 3). \tag{2.11}$$

The factors I_c and II_c are the first and second invariants determined from the deformation of the soft matrix, and δ_1 and δ_2 are arbitrary stress like parameters chosen to minimize the error between theoretical and experimental results. The strain energy of the fibres is defined as

$$W_{kf} = \frac{1}{2} E_f (\lambda_{kf} - 1)^2 \tag{2.12}$$

where E_f is the elastic modulus of one individual fibre and λ_{kf} is the stretch ratio of the family of fibres, depending on the original fibre angle shown in figure 2.11. The fibre stretch for cylindrical tubes is outlined as

$$\lambda_{kf}^2 = \cos^2 \theta_{fc} \left(\tan^2 \theta_{fc} \frac{r^2}{R^2} + \lambda_z^2 \right) \tag{2.13}$$

where λ_z is the stretch ratio of the entire composite tube in the z direction, r is the radius of the deformed tube, and R is the initial radius of the tube with the applied constraints:

$$R_{int} \leq R \leq R_{ext} \quad \text{and} \quad r_{int} \leq r \leq r_{ext}. \tag{2.14}$$

The fibre angle of the deformed SC, θ_{fc}, is defined by

$$\tan^2 \theta_{fc} = \frac{1}{\lambda_z^2} \frac{r^2}{R^2} \tan^2 \theta_f. \tag{2.15}$$

The parameters were selected to optimize the accuracy of the predicted tensile test results when compared to the experimental data. Figure 2.12 illustrates good agreement between experimental and theoretical tensile test results. There is a variation between the slope of each curve under in the toe region and at the end of the linear region. It is not clear if the results were consistent at higher strains past what is shown in figure 2.12.

A similar method was used by Mollica *et al.* [24] to model the tensile response of their hyper-elastic, SC prosthetic ligament presented in section 2.2.1. They employed the same additive split to the strain energy function of the composite W_c that Vena *et al.* [37] did in (2.10), except they

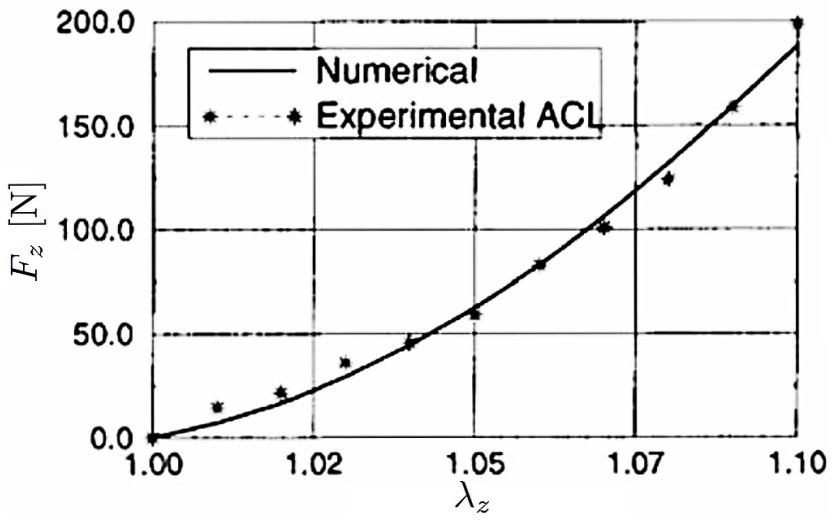

Figure 2.12: Axial force versus stretch ratio along the z axis for experimental and theoretical tensile test results for the SC prostheses created by Vena *et al.* [37].

added a parameter ζ to yield

$$W_c = (1 - 2\phi)\zeta W_m + \phi W_{+\alpha} + \phi W_{-\alpha}. \tag{2.16}$$

The subscripts $+\alpha$, $-\alpha$ represent the helical fibres with equal and opposite orientations based off of the initial fibre angle α. The parameter ϕ is defined as half of the total fibre volume fraction. The added parameter ζ, defined by

$$\zeta = \frac{1}{1 - 2\phi}, \tag{2.17}$$

was implemented by the researchers as a modulus to help estimate some of the transverse properties of the composite.

The strain energy of the matrix W_m was modelled as a Mooney-Rivlin material [39, 40] identical to the form shown in (2.11). Mollica *et al.* [24] chose to test only the elastomeric matrix, and not the full composite, to optimize the material constants δ_1 and δ_2. They argued that the optimization need only be completed once, on the matrix material only, instead of having to reoptimize individual SC specimens separately. The constants were optimized using the Least Squares algorithm.

The embedded fibres were assumed linearly elastic and the strain energy function W_f that was used to model them was identical to that shown in (2.12). The modulus of elasticity based off of

properties of the PET fibres, and the fibre stretch ratio is modelled as

$$\lambda_f = \sqrt{\lambda_\theta^2 \sin^2 \alpha + \lambda^2 \cos^2 \alpha} \tag{2.18}$$

where λ and λ_θ are represented as the axial and azimuthal stretch ratios, respectively.

The strain energy model of the composite, which was obtained from the additive split of W_m and W_f, was used to predict the tensile response of the SC and the results are shown in figure 2.13. It is seen that, even with the use of a parameter to estimate transverse shear properties, the predicted results were incapable of modelling the experimental data.

Groups 1 and 4, in figure 2.13, illustrate the experimental results of composite ligaments made from PET fibres that were not plasma treated, while Groups 2 and 5 illustrate the results of the PET fibres that were plasma treated. As mentioned in section 2.2.1, plasma treating PET fibres creates better adhesion between the fibres and the matrix. The theoretical model did not take into account any slippage between the fibres and the matrix during deformation which adequately explains why the model predictions are more representative of the plasma treated groups. Still, the fibre predictive model was incapable of fully estimating the linear region of each composite material.

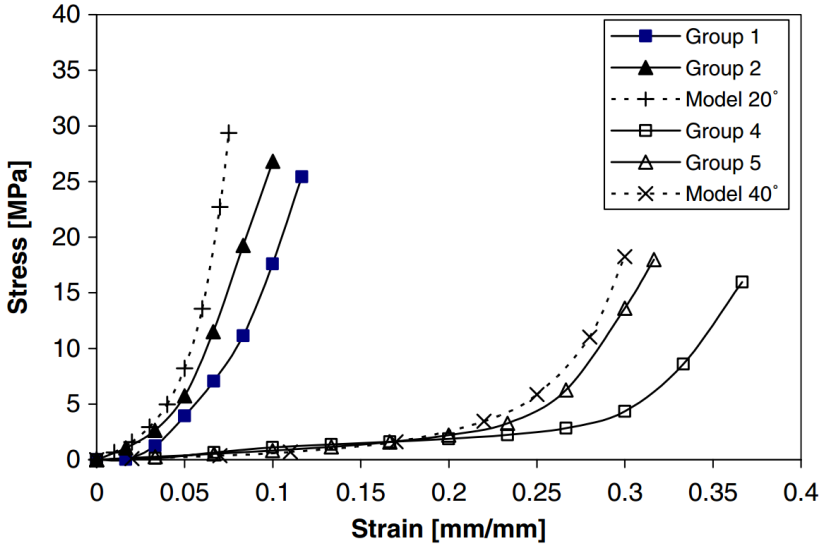

Figure 2.13: Comparison of predicted and experimental tensile test results on the SC prostheses created by Mollica *et al.* [24].

Soft biological tissue, such as ligaments, tendons, and arteries, have a similar structure to the

SC materials being discussed in this research. Many models that have been used to represent the mechanical behaviour of a SC can be used to model the behaviour of soft tissues, and the same can be done with models used to represent soft tissues for modelling SC materials. For example, models presented by Vena *et al.* [37] and Mollica *et al.* [24] were also employed by Hirokawa and Tsurono [41] to characterize the mechanical behaviour of an Anterior Cruciate Ligament.

Ligaments and tendons, for the most part, are assumed to have their fibres oriented along the axis of deformation. When creating a strain energy model, this assumption of axially aligned fibres leads to the creation of a transversely isotropic model with one preferred direction [42], which does not accurately represent the helical winding of the fibres presented in the structure of the SCs that are discussed in this research.

The structure of a SC material, similar to those mentioned in this research, can actually be related to the medial layer of an arterial segment. The medial layer of an artery has been described as an incompressible, soft matrix embedded with helically wound collagen fibres and has been assumed axisymmetrical as well [36]. This means that continuum mechanical formulae used to model the mechanical response of arterial segments have potential to be useful for the application of this research.

Holzapfel *et al.* [36] proposed a model that provided a mechanical characterization of the medial arterial layer. The model assumed that the fibres in the medial layer of the artery were axisymmetrically, helically wound around the axial direction of the artery with a constant fibre angle throughout the entire segment. The fibres were assumed to be active only when extended and inactive when compressed. The action of the fibres was assumed in the axial and circumferential directions only, and therefore any components within the radial direction were neglected.

Holzapfel's model took the form of a strain energy function, similar to those introduced earlier in this section, where the strain energy of the artery was expressed as an additive split between the isotropic matrix and the embedded collagen fibres. Denoting the matrix response as W_{iso}, for the isotropy of the matrix material, and the fibrous response as W_{aniso}, for the anisotropy that embedded collagen fibres add to the artery, the strain energy is expressed as

$$W(\mathbf{C}, I_4, I_6) = W_{iso}(\mathbf{C}) + W_{aniso}(\mathbf{C}, I_4, I_6). \tag{2.19}$$

The second order tensor $\mathbf{C}$ is the right Cauchy-Green tensor and scalar values I_4 and I_6 are invariants of whose integrity is based on the properties of the fibres and the deformation of the full specimen. They are a direct function of the initial fibre angle β. A more detailed explanation of $\mathbf{C}, I_4$, and I_6 is outlined in chapter 4.

The isotropic portion of the strain energy is modelled as a Neo-Hookean material [40] as

$$W_{iso}(\mathbf{C}) = \frac{c_1}{2}(I_1 - 3) \tag{2.20}$$

where $c_1 > 0$ is a stress like material parameter representing features of the isotropic matrix. The anisotropic response exhibited by the fibres during experimentation, as they became aligned with the tensile axis, is largely contributed to the exponential increase within the force response of the artery. It was proposed by [36] that the anisotropic strain energy response be modelled as

$$W_{aniso}(I_4, I_6) = \frac{c_2}{2c_3}\left[\exp\left(c_3(I_4 - 1)^2 - 1\right) + \exp\left(c_3(I_6 - 1)^2 - 1\right)\right], \tag{2.21}$$

where the parameters $c_2 > 0$, a stress-like material parameter, and $c_3 > 0$, a dimensionless parameter, both describe properties regarding the embedded fibres.

Holzapfel *et al.* [36] chose to use the strain energy function presented in (2.19) to model both the media and adventitia in a healthy and young carotid artery segment from a rabbit. They assumed an arterial segment, with residual strains, similar to scenario shown in figure 2.14. This figure also

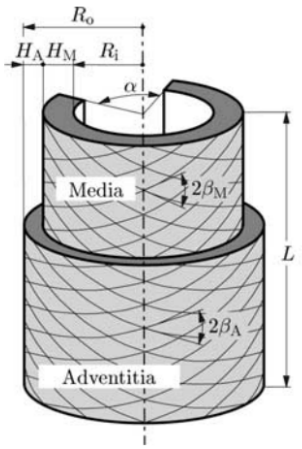

	Material	Geometry
Media	$c_M = 3.0000$ [kPa] $k_{1M} = 2.3632$ [kPa] $k_{2M} = 0.8393$ [–]	$H_M = 0.26$ [mm] $\beta_M = 29.0°$
Adventitia	$c_A = 0.3000$ [kPa] $k_{1A} = 0.5620$ [kPa] $k_{2A} = 0.7112$ [–]	$H_A = 0.13$ [mm] $\beta_A = 62.0°$

$R_i = 0.71$ [mm] for $\alpha = 0.0°$
$R_i = 1.43$ [mm] for $\alpha = 160.0°$

Figure 2.14: Material parameters selected to model the medial and adventitial layers of an artery by Holzapfel *et al.* [36]. Experimental data was taken from experiment 71 performed by Chuong and Fung [43].

illustrates the parameters that were used to form the strain energy function, $W(\mathbf{C}, I_4, I_6)$, that were a resultant of curve fitting theoretical to experimental data from tests performed by Chuong and Fung in experiment 71 of [43]. The Levenberg-Marquardt algorithm was used optimize the material constants c_i and k_i.

The trends of the model are shown, only with numerical results, in figure 2.15 and these results were not compared to any experimental data. According to [36], the strain energy function is able to determine the typical evolution of the reduced axial force with inflation of the artery during an extension-inflation test. It was said, by Holzapfel *et al.* [36], that the fully 3-D formulation of (2.19) allows the anisotropic behaviour of healthy arteries under combined bending, inflation, axial extension, and torsion to be predicted. They also mention that the model was not restricted to axisymmetry and it was accessible to approximation techniques such as FEA.

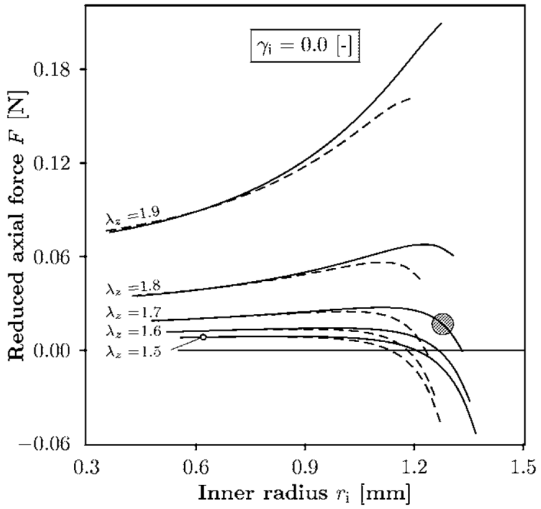

Figure 2.15: Numerical results for reduced axial force versus internal radius for different axial stretch ratios λ_z based off of Holzapfel's strain energy function for an arterial segment [36]. Residual strains included $(-)$ with opening angle value of $\alpha = 160°$ and no residual strains $(--)$ with an opening angle value of $\alpha = 0°$.

The major limitation presented by the Holzapfel strain energy function for hyperelastic materials is that it does not take into account the variation in angular distribution of the fibres embedded within the soft matrix. It assumes a completely uniform angular distribution through the entire specimen. The work of Zulliger *et al.* [44] proposed the first attempt at modelling an angular distribution of the fibres throughout an arterial specimen using a continuum mechanical basis.

Zulliger *et al.* employed the same additive split as every other structural based strain energy

function examined in this review, where

$$W = f_{elast} W_{elast} + f_{coll} W_{coll}. \tag{2.22}$$

The term $f_{elast} W_{elast}$ represents the values related to the elastin matrix, or more importantly, the isotropic portion of the artery. The term $f_{coll} W_{coll}$ represents the values related to the collagen fibres, which formulates the anisotropic strain energy W_{aniso} of the artery. The fraction of the total artery composed of either elastin f_{elast}, or collagen f_{coll} was determined histologically as described in [45], and respectively weigh the functions W_{elast} and W_{coll} in W.

The behaviour of the matrix material W_{elast} was further defined as

$$W_{elast} = c_{elast} \left(I_1 - 3\right)^{\frac{3}{2}} \tag{2.23}$$

where c_{elast} is an experimentally determined elastic constant that must be greater than zero.

The function W_{coll} was derived to express the non-uniform variation of the fibre angle throughout the matrix by expanding the strain energy of a single fibre W_{fibre} over the entire artery. A log-logistic probability distribution function $\rho_{fibre}(\varepsilon)$ was employed, where

$$\rho_{fibre}(\varepsilon) = \begin{cases} 0 & \text{for } \varepsilon \leq \varepsilon_0, \\ \dfrac{k}{b} \dfrac{\left(\varepsilon - \varepsilon_0/b\right)^{k-1}}{\left[1 + \left(\varepsilon - \varepsilon_0/b\right)^k\right]^2} & \text{for } \varepsilon > \varepsilon_0. \end{cases} \tag{2.24}$$

The parameters $b > 0$ and $k > 0$ scale and shape the distribution, respectively, and the strain at the lower bound ε_0 was set to zero to prevent any collagen fibres from being loaded when the tissue was at rest or in compression. The engagement strain ε was defined as

$$\varepsilon = \lambda - 1 \tag{2.25}$$

where λ represents the stretch ratio of a collagen fibre. The stretch ratio was decomposed into its axial and azimuthal directions through

$$\lambda = \sqrt{\lambda_\theta^2 \cos^2 \alpha + \lambda_z^2 \sin^2 \alpha}, \tag{2.26}$$

where the fibre angle α represents the average fibre angle with respect to the circumferential direction.

The strain energy of an individual collagen fibre W_{fibre} was represented as

$$W_{fibre}(\varepsilon) = \begin{cases} 0 & \text{for } \varepsilon \leq 0, \\ c_{coll}\left(\varepsilon - \log\left(\varepsilon + 1\right)\right) & \text{for } \varepsilon > 0 \end{cases} \tag{2.27}$$

where c_{coll} was represented by the Young's modulus of collagen. The collective behaviour of all the collagen fibres was described by a convolution of the individual fibre strain energy and the probability distribution function, which is written as

$$W_{coll}(\varepsilon) = W_{fibre} * \rho_{fibre} = \int_{-\infty}^{\infty} W_{fibre}(x) \cdot \rho_{fibre}(\varepsilon - x)dx, \tag{2.28}$$

and illustrated in figure 2.16.

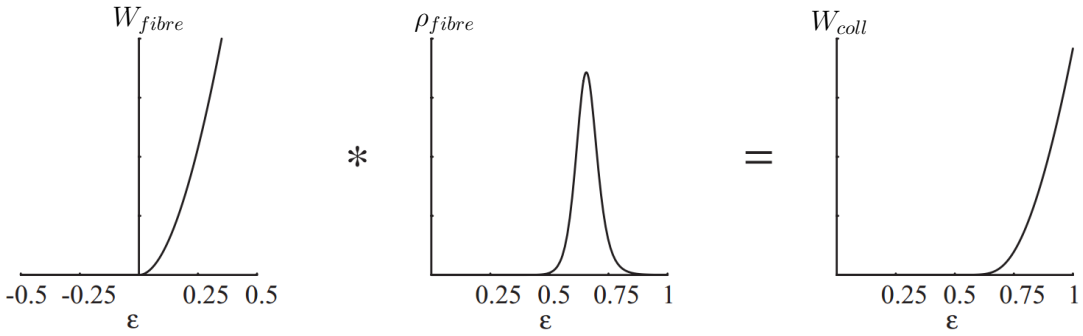

Figure 2.16: Convolution of the strain energy function of an individual fibre W_{fibre}, with the log-logistic distribution ρ_{fibre}, resulting in the overall strain energy function of the entire collagen fibre ensemble W_{coll}. Adapted from [44].

The total anisotropic strain energy W_{aniso}, represented by each family of collagen fibres, is

$$W_{aniso} = f_{coll}\left(\frac{1}{2}W_{coll}\left(\lambda - 1\right) + \frac{1}{2}W_{coll}\left(\lambda' - 1\right)\right) \tag{2.29}$$

where λ' corresponds to the fibre angle $-\alpha$. Thus the final strain energy function W relating to (2.22) was derived as

$$W = f_{elast}c_{elast}\left(I_1 - 3\right)^{\frac{3}{2}} + f_{coll}\left(\frac{1}{2}W_{coll}\left(\lambda - 1\right) + \frac{1}{2}W_{coll}\left(\lambda' - 1\right)\right). \tag{2.30}$$

The researchers employed the strain energy function presented in (2.30) to predict the data from experiments performed by Fridez *et al.* [46] on left carotid arterial segments from eight-week-old Wistar rats. W was fitted to experimental data by optimizing the four parameters, b, k, c_{coll}, and c_{elast}. Finding the global minimum of the error function between the theoretical and experimental data, for this specific strain energy function, was computationally taxing when trying to optimize four parameters. It was decided to fix c_{coll} at 200 MPa.

The results of the fits for the internal pressure versus the radius of an artery during an inflation-extension test are shown in figure 2.17. The Zulliger strain energy function can predict the arterial response at low stretch ratios, but is not able to fully predict the linear region of the response curve at higher strains. According to the researchers, the curve fitting was a computationally costing procedure and assumptions needed to be made about the fitted parameters in order to ease the process in finding the global minimum of the error function.

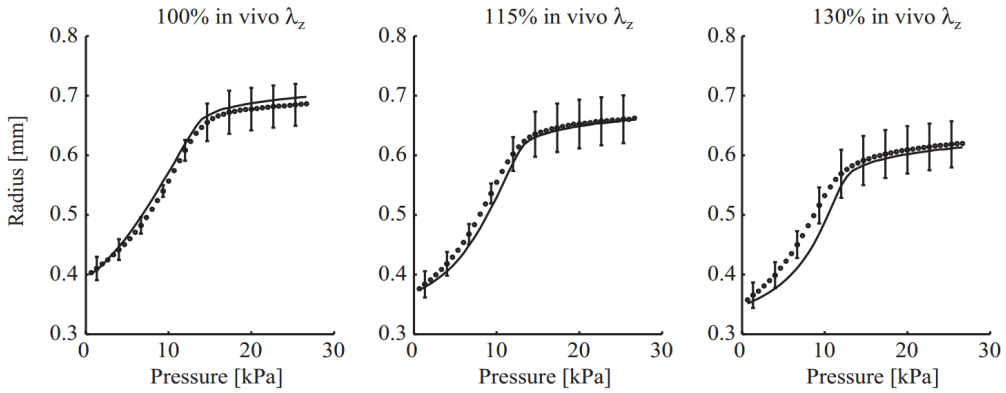

Figure 2.17: Comparison of radius and pressure with the Zulliger strain energy function (−) for three different axial stretch ratios λ_z [44].

2.3.4 Summary of material characterization models

The SC material that is being proposed in this study will need to be characterized in order to fully comprehend and predict its behaviour based on certain design aspects. The literature discussed within this research reviewed many material characterization models that involved the use of either composite laminate theory, or the continuum hypothesis to characterize the mechanical behaviour of a SC specimen. Both methods of modelling have the ability to provide the basis to a fully feasible FEA of the proposed SC, in future works.

It was noticed that the results relating to composite laminate models shown in figures 2.2 and 2.10 tend to not conform to the nonlinear shape of the stress-strain curve presented by experimental data. The models can predict the initial response, for strain less than 20 % in both cases, but fail to predict the remaining data. It is, for this reason, that composite laminate theory will not be used to model the proposed SC design within this research.

The continuum models presented in this review were separated into phenomenological and structural functions. The first type of function characterizes the material based on macroscopic qualities only, while the latter incorporates a form of structural geometry into the function. It is hoped that utilizing a function with a structural component will provide a more general representation of the material that can be altered without needing to re-fit data to the predictive model for every separate specimen. Since there is no conclusive evidence in literature as to which type of function is more accurate, this research will conduct a study on, both, a phenomenological and structural function type. The phenomenological function that will be used within this research will be of Fung's type because it is one of the, if not the most, commonly used functions to model a soft tubular composite or biological tissue with embedded fibres.

Several models were inspected for use regarding a structural material characterization function. The functions suggested by Vena *et al.* [37] and Mollica *et al.* [24] provided theoretical predictions shown in figures 2.12 and 2.13, respectively. In the case of Vena *et al.*, the results shown by the stretch ratio were not conclusive because the results were only shown for strains of up to 10 %. For what was shown, however, the results were more linear than the experimental data and could not seem to predict the exponential curve of the response. It is estimated that the error within the prediction came mostly from the use of linear elastic constants to describe the matrix, which is a highly nonlinear elastic material. The predictive models in [24] grossly over predicted the tensile stress of the tested composites. The function utilized a transverse shear modulus in order to compensate for only optimizing the isotropic strain energy function by individually testing the elastomeric matrix, once, without the embedded fibres. This shear modulus increased the stiffness, in every case, of the predictive model stress-strain response and failed to replicate experimental data.

The Holzapfel strain energy function has promising traits. It utilizes an exponential function to characterize the exponential increase of the tensile response as the composite is elongated past the

jamming state and the fibres become aligned with the deformed axis. The most evident limitation within the model is that it assumes a constant fibre angle throughout the SC.

The probability distribution that was utilized in Zulliger's strain energy function to compensate for the non-uniform angular distribution of the embedded collagen fibres presented results that conformed to experimental data. These results, however, were calculated at the cost of increased mathematical complexity and greater computational power. Other similar models have been proposed to alleviate the computational power required to calculate the global minimum of the error function between theoretical and predictive models. The most popular of these models is proposed by Gasser, Holzapfel, and Ogden [47], in 2006, which uses a generalized structure tensor to reduce the amount of integration performed on each iteration of the optimization algorithm.

Models that predict non-uniform angular distribution were originally created for arterial mechanics. The angular distribution of collagen within an artery, as shown in figure 2.18a, is non-uniform due to the unpredictable, winding nature of a collagen fibre. The composite that is proposed in this research utilizes a helically wound mesh sleeve that resembles the configuration shown in figure 2.18b and is clearly much more uniform than the collagen. It is understood that the angular

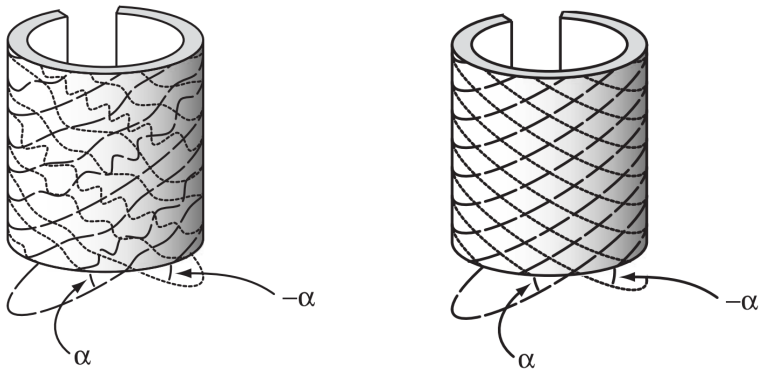

(a) Theoretical artery **(b)** Proposed SC

Figure 2.18: The difference in fibre angle distribution for an arterial segment and a proposed SC for initial fibre angle $\pm\alpha$ [44].

distribution within the SC is not perfect, but it can be stated with great confidence that it is not as unpredictable as an arterial segment. This leads one to question if the added computational cost and mathematical rigour from using a probability density driven strain energy function is worthwhile for characterizing the SC. It was decided that, due to the fact that the fibre distribution in

the SC is much more uniform than in an arterial segment, the Holzapfel strain energy function will be used as a structural based method to characterize the mechanical response of the SC proposed within this research.

Chapter 3

Soft Composite Development and Testing

This chapter introduces the development of the proposed SC as an actuation solution for passively powered exoskeletons. It discusses several experimental setups and tests, with variable control parameters, that highlight the versatility of the SC's mechanical behaviour. Most tests are performed on the SC as a whole, however, initial tests are also performed on the braid and matrix materials, separately, with the intent of determining the mechanical properties of the individual materials.

3.1 SC development

The development of the proposed SC is primarily inspired by the objective of converting the PAM into a passive fluidless actuator. Figure 3.1 shows a PAM prototype that was fabricated at the University of Ottawa [4, 48], which consists of an elastic bladder wrapped by a braided mesh and is secured with end fixtures. It was desired to retain the governing geometric relationship offered by the PAM braid without the need of a fluid supply so that pressure dissipation over time would be avoided. This objective was accomplished by embedding an elastomer between the braided fibres.

The secondary objective is to create a SC specimen with an elongation potential greater than that offered by the PAM, which is only 30 % of its contracted length [4]. The contraction limit of the PAM is controlled by the jamming angle of the braid when the PAM is inflated, and the equilibrium state of the contraction force when the PAM reaches maximum contraction. This equilibrium state,

Figure 3.1: Deflated (top) and inflated (bottom) PAM [4].

as stated in [4], corresponds to the balance of forces contributed by the longitudinal and hoop stresses acting on the braid. This occurs when the fibre angle is at 54.7°, which is also known as the "Magic Angle", in braid analysis. While this represents the maximum theoretical fibre angle obtainable by the PAM during contraction, experimentally, the PAM can only achieve a maximum contraction up to 40°. This reduction is attributed to other unaccounted resistive forces such as friction and bladder resistance within the PAM. Figure 3.2 shows a typical braid in its three principal states which are the contraction jamming state, the equilibrium state (Magic Angle), and the tensile jamming state.

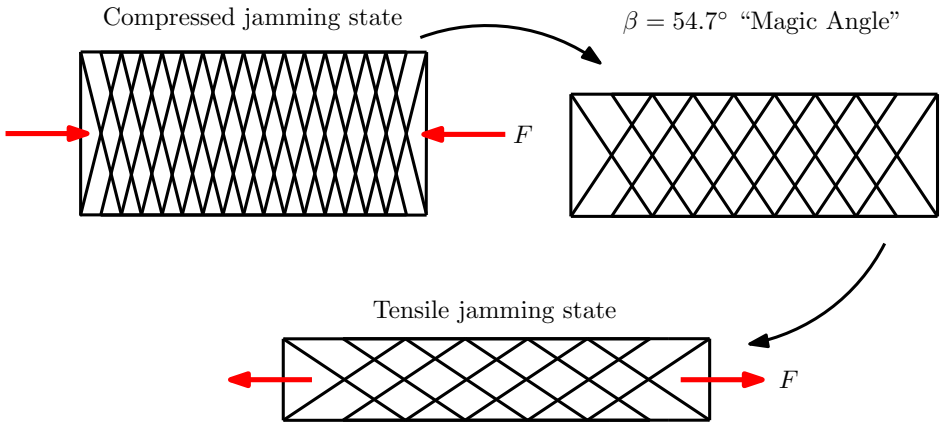

Figure 3.2: A typical braid in its three states: compressed jamming state, the equilibrium state (Magic Angle), and tensile jamming state.

A decision was made to fabricate some of the SC specimens with an initial fibre angle beyond the 54.7° Magic Angle. This achieves a greater range of elongation potentials which leads to designs that are more suitable to mimic the force response of soft tissue in varying applications. This design, to the knowledge of the author, has not been previously attempted. It is only achievable by locking

the braid at a higher initial fibre angle which is most conveniently done by suspending the braid in a polymer matrix. Using a braid wrapped around an elastic core, as discussed in the literature review, is not feasible for initial fibre angles larger than the Magic Angle. The fibre orientation and geometry, in its resting state, is unrestricted and therefore predicting its deformation for design purposes becomes very difficult.

Figure 3.3 illustrates a typical SC specimen that was developed for this research. In order to gain a better understanding of its mechanical behaviour, it was deemed important to be able to develop the SC using a variety of different combinations of physical key design parameters. The design parameters of interest are of those related to the braided sleeve and the silicone matrix.

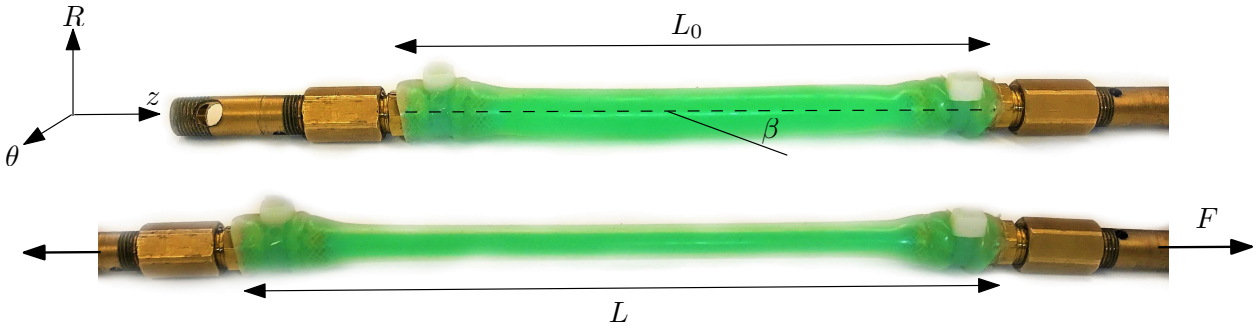

Figure 3.3: A SC specimen made with a regular braid and soft silicone matrix shown in a resting (top) and stretched (bottom) configuration.

With reference to figure 3.3, geometric components of the SC are defined such that: β is the initial fibre angle measured from the z axis, L is the deformed length, L_0 is the relaxed length, R_i and R_o are the relaxed inner and outer radii, respectively, and r_i and r_o are the deformed inner and outer radii, respectively.

3.1.1 Material selection

The SC only consists of two materials, namely, the fibres and the matrix. Given that hyperelasticity is a desired property of the SC, an elastomeric matrix is considered over a stiffer resin that would be typically used in composite design. Three different silicone rubbers of varying stiffness were selected from Smooth-On Inc. [49]. It was decided that Ecoflex®00-30 would be chosen as the softest silicone rubber, Mold Star®20T would be chosen as the rubber of medium stiffness, and Oomoo®30 would be chosen as the stiffest rubber. These silicone rubbers are available in two part

prepolymers that were mixed by weight and then allowed to cure to yield the final silicone rubber. Mechanical properties of each selected rubber are displayed in table 3.1.

Table 3.1: Material properties of the silicone rubber selected as the matrix for the SC design.

Material property	Ecoflex®00-30 [50]	Mold Star®20T [51]	Oomoo®30 [52]
Referred to as	Ecoflex	Moldstar	Oomoo
Silicone base	Platinum	Platinum	Tin
Mixing ratio	$1A:1B$	$1A:1B$	$100A:130B$
Pot life	45 min	6 min	30 min
Mixed viscosity	3 Pa s	11 Pa s	$1.34\,\mathrm{g\,cm^{-3}}$
Cure time	4 h	30 min	6 h
Tensile strength	1.38 MPa	2.90 MPa	1.65 MPa
Elongation at break	900 %	470 %	250 %
Shore Hardness	30-00	20-A	30-A

The silicone material properties regarding the mixing ratio, pot life, mixed viscosity, and cure time were important to consider for the fabrication process of the SC. Tensile strength, elongation at break, and Shore Hardness ratings are properties that describe the strength and stiffness of the silicone rubber after it cured. The shore hardness ratings are not necessarily intuitive so, for a point of reference, one may compare the hardness of Ecoflex, the softest rubber, to that of a rubber shoe insole and the hardness of Oomoo, the stiffest rubber, to that of a pencil eraser [53].

One of the major control parameters investigated in this research was the effect of the fibre braided sleeve properties on the overall mechanical response of the SC. To perform this analysis, two different braid types were selected from TechFlex Inc. [54]. The first braid selection was the Flexo PET® (PT) sleeve. Figure 3.4a illustrates that this braiding style uses only one fibre helically wound around the axial direction using a regular fibre braiding pattern. This braiding style, henceforth referred to as the "regular" braid, has a nominal diameter of 3.175 mm, and a monofilament thickness of 0.254 mm. The advertised minimum and maximum achievable diameters of this braid are 2.381 mm and 6.350 mm, respectively. The second selection was the TechFlex Inc. Flexo Tight Weave® sleeve which, in contrast to the Flexo PET® (PT) sleeve, has a greater fibre braiding density. Figure 3.4b illustrates that there are two fibres that are helically wound around the axial direction. This braiding style, henceforth referred to as the "tight" braid, has a nominal

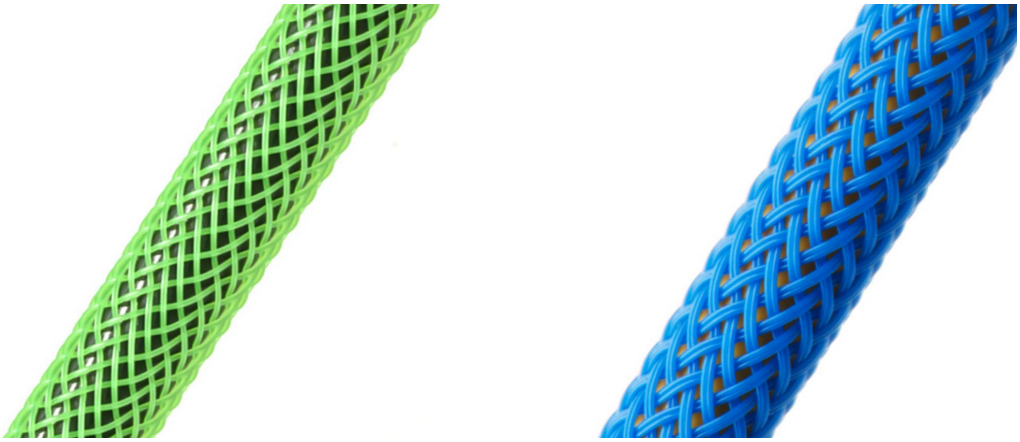

(a) Regular Braid **(b)** Tight Braid

Figure 3.4: TechFlex Inc. Flexo PET® in neon green [55] and in neon blue [56].

diameter of 6.350 mm, and a monofilament thickness of 0.254 mm. The advertised minimum and maximum achievable diameters of this braid are 4.360 mm and 8.730 mm, respectively.

Using a combination of selected materials and initial fibre angles, 18 unique SC specimens were fabricated for experimental testing. Due to the large number of developed SC specimens a nomenclature system of the format **X1Y4Z_XX** is used for identification. Parameter **X** represents the braiding style, parameter **Y** represents the class of initial fibre angle, parameter **Z** represents the choice of silicone for the composite matrix, and the number **XX** represents the initial fibre angle β, measured in degrees. The associated choices of physical features for each parameter are outlined in table 3.2.

Table 3.2: Classification of parameter nomenclature with associated physical representations.

X	**R** for a regular braiding style	**T** for a tight braiding style	__
Y	**A** for a small fibre angle ($\beta \leq 49°$)	**B** for a medium fibre angle ($50° \leq \beta \leq 59°$)	**C** for a large fibre angle ($\beta \geq 60°$)
Z	**A** for the softest silicone	**B** for a medium stiffness silicone	**C** for the stiffest silicone

For example, a specimen name of R1A4A_45 implies that the specimen was made from a braided sleeve that had a regular braiding style, a low stiffness silicone matrix, and a small initial fibre angle. The numbers 1 and 4 are simply placeholders. A complete list of these specimens is given in table 3.3.

Table 3.3: List of fabricated specimens sorted by the design parameters of interest.

Regular Braiding Style	Fibre Angle (°)	Matrix Type	Specimen Name
Small fibre angle	45	Ecoflex®00-30	R1A4A_45
	49	Mold Star®20T	R1A4B_49
	48	Oomoo®30	R1A4C_48
Medium fibre angle	54	Ecoflex®00-30	R1B4A_54
	55	Mold Star®20T	R1B4B_55
	56	Oomoo®30	R1B4C_56
Large fibre angle	61	Ecoflex®00-30	R1C4A_61
	62	Mold Star®20T	R1C4B_62
	64	Oomoo®30	R1C4C_64
Tight Braiding Style	Fibre Angle (°)	Matrix Type	Specimen Name
Small fibre angle	40	Ecoflex®00-30	T1A4A_40
	43	Mold Star®20T	T1A4B_43
	45	Oomoo®30	T1A4C_45
Medium fibre angle	53	Ecoflex®00-30	T1B4A_53
	52	Mold Star®20T	T1B4B_52
	56	Oomoo®30	T1B4C_56
Large fibre angle	60	Ecoflex®00-30	T1C4A_60
	63	Mold Star®20T	T1C4B_63
	65	Oomoo®30	T1C4C_65

3.2 SC fabrication process

This section provides a detailed explanation of the single step impregnation process that was implemented to fabricate the SC. An outline of the mold design and fabrication, impregnation process, demolding process, and application of end fixtures will be discussed.

3.2.1 Mold design and fabrication

All composite specimens were fabricated using molds with the equal geometries to assure consistency between experimental tests. 3-D printed molds were originally considered due to their customizability and ability to create unique geometries for the final SC, however, major drawbacks were encountered. The most predominant drawbacks of 3-D printing the molds included the sur-

face finish, prepolymer leakage, and lengthy print times. Therefore, it was decided that off-the-shelf tubing and rods were to be used to create the molds. The mold shown in figure 3.5 was used to suspend one of the PET braids shown in figure 3.4a and 3.4b for the prepolymer impregnation process.

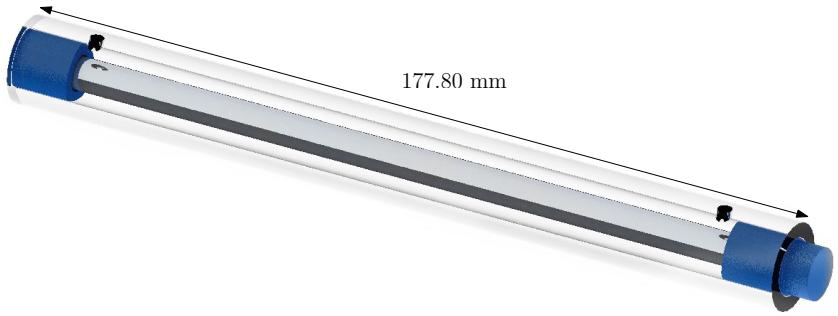

Figure 3.5: A CAD render of the mold used to suspend the PET braid for impregnation. Render created with SolidWorks 2016.

The apparatus that was used to form the molds is shown, as individual components, in figure 3.6. The acrylic tubing had an inner diameter of 12.70 mm and was cut to a length of 177.80 mm. The metal rod was chosen to be brass, due to strength and availability, and it had an outer diameter of 7.14 mm. When the brass rod was inserted into the acrylic tube, the resulting gap was 2.78 mm which corresponds to the wall thickness of the SC after impregnation. The 3-D printed end caps were created to be removable so that the mold could be reused for multiple processes. A more detailed view of the mold geometry can be seen in the assembly drawing shown in appendix A.

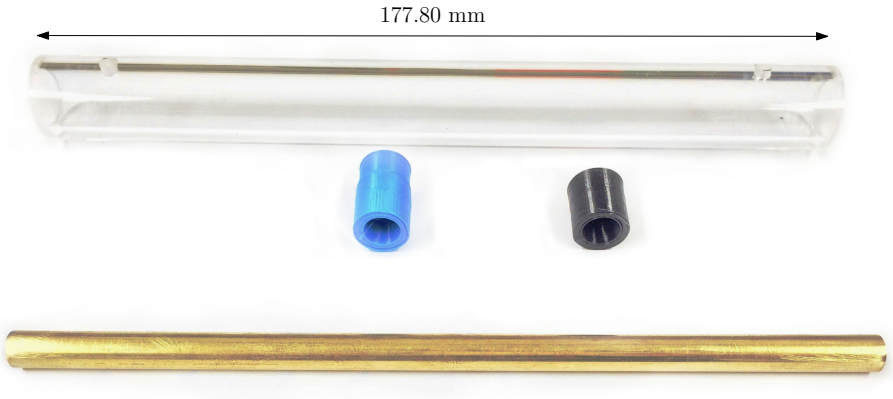

Figure 3.6: Apparatus used to fabricate the mold that suspends the PET braid for impregnation.

The first step to making the mold, as shown in figure 3.7, involved wrapping each end of the brass rod with Teflon tape. The tape created a compressible seal so that the end caps would fit snugly over the brass rod and prevent silicone prepolymer from flowing between the end caps and brass rod during impregnation. Sliding the PET sleeve over the brass rod was also less strenuous due to reduced frictional forces created the by Teflon tape.

Figure 3.7: The first step of the mold fabrication process.

Next, PET braid was cut from the spool to a length that was longer than the brass rod. The desired initial fibre angle was obtained by retaining an open ended mesh and compressing a length of braid to achieve a shorter length of braid, with a larger diameter, resulting in a larger initial fibre angle. This manual method of changing the initial fibre angle lead to inconsistencies within the fibre angles between the final specimens. A theoretical braid model could be used to predict the initial lengths of braid to achieve a desired initial fibre angle, however, this method was not feasible for this fabrication process. When the braid was slipped over the brass rod, there was fibre fraying, similar to figure 3.8, which needed to be trimmed and cleanly cut in order to have a homogeneous SC after impregnation. This unavoidable fibre fray caused an unpredictable change in length of the PET braid during this step of the manufacturing process.

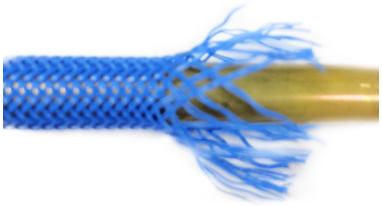

Figure 3.8: Unpredictable fibre fray of the PET braid when it is slipped over the brass rod.

After the fibre fray was removed with a hot blade and the braid was securely placed over the brass rod, the end caps were assembled to the brass rod. Figure 3.9 illustrates this assembly. It is at this point that the initial fibre angle was measured and recorded, manually, with a measurement error of $\pm 2^{\circ}$. It is important to note that, for the regular braid, only initial fibre angles between

45° and 63° were achievable. Likewise, for the tight braid, only initial fibre angles between 40° and 65° were achievable. The braided sleeve would buckle if the initial fibre angle were too large, and its diameter would have been too small to fit over the brass rod if the initial fibre angle were too low.

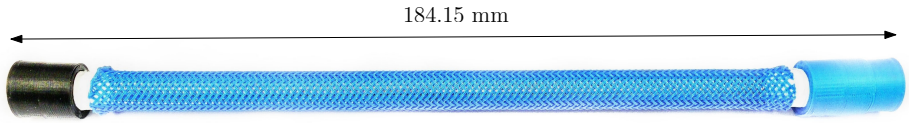

Figure 3.9: Tight braid over the brass rod with end caps assembly photo.

An attempt was made to create SC specimens with equal initial fibre angles for similar control groups. However, due to problems related to fibre fraying, exact initial fibre angles within similar composites could not be created as desired. This led to the initial fibre angle parameters being grouped in sizes small, medium, and large to maintain a level of uniformity between samples.

The final step to making the mold involved wrapping the end caps with Teflon tape, for an airtight seal, and then inserting this assembly into acrylic tubing until the bottom of the end cap was flush with the bottom of the acrylic tube. The geometry of the mold was constructed to assure that the input and exhaust holes on the acrylic tubing were properly aligned for injection. Figure 3.10 illustrates the final mold ready for impregnation.

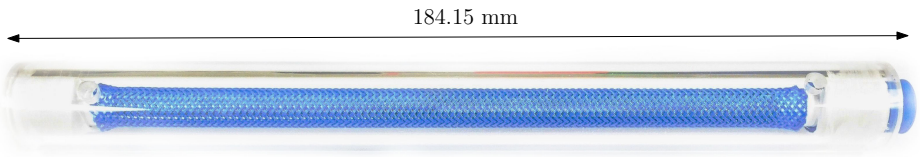

Figure 3.10: The composite mold. Illustrated with a tight braid and a small initial fibre angle.

3.2.2 Impregnation process

The selected elastomers are safe and non-toxic according to their manufacturer, Smooth-On Inc. Safety procedures were followed according to the technical specification sheets for each rubber

[50, 51, 52]. Special precautions included regular hygiene protocol, properly ventilated areas, safety glasses, long sleeves, and vinyl gloves.

All of these silicones came as prepolymer A/B forms and were mixed in a plastic container to create the final elastomer. The mixture was stirred thoroughly to assure a proper solution without any lumps or inconsistencies. Thorough stirring of the mixture created air bubbles within the silicone rubber that would greatly diminish the structural integrity of the final SC. Consequently, a vacuum chamber was developed in the laboratory to degas the prepolymer and eliminate any presence of air bubbles within the silicone rubber.

The main components of the degassing system is the pump and chamber which include an easily removable lid, a gasket, a release valve, and rubber hoses to connect the chamber to the vacuum pump. A rotary vane vacuum pump, by Norman, equipped with a 248.5 W motor that can achieve an absolute vacuum pressure of 30 Pa at $6.80\,\mathrm{m^3\,h^{-1}}$, was selected.

The vacuum chamber was fabricated from acrylic slabs and tubing. Figure 3.11 illustrates the key components of the chamber. The bottom slab of the 12.70 mm thick acrylic was glued on to

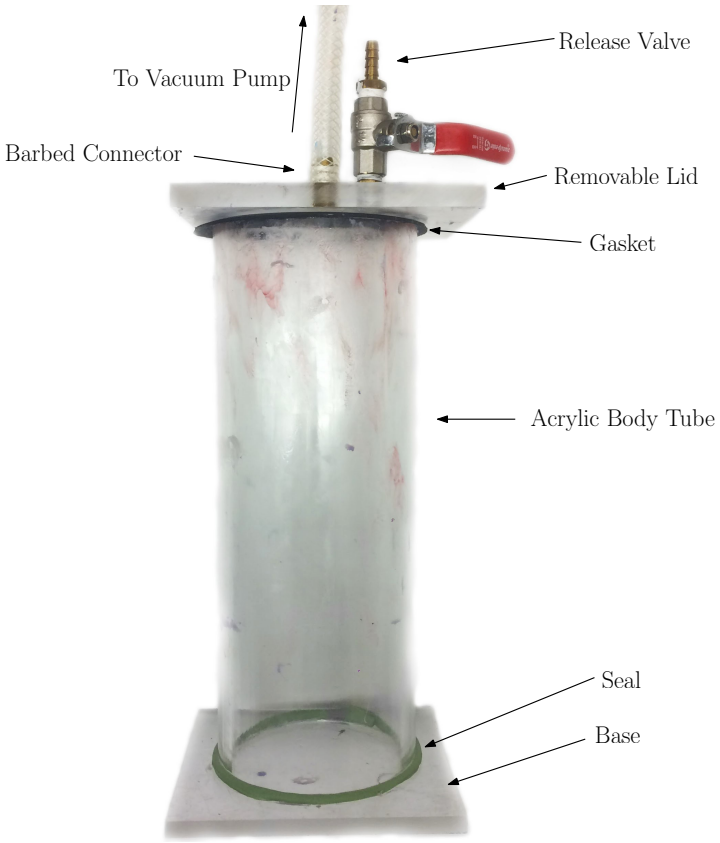

Figure 3.11: A cost-effective vacuum chamber that was fabricated in-house.

the 6.25 mm thick acrylic tube using Weld-On 16 acrylic glue. Plumbers putty was used to line the bottom seam to ensure that this junction was air tight. The top piece of acrylic, which was also 12.70 mm thick, served as a lid to open and close the vacuum chamber. A gasket made from foam was put in between the top acrylic slab and the acrylic tube, and it was coated with Red "N" Tacky #2 multi-purpose EP grease to make sure that the seal was air tight. The acrylic lid was tapped and threaded to fit a barbed connector that would attach to a hose connected to the vacuum pump. The acrylic lid was tapped and threaded, again, to fit a release valve to control the airflow into the vacuum chamber during the degassing process.

During the degassing process, the mixture was observed for the escape of air bubbles, and the process ended when no more air bubbles were observed leaving the mixture. The Moldstar silicone had a pot life of only six minutes, therefore, its degassing time was much less than all of the other silicones. However, its low viscosity allowed for adequate removal of entrapped air during the quick degassing period. The Oomoo silicone required the longest period to degass due to its high viscosity. Since it was not translucent, unlike the other silicone prepolymers, extra time was taken for degassing, after bubbling ceased, to assure that all of the air was removed.

Once the prepolymer was degassed, it was poured into a syringe and injected through the injection hole of the mold shown in figure 3.10. Figure 3.12 illustrates the final step of the fabrication process before the composite was allowed to cure. Plumbers putty was used to seal the injection and exhaust ports so that no silicone would leak during the curing process. All molds were cured in an upright position, overnight, at room temperature and atmospheric pressure.

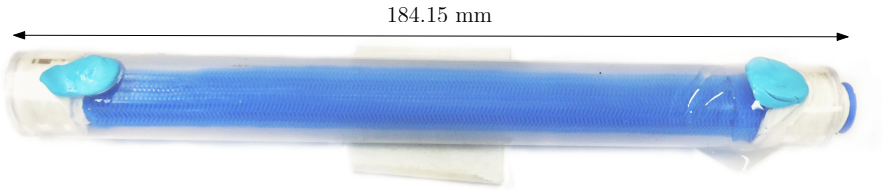

Figure 3.12: An impregnated mold shown with a tight braid and Ecoflex silicone rubber.

3.2.3 Demolding the SC and applying end fixtures

The SC was demolded after curing overnight. First, the end cap with the flange (the blue end cap in figure 3.6) was removed, and then the whole SC, including the inner brass rod, was pushed out

of the acrylic tube using a rod of slightly smaller diameter than the inner diameter of the acrylic tube. The SC was then pulled off of the brass rod to yield the final SC shown in figure 3.3.

End fixtures, shown in figure 3.13, were manufactured using off-the-shelf plumbing hardware. A brass barbed connector, with a nominal diameter of 7.93 mm, was connected to a brass pipe

Figure 3.13: End fixtures manufactured using off-the-shelf plumbing products.

machined with a hole to allow connection to the load cell of the Instron universal testing machine. The barbed connectors were inserted into the ends of the SC and secured using multiple cable ties. The size and quantity of cable ties were determined based on the stiffness of the rubber and the type of braid used. Figure 3.14 illustrates a full prototype of a SC that is ready for testing.

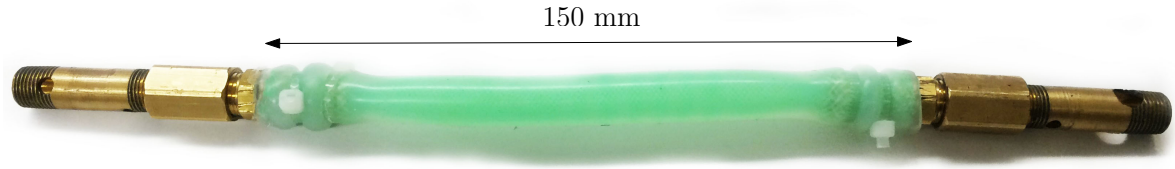

Figure 3.14: Full prototype of a SC that is ready for testing.

3.3 Experimental results

Experimental tests were performed on 18 unique SC specimens that were previously defined in table 3.3, as well as the matrix and fibre materials. Each test tracked the linear elongation and the resulting tensile force while the material was linearly strained along its longitudinal axis. The linear elongation is represented as a ratio with respect to its original length and will henceforth be referred to as the stretch ratio λ.

3.3.1 Experimental setup

Tensile tests were performed on the proposed SC, as well as on the variety of different braid and matrix materials used to construct it, using an Instron universal testing machine, model 4482. An Instron load cell rated at 1 kN, 2525 series, with a linearity and repeatability of 0.25 %, was used to accurately measure the tensile load while the SC specimens were stretched at a constant crosshead speed of $1\,\mathrm{mm\,s^{-1}}$. Cyclical loading tests were also performed, using the same experimental setup,

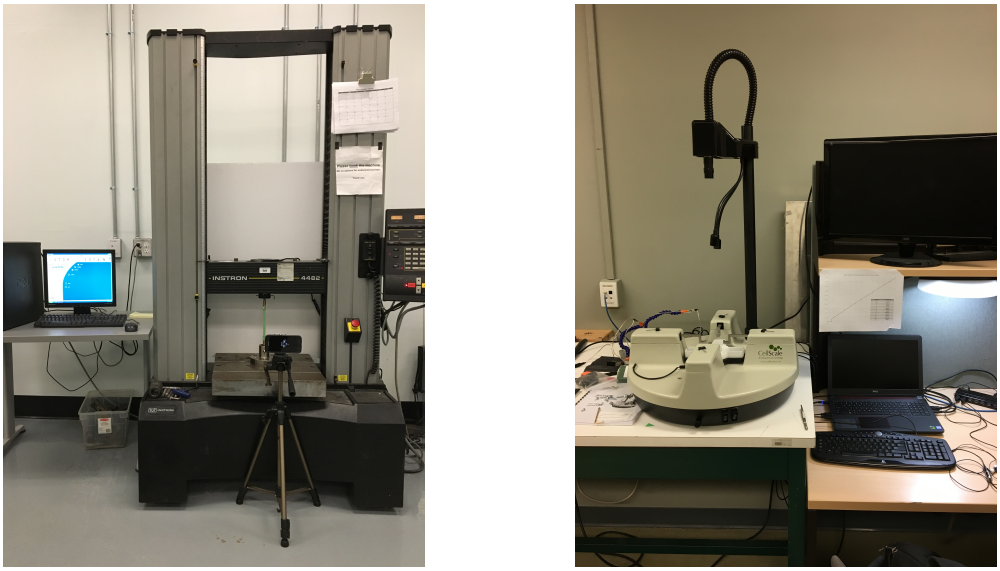

(a) Tensile testing setup **(b)** Biaxial testing setup

Figure 3.15: Tensile testing setup on Instron universal testing machine, model 4482, and biaxial testing setup on CellScale biaxial testing machine.

in order to observe the variant hysteresis effects of the proposed SC. For this setup, experimental data were acquired at a frequency of 10 Hz using Instron Bluehill software and then exported into a .csv file to be analysed. This configuration is shown in figure 3.15a.

To further comprehend the mechanical behaviour of the matrix materials biaxial, tension tests were performed using the CellScale BioTester biaxial testing machine as shown in figure 3.15b. The BioTester uses semiconductor strain gauge based 23 N load cells with an accuracy of 0.2 % of the rated full scale load. For these tests flat, rectangular silicone samples were molded and stretched at a uniform deformation rate of $0.025\,\mathrm{mm\,s^{-1}}$, simultaneously, in the x and y directions. Experimental data were acquired at a frequency of 1 Hz using BioTester software and exported into a .csv file to be analysed.

In the analysis of elastic materials, it is customary to precondition each material prior to testing. Elastomers exhibit viscoelastic effects under many loading conditions, so preconditioning the SC until the behaviour becomes repeatable is important. Section 3.3.4 shows the effects of energy loss and creep during preconditioning. Therefore, all test subjects were subjected to cyclical loading of ten cycles prior to testing unless otherwise explicitly stated.

Resulting data of the SC specimen and material tests were analysed and are presented in the remainder of this section.

3.3.2 Testing individual components of the SC

The SC is a two phase material that combines the properties of both constituent phases such that a desirable combination of mechanical properties is obtained. The two phases of the SC are defined as the dispersed phase and the matrix phase. In this case, the dispersed phase is a braided mesh sleeve and the matrix phase is a soft silicone rubber. In this section, both phases have been analysed, separately, with the purpose of observing the individual actions that combine to produce the behaviour of the final SC.

3.3.2.1 Tensile response of the silicone rubbers

Silicone rubbers that were used as matrix materials for the SC were introduced in section 3.1.1 as Ecoflex, Moldstar, and Oomoo silicone rubbers. Each rubber specimen was fabricated using the exact same tubular geometry as was used for the final SC, and each was loaded by the Instron machine, to failure, at an elongation rate of $1\,\mathrm{mm\,s^{-1}}$. The resulting data have been smoothed, for demonstration purposes, and are illustrated in figure 3.16. It is important to observe the shape of each curve from the tensile test results rather than the maximum strength of each silicone, even though all of the three silicone rubbers have failed below a significant load of 30 N.

The deformation of the three silicone rubbers, as illustrated by the J-shaped response curves, deformed according to typical elastomeric force-elongation behaviour. In accordance with expectations, the Ecoflex rubber achieved a total deformation of 450 % while the Moldstar and Oomoo rubbers deformed at only 275 % and 160 % of their respective original lengths. The toe region of the Ecoflex silicone was significantly larger than the other rubbers who, in fact, exhibited very limited toe regions. The Oomoo rubber demonstrated the largest stiffness within the linear region, while

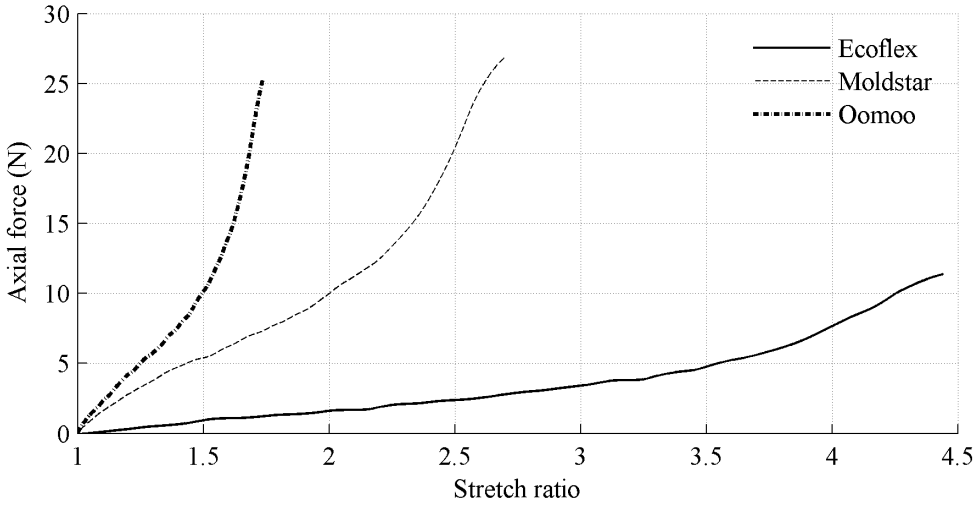

Figure 3.16: Tensile test results for the silicone rubber specimens, without an internal braid, for Ecoflex, Moldstar, and Oomoo silicone rubber types.

the Moldstar and Ecoflex rubbers displayed decreasing stiffness. It can be seen that the Moldstar rubber unexpectedly achieved a higher maximum tensile force at failure than the Oomoo rubber did. This observation is explained by the high stiffness and Shore Hardness rating of the Oomoo rubber, which made it more susceptible to tearing than either the Moldstar or Ecoflex rubbers.

Properties regarding the silicone rubbers will be further discussed in section 3.3.3, where planar silicone samples are biaxially tested.

3.3.2.2 Tensile response of the PET braids

The regular and tight braided sleeves used to form the SC were separately tested on the Instron machine without embedding them into a silicone matrix. Each braid was cut to an initial length equal to the final SC and then loaded into the Instron machine using the end fixtures illustrated in figure 3.13. An initial slack of 30 % of the original braid length was applied to each braid to help illustrate the change in axial force response when the braid is stretched past a certain elongation point. The results were smoothed for demonstration purposes and illustrated in figure 3.17.

As the Instron machine began to stretch the braid, the fibre angle decreased and the braid began to tighten, causing a minimal increase in force. Each braid was continuously elongated past 30 % of its original length and the fibre angle decreased even more. Once the braid reached its tensile jamming state, the tensile response became linear. The abrupt exponential increase in force, shown

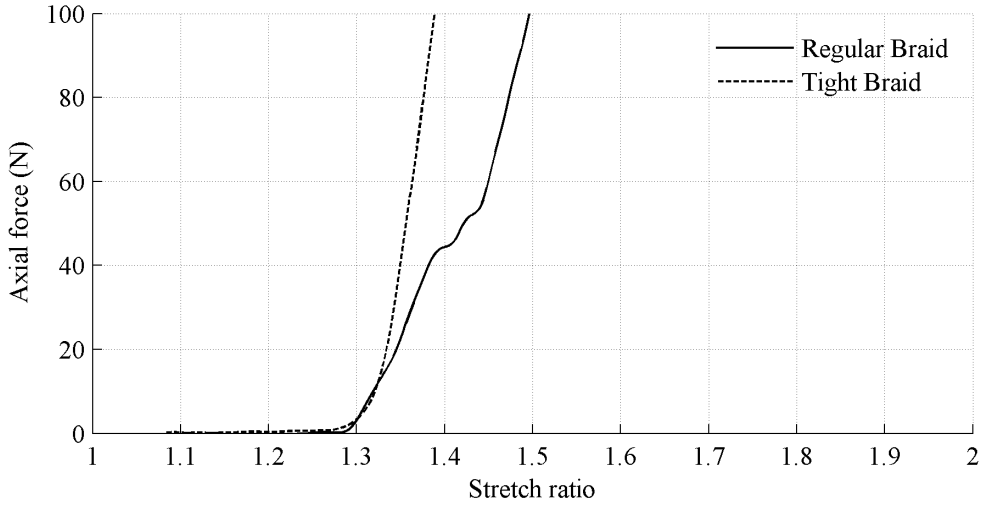

Figure 3.17: Tensile test results for the braid, without any silicone rubber, for the regular and tight braiding styles.

by each braid, occurred between 30 % and 35 % elongation. This was caused by the small initial fibre angles of the braided sleeves since there was no silicone rubber present to hold the braids at a larger initial fibre angle. The linear region of the response curve was largely based on the stiffness of the actual fibres rather than the braid geometry.

The response of the tight braid, when compared to the regular braid, demonstrated a steeper slope within the linear region. This result was expected when observing how figure 3.4b illustrates an extra fibre helically wound in each direction in the tight braid. These extra fibres not only increased the stiffness of the tight braid during its linear response, but they also caused the tight braid to reach its tensile jamming state slightly faster than the regular braid. The irregularities within the response curve of the regular braid, seen at 40 % elongation, were due to a few individual fibres slipping at the end connections. It is expected that the selection of braid style will largely influence the mechanical response of the SC.

3.3.3 Biaxial testing on planar silicone segments

Planar rectangular silicone samples were fabricated with the purpose of analysing the response of each polymer under biaxial loading conditions. Each specimen was mounted in the CellScale biaxial testing machine and stretched, with equal elongation rates, in the x and y directions. Sample specimens can be seen in their mounted configuration, in figure 3.18, where the horizontal direction

corresponds to the x axis and the vertical direction corresponds to the y axis.

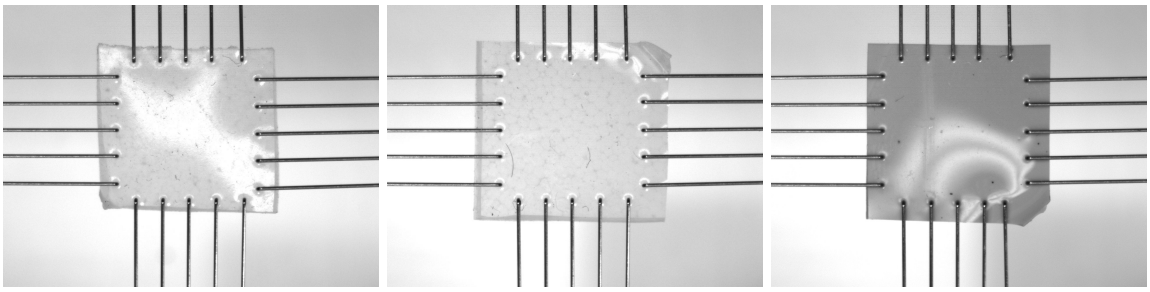

(a) Ecoflex **(b)** Moldstar **(c)** Oomoo

Figure 3.18: Ecoflex, Moldstar, and Oomoo planar square samples hooked into the Cell Scale biaxial testing machine and ready to be tested.

Each sample was cut into a 15 mm × 15 mm square that was then mounted onto tines that formed a 12 mm × 12 mm square. The tines had a diameter of 305 mm, were spaced 2.2 mm apart, and had a puncture depth of 2.4 mm. Recall, from section 3.1.1, that the thickness of the composite tubes was defined to be 2.78 mm. However, the maximum thickness of the planar silicone samples cannot exceed the puncture depth of the tines. Therefore, planar samples with a thickness less than 2.4 mm were created.

The thickness of the Ecoflex, Moldstar, and Oomoo planar sample were 1.60 mm, 2.10 mm, and 1.30 mm, respectively. Each specimen was mounted and strained at a rate of $0.025\,\mathrm{mm\,s^{-1}}$. It was decided, due to the stiffness of each rubber, to strain the Ecoflex, Moldstar, and Oomoo specimens to a respective 100 %, 50 %, and 37.5 % of their original lengths. The specimens were not preconditioned prior to testing and each sample was loaded and unloaded without a resting phase at the peak elongation point. The resulting curves were smoothed, for demonstration purposes, and are illustrated in figure 3.19.

It was concluded that each rubber exhibited isotropic behaviour since the curves in figure 3.19 in the x direction closely resembled the curves in the y direction. The Oomoo silicone failed due to the tines tearing out, whereas the other silicones failed by tearing in the middle of the specimen. The Moldstar rubber exhibited larger biaxial forces than the Oomoo due to its larger thickness and the fact that the Oomoo rubber tore at the tines because of its higher stiffness and Shore Hardness rating.

It is important to verify if the silicone rubbers deformed isotropically in order to predict the

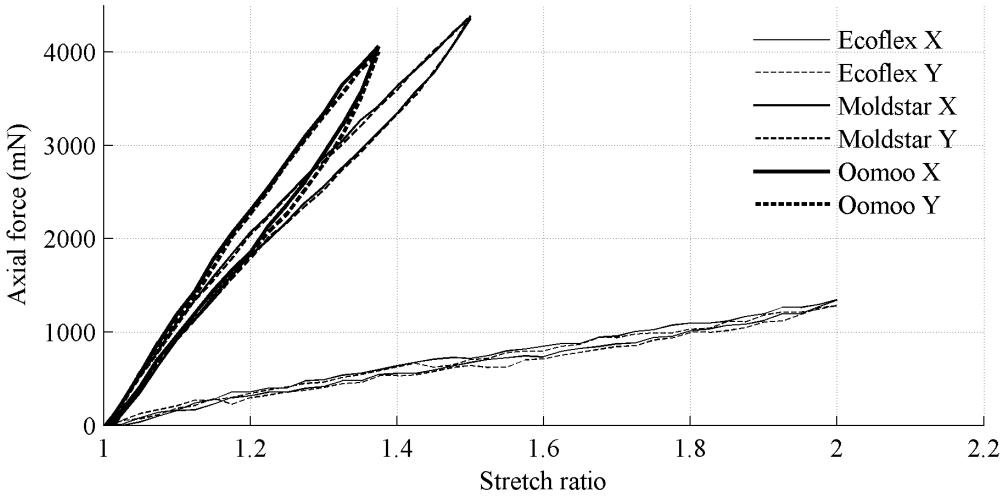

Figure 3.19: Biaxial test results from equal, simultaneous x, y directional elongation rates of $0.025\,\mathrm{mm\,s^{-1}}$. Tests were performed using Ecoflex, Moldstar, and Oomoo silicone rubbers.

behaviour of the mechanical response of the SC. In any given SC specimen, the geometry of the fibres form a diamond shape that is filled with silicone rubber during the impregnation process. As the SC is stretched, the fibres begin to align parallel to the axis of the applied force which causes the fibres to scissor shut onto the silicone rubber. The scissoring motion creates compressive forces on the silicone rubber in the horizontal direction while the silicone is simultaneously being stretched in the axial direction, along with the rest of the specimen. The silicone that fills each diamond shaped spaced between the fibres is applying resistance to both the horizontal and vertical forces during the tensile elongation of the SC. The isotropic property of the silicone rubbers is expected to dictate the overall stiffness of the SC specimens.

3.3.4 Viscoelasticity demonstrated through cyclical load-unload tensile tests

Cyclical load-unload tensile tests were performed on the SC in order to illustrate the energy loss due to viscoelastic effects. One set of tests were performed using a constant loading rate over multiple cycles, and another set of tests were performed using a different loading rate for each cycle.

3.3.4.1 Multiple load-unload cycles performed at the same loading rate

Specimen T1B4B_56 was cyclically loaded, well below its failure point, at a constant elongation rate of $3\,\mathrm{mm\,s^{-1}}$ for ten cycles. Figure 3.20 illustrates the first, middle, and last cycle of this test.

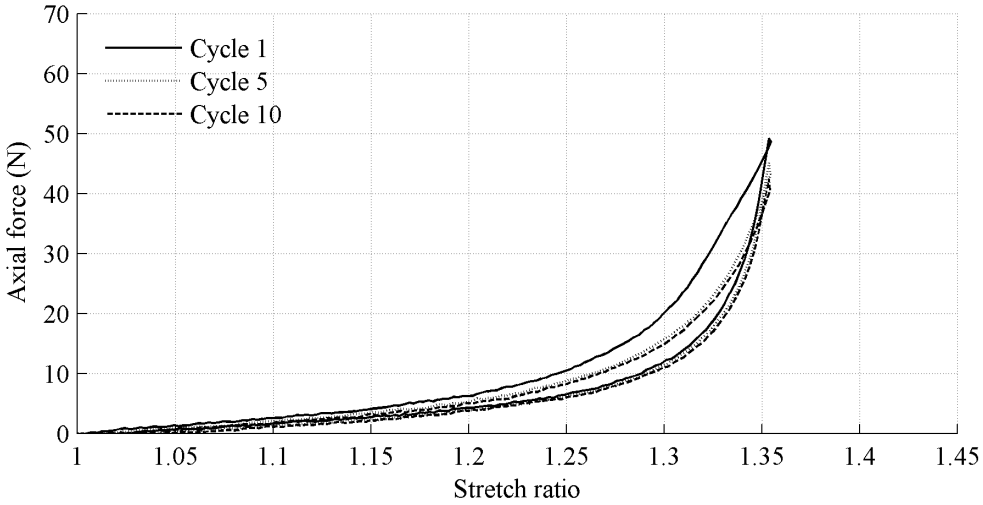

Figure 3.20: Load-unload cyclical tensile test results for the T1B4B_56 specimen for ten cycles a constant elongation rate of $3\,\mathrm{mm\,s^{-1}}$.

Each cycle exhibited hysteresis which means that there was energy lost between the load and unload curves due to frictional forces between the individual fibres, the fibres and the silicone, and the polymeric chains in the microstructure of the silicone. This specific specimen was not preconditioned prior to testing, and it was noticed that the first cycle exhibited a much larger energy loss than the following cycles. Cycles 2 through 10 exhibited loading curves and peak forces that decreased for each repeated cycle but converged after the fifth repetition. The convergence of the load curves was caused by the permanent elongation of some polymeric fibres in the microstructure of the silicone as well as any creep deformation caused by the previous cycles. These results illustrated the viscoelastic and creep effects within the material and proved the importance of preconditioning the SC specimens for atleast ten cycles prior to testing to achieve repeatable behaviour.

3.3.4.2 Multiple load-unload cycles performed at different loading rates

Specimen T1B4B_52 was cyclically loaded well below its failure point at a different elongation rate between each cycle. Cycles were performed at $2\,\mathrm{mm\,s^{-1}}$ and $4\,\mathrm{mm\,s^{-1}}$ elongation rates. Figure 3.21 illustrates each of the two cycles.

Hysteresis effects were observed in each cycle. The composite experienced a loss in energy from the loading to the unloading phase of the cycle that seemed to reduce as the elongation rate increased. Cycles were also administered at $6\,\mathrm{mm\,s^{-1}}$ and $8\,\mathrm{mm\,s^{-1}}$, however, the results were

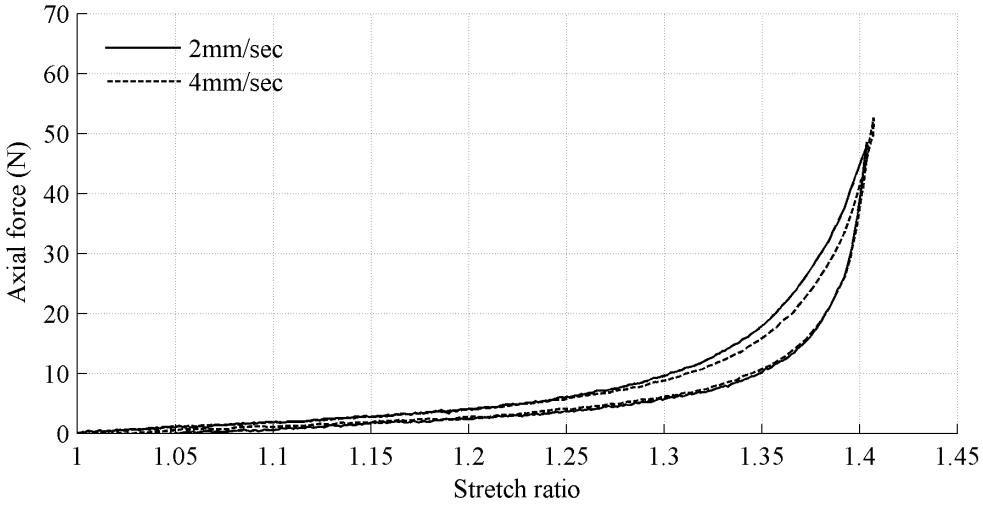

Figure 3.21: Load-unload cyclical tensile test results for the T1B4B_52 specimen for two different extension speeds of $2\,\mathrm{mm\,s^{-1}}$ and $4\,\mathrm{mm\,s^{-1}}$. One complete cycle is shown for each loading rate.

omitted from the analysis. The loading cell on the Instron machine was incapable of tracking the change of force at the peak elongation point at high speeds accurately.

3.3.5 Time dependency of the loading response

The time independant loading response of the SC may be found by performing tests at an infinitely slow rate, but a more practical method follows that of Hossain *et al.* [57] where a multi-step relaxation test is performed.

A multi-step relaxation test was performed with the purpose of analysing the time independent force response of the SC. The specimen was loaded and allowed to rest until the load response would equalize. This process was repeated to create 16 discrete data points. For each point, the resulting elongation and initial, or peak, axial force was recorded, followed by the axial force after equilibrium was reached. Figure 3.22 illustrates a multi-step test that was completed on composite specimen T1B4B_55.

The upwards facing triangles illustrate the peak forces experienced by the specimen whereas the downwards triangles represent the axial force after the composite was allowed to rest for over 30 min. It can be seen that there was upwards of 35 N variance near the end of both curves. These results will be implemented to help form an assumption about the SC in section 4.1 regarding the analytical model.

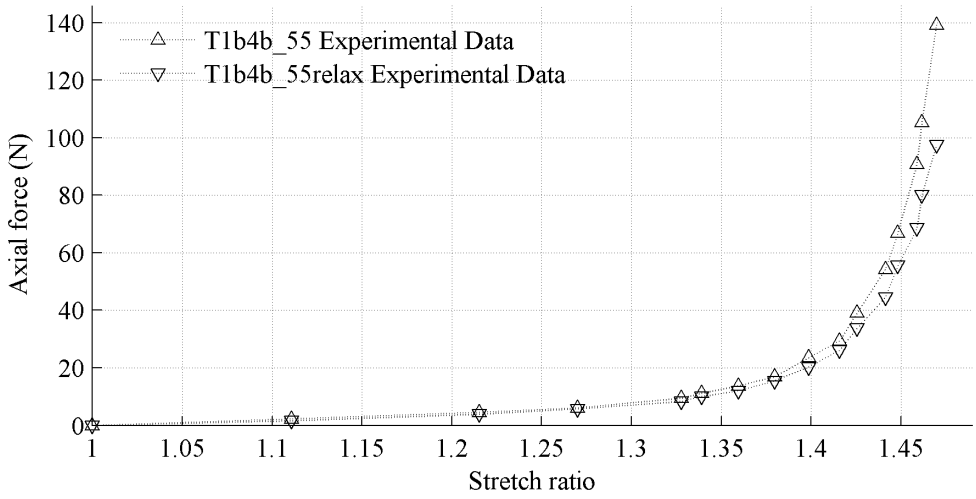

Figure 3.22: Multi-step relaxtion tensile test results for specimen T1B4B_55 to illustrate the time independent loading response of the SC over a 30 min resting period for each step.

3.3.6 Tensile test results on the full SC specimen

Tensile tests were performed using the Instron machine on the 18 SC specimens outlined in table 3.3. This subsection defines a set of results formed into groups based on which silicone matrix was used fabricate the SC specimen. The results are demonstrated for both the regular and tight braided sleeves.

3.3.6.1 Specimens made with Ecoflex silicone rubber

Six specimens were manufactured using the Ecoflex silicone as the elastomeric matrix for the SC. Three of these specimens, R1A4A_45, R1B4A_54, and R1C4A_61, were manufactured using a regular braid. The results of these tests were plotted and smoothed for demonstration purposes in figure 3.23.

The other three specimens, T1A4A_40, T1B4A_53, and T1C4A_60, were manufactured using a tight braid. The results of these tests were plotted and smoothed for demonstration purposes in figure 3.24.

Figures 3.23 and 3.24 illustrate the effects of varying the fibre angle for a SC specimen with a matrix made from Ecoflex silicone rubber. It is evident that changing the initial fibre angle dictates the length of the toe region in the curve. The slope of the toe region is small, while the slope of the linear region is large, and there is an abrupt change in the transition of the toe and the linear

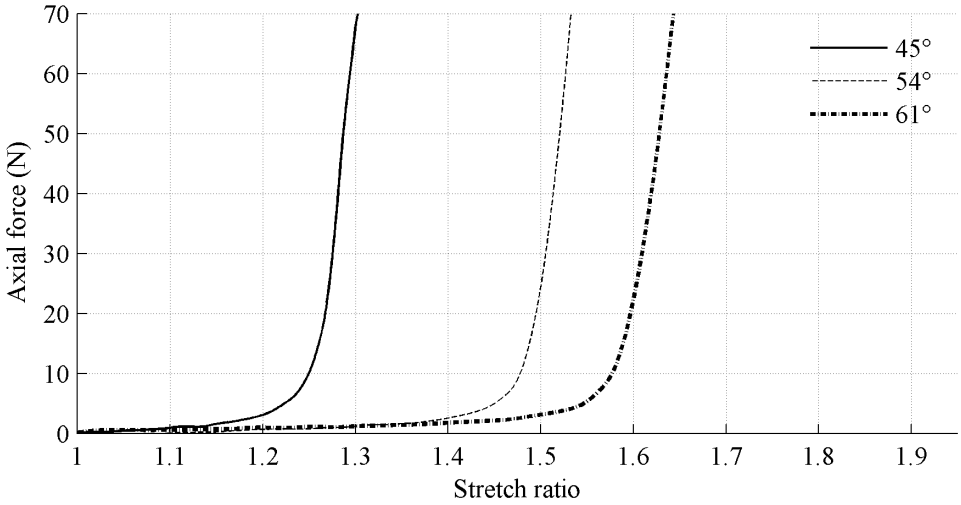

Figure 3.23: Tensile test results for specimens R1A4A_45, R1B4A_54, and R1C4A_61. The specimens are fabricated using Ecoflex rubber, regular braid style, and three different initial fibre angles of 45°, 54°, and 61°.

region of the curve. The resulting curves largely resemble the force versus stretch ratio graphs for the braided sleeves that are shown in figure 3.17 which implies that the Ecoflex silicone matrix does not greatly affect the overall mechanical response of the SC. It is seen that all specimens made with a regular braid achieved greater elongation potentials than specimens made with a tight braid for similar initial fibre angles.

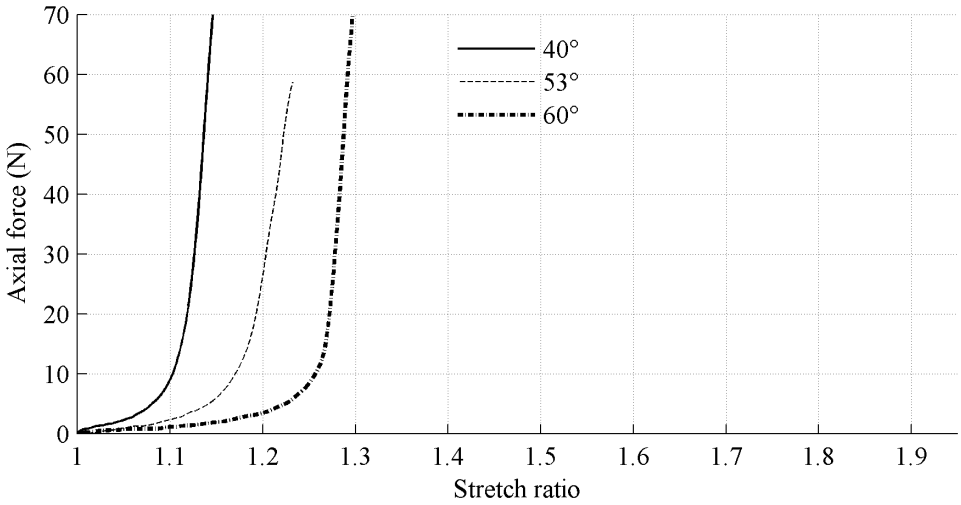

Figure 3.24: Tensile test results for specimens T1A4A_40, T1B4A_53, and T1C4A_60. The specimens are fabricated using Ecoflex rubber, tight braid style, and three different initial fibre angles of 40°, 53°, and 60°.

The specimen T1A4A_53, in figure 3.24, failed at an axial force less than 60 N. Multiple tests were run with different specimens that had the similar geometries, and the results did not vary from those shown in the image. The reason as to why this occurred will be discussed in section 3.3.8.

3.3.6.2 Specimens made with Moldstar silicone rubber

Six specimens were manufactured using the Moldstar silicone as the elastomeric matrix for the SC. Three of these specimens, R1A4B_49, R1B4B_55, and R1C4B_62, were manufactured using a regular braid. The results of these tests were plotted and smoothed for demonstration purposes in figure 3.25.

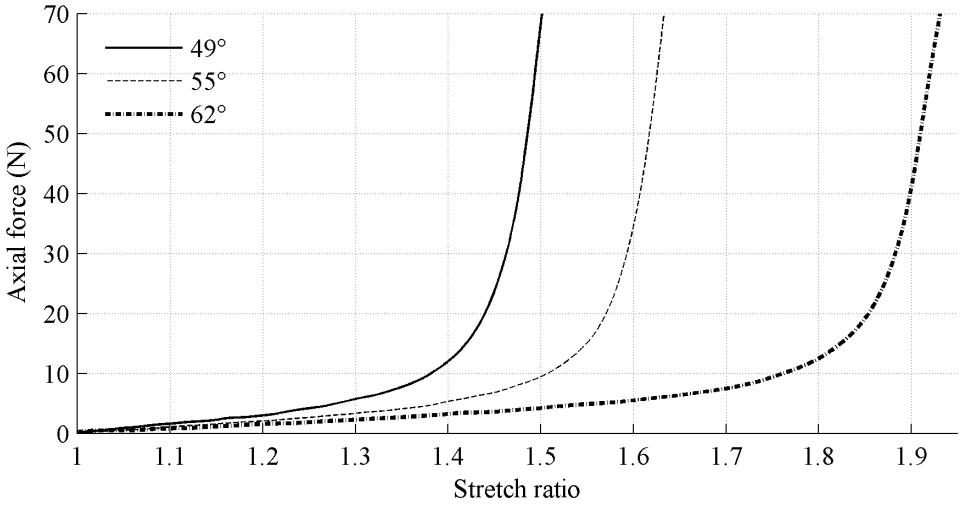

Figure 3.25: Tensile test results for specimens R1A4B_49, R1B4B_55, and R1C4B_62. The specimens are fabricated using Moldstar rubber, regular braid style, and three different initial fibre angles of 49°, 55°, and 62°.

The other three specimens, T1A4B_43, T1B4B_52, and T1C4B_63, were manufactured using a tight braid. The results of these tests were analysed, smoothed for demonstration purposes, and shown in figure 3.26.

Figures 3.25 and 3.26 illustrate the effects of varying the fibre angle for a SC specimen with a matrix made from Moldstar silicone rubber. It was noticed that the initial fibre angle dictated the length of the toe region in the curve, just as it did for the specimens made with Ecoflex silicone rubber. Unlike the specimens made from Ecoflex, the transition from the toe region to the linear

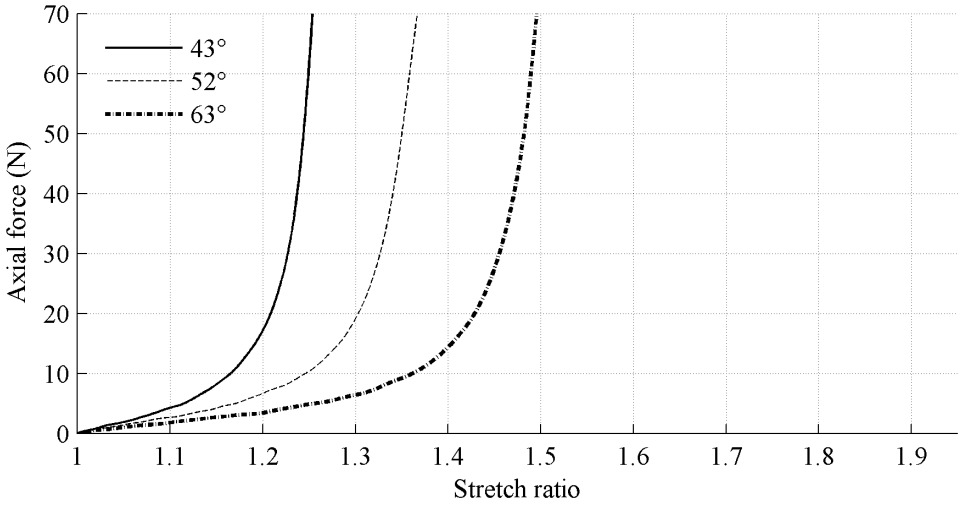

Figure 3.26: Tensile test results for specimens T1A4B_43, T1B4B_52, and T1C4B_63. The specimens are fabricated using Moldstar rubber, tight braid style, and three different initial fibre angles of 43°, 52°, and 63°.

region was more gradual. The slope of the toe region was larger while the slope of the linear region was smaller than the Ecoflex specimens. It is seen that all specimens made with a regular braid achieved greater overall elongation than those made with a tight braid. The specimens fabricated from Moldstar silicone rubber achieved larger elongation potentials than those made with Ecoflex for similar angle classes.

3.3.6.3 Specimens made with Oomoo silicone rubber

Six specimens were manufactured using the Oomoo silicone as the elastomeric matrix for the SC. Three of these specimens, R1A4C_48, R1B4C_56, and R1C4C_64, were manufactured using a regular braid. The results of these tests were plotted and smoothed for demonstration purposes in figure 3.27.

The other three specimens, T1A4C_45, T1B4C_56, and T1C4C_65, were manufactured using a tight braid. The results of these tests were plotted and smoothed for demonstration purposes in figure 3.28.

Figures 3.27 and 3.28 illustrate the effects of varying the fibre angle for a SC specimen with a matrix made from Oomoo silicone rubber. It was noticed that changing the initial fibre angle dictated the length of the toe region, just as it did for the specimens made with the Ecoflex

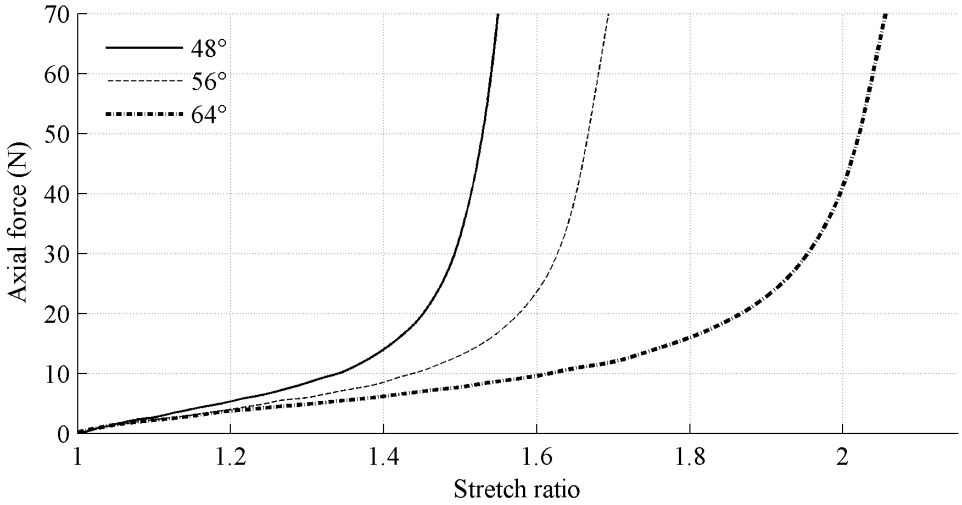

Figure 3.27: Tensile test results for specimens R1A4C_48, R1B4C_56, and R1C4C_64. The specimens are fabricated using Oomoo rubber, regular braid style, and three different initial fibre angles of 48°, 56°, and 64°.

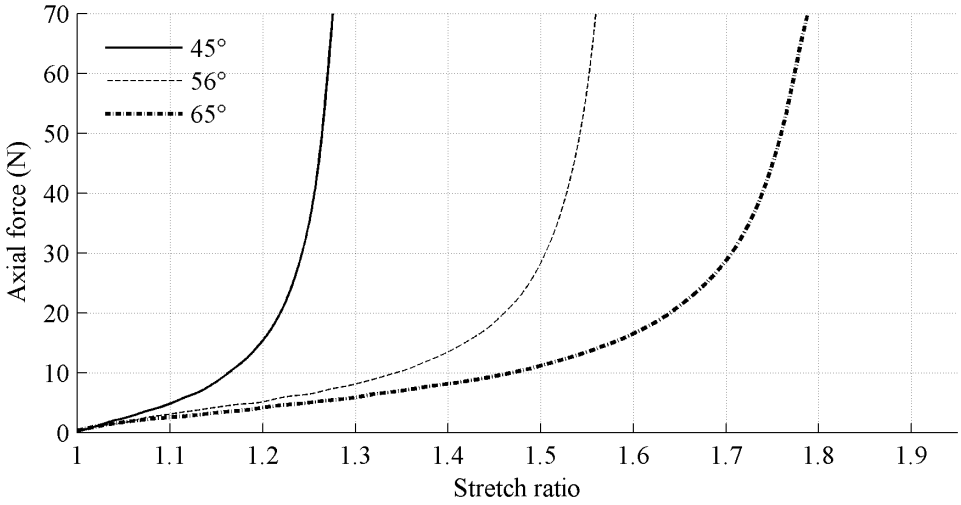

Figure 3.28: Tensile test results for specimens T1A4C_45, T1B4C_56, and T1C4C_65. The specimens are fabricated using Oomoo rubber, tight braid style, and two different initial fibre angles of 45°, 56°, and 65°.

and Moldstar silicone rubbers. The transition between the toe region and the linear region was more gradual than for the specimens made with a Moldstar silicone matrix. The slope of the toe region was larger, while the slope of the linear region was lower, than both of the other types of specimens. It is clearly shown that all specimens made with a regular braid achieved greater elongation potentials than those made with a tight braid. The specimens fabricated from Oomoo

silicone rubber achieved larger elongation potentials than any other specimen for a similar initial fibre angle range.

3.3.7 SC stiffness

The stiffness k of a SC at a given change in elongation can be calculated by

$$k = \frac{F_{n+1} - F_n}{q_{n+1} - q_n}, \tag{3.1}$$

where F represents the axial force at a point n with corresponding elongation q. The stiffness of specimens R1C4A_61, R1C4B_62, and R1C4C_64 are plotted versus their elongation, and smoothed for demonstration purposes, in figure 3.29.

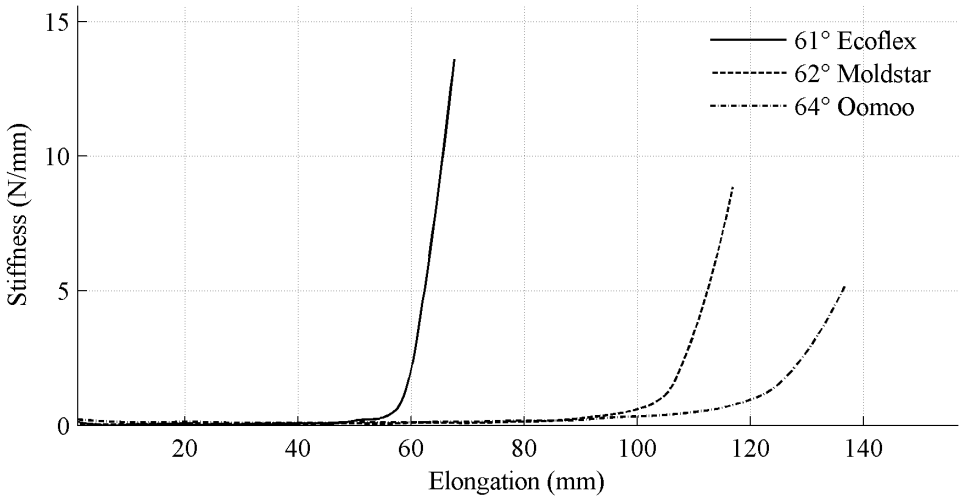

Figure 3.29: Stiffness versus elongation test results for specimens R1C4A_61, R1C4B_62, and R1C4C_64.

The stiffness of specimens T1C4A_60, T1C4B_63, and T1C4C_65 are plotted versus their elongation, and smoothed for demonstration purposes, in figure 3.30.

These figures were created with the intention of illustrating the effect of the silicone matrix selection on the overall stiffness of the composite. A trend that is seen in both figures 3.29 and 3.30 is that the stiffness of the overall SC decreases as the stiffness of the selected silicone matrix increases. It is also noticed that specimens made with the tight braid style were stiffer than those fabricated with a regular braid style.

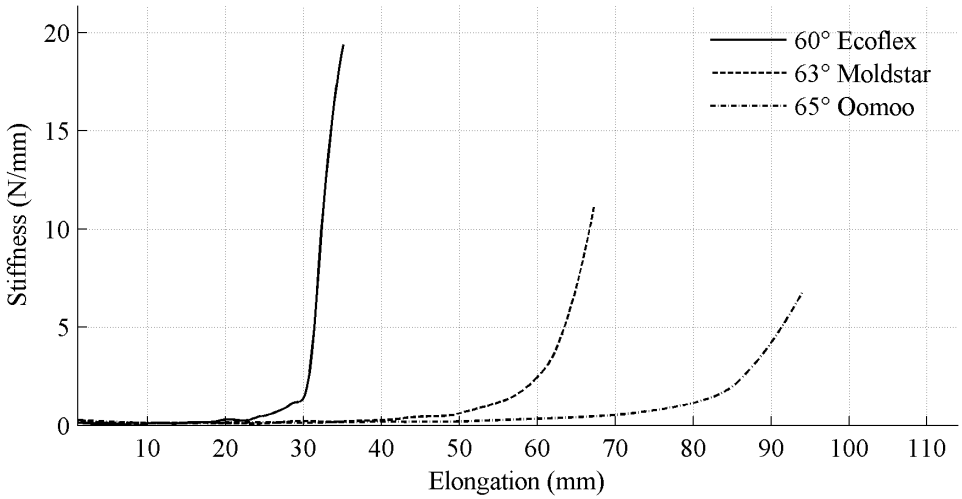

Figure 3.30: Stiffness versus elongation test results for specimens T1C4A_60, T1C4B_63, and T1C4C_65.

The SC specimens fabricated using softer silicone rubbers exhibit a larger response from the fibres. Specimens made with stiffer rubbers inhibit the fibres from becoming fully aligned with the axis of elongation and therefore exhibit a less stiff response curve. More details regarding this trend are explained in section 3.3.8.

3.3.8 Discussion of experimental results

Tensile tests have been performed on 18 unique SC specimens that were controlled by three key parameters, namely: the initial fibre angle, the stiffness of the silicone matrix, and the choice between a regular braided sleeve or a tight braided sleeve. Section 3.3.6 shows the graphical results of these tests.

Each SC specimen exhibited a toe region followed by an exponential change into a linear region. The results of every SC specimen replicated the tensile behaviour of the PAM and natural fibrous tissue shown in figure 1.1b. The elongation potential over all specimens ranged from 15 % to 110 % of their original length. For the six specimens that were fabricated with an initial fibre angle larger than the Magic Angle, the range of elongation potentials was from 30 % to 110 % of their original length. Specimens made from a regular braid style exhibited a greater overall elongation potential than those fabricated from a tight braid style. Specimens made from the Oomoo silicone rubber exhibited a greater elongation potential than those made from softer rubbers.

The variation of the initial fibre angle for the SC specimen had the greatest influence on its resulting mechanical behaviour. The initial fibre angle determined how long the composite would stretch before it started exerting any significant resistance forces. The reasoning behind this was briefly outlined in section 3.3.2.2. Essentially, when the composite was elongated, the fibres tended to scissor shut and become aligned with the applied axial force. During this alignment process, the fibres reached a tensile jamming state and the fibre angle could no longer decrease, resulting in the rapid increase in resistive force.

The mechanical response of the toe region was governed mostly by the silicone matrix properties, however the initial fibre geometry did influence the length of the toe region. The stiffer silicone rubbers portrayed a toe region with a larger slope while the softer silicone rubber portrayed a material response that was comparable to that of the braided sleeve, without a silicone matrix, seen in figure 3.17. These results are supported by figure 3.16 where the tensile test results of the pure silicone samples were shown. It was seen that the Ecoflex silicone could not apply a resistance past 10 N under 400 % elongation, whereas the Oomoo rubber was exerting a force of 25 N at 175 % elongation. The toe region of the tensile loading response of each SC resembles the shape of the curves of their respective silicone tensile response shown in figure 3.16.

The most interesting aspect of the mechanical response of the SC was the transition between the toe region and the linear region. The transition between the toe region, which was governed mostly by the silicone matrix, and the linear region, which was governed largely by the fibre properties, was different for each silicone matrix type. The stiffer silicone rubbers exhibited a more gradual change while the change in the specimens with softer rubbers was abrupt. As the fibre angle decreased, the fibres applied a compressive force on the silicone rubber. Section 3.3.3 introduced this topic, and it was seen that the isotropy of each silicone did not allow for the mechanical response of the SC to negate the presence of the silicone past the toe region.

The silicone resisted the compressive forces of the fibres while simultaneously resisting tensile forces as the SC was stretched. The stiffer silicones demonstrated more resistance to the compressive forces of the fibres. Since the compressive forces of the fibres were proportional to the tensile force applied to the entire SC, it demanded a greater tensile force for the fibres to close over the stiffer silicones. Therefore, the specimens made with a softer silicone matrix exhibited an overall stiffer mechanical response over the same elongation, which is supported by the stiffness plots shown in

figures 3.29 and 3.30. The resultant force versus stretch ratio curve of the SC had an elongated transition period between its toe and linear regions for stiffer silicone rubbers.

Properties of the PET fibres had a large impact on governing the response of the linear region for the SC. The tensile resistance of the SC greatly increased when its fibres reached the tensile jamming state. This behaviour is very similar to that of the braided sleeves, without the silicone matrix, shown in figure 3.17. The response of the linear region was not governed entirely by the fibres. The parallel action of both the fibres and the silicone matrix during the linear response dictated the slope of the linear region. The stiffer silicone rubbers, such as the Ooomoo silicone rubber, exhibited a linear region with a smaller slope than those presented by the specimens made with either of the softer silicone rubbers.

The effect of using different braided sleeves was controlled through the use of a regular or tight braiding style. The most noticeable difference between specimens using a regular or tight braid was the point at which the graph would hit the tensile jamming state. These results agreed with the results shown in figure 3.17, where the tight braid also began to linearly increase faster than the regular braid did. The extra fibre used in the tight braid gave less room for silicone to fill the space between the fibres and more of the resulting mechanical response was attributed to the braid rather than the silicone. The ultimate tensile strength of the SC specimens formed with the tight braid was also higher than those formed with the regular braid, since the tight braid has one extra monofilament helically wound in each direction.

Apart from the issue of fraying, as discussed in section 3.2.1, a problem that occurred during the manufacturing process was that the initial fibre angle could not be made constant throughout the entire SC. It was very difficult to assure that the angle was consistent throughout the individual SC, or between separate SCs. For example, when the tight braid was compressed to an angle greater than 60° it would begin to wave throughout the composite. This would create a larger elongation than expected due to the extra braid within the same amount of length.

Since the fibres were compressed in the mold, and then injected and cured with a silicone rubber, the final composite yielded some residual stresses. These residual stresses were evident when measuring the external and internal radii before testing. It was noticed that all of the SC specimens had smaller internal and external radii than the geometry of the mold that they were cast in. The compressed braided sleeve, when released from the bind of the mold, expanded enough

to slightly change the resulting specimen geometry. In the stiffer rubbers, such as the Moldstar and Oomoo, these changes were less apparent. The geometrical changes were more noticeable in the Ecoflex silicone rubber.

The end fixtures that were used in the experiments, seen in figure 3.13, were chosen with an external radius of 7.94 mm and not changed between each specimen test in order to assure consistency. Since the Ecoflex specimens were influenced by the change in geometry created by the residual stress from the braided sleeve, they needed to be forced onto the end fixtures. This created a change in the braiding diameter that was very evident in all Ecoflex specimens, but especially those with larger initial fibre angles. The process of stretching the SC over the end fixture meant that the portion wrapped around each end piece, as well as the portion just before each end piece, could not elongate the same way as the rest of the SC could. This shortened the expandable length of each composite made from Ecoflex rubber, and this is clear when looking at figures 3.23 and 3.24 by their minimal elongation potentials.

The decrease in radius for the Ecoflex specimens was most evident in those made with the tight braid. The extra fibre that is wound on each family of fibres amplified the decrease within the radius when compared to specimens made with the regular braid. This created issues while using the end fixtures because the specimen would not fit on them as well as the others made with stiffer silicones. Figure 3.24 showed specimen T1A4A_53 failing at an axial force less of than 60 N. It was mentioned in section 3.3.6 that multiple specimens with the same geometry have been tested, and they all failed around the same point. The combined softness of the silicone and the inability to properly fit the specimen over the end piece caused the end piece to rip through the silicone and pull out at a fairly low tensile force, with respect to those achieved by other composites. The specimens made with Ecoflex silicone rubber, and a smaller initial fibre angle, did not exhibit this behaviour because the braid did not create high enough residual stresses that would highly influence the geometry of the specimen.

3.3.9 Testing several composite specimens until failure

The tests outlined in this section were performed to gauge the initial reaction of the composite specimens in order to help quantitatively understand the initial mechanical response of the material. Some specimens were tested until failure in order to gain some qualitative insight about the SC.

Figure 3.31 shows the failure curves for these specimens; the resulting data were smoothed for demonstration purposes.

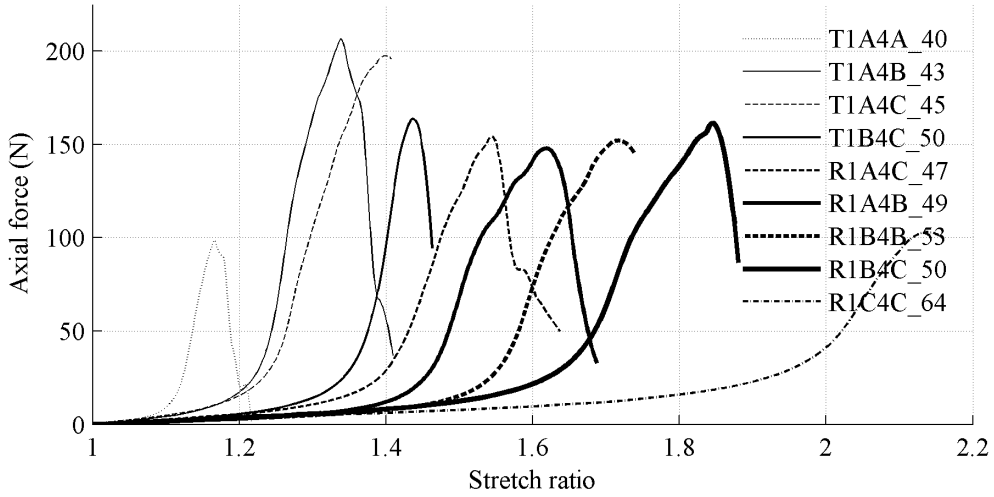

Figure 3.31: Tensile test results, until failure, for specimens R1A4B_49, R1A4C_47, R1B4B_53, R1BC_50, R1C4C_64, T1A4A_40, T1A4C_45, T1A4B_43, and T1B4B_50.

It can be seen that the the largest tensile load that a composite reached was just slightly over 200 N. Most other specimens had a maximum tensile load of around 150 N and some specimens exhibited a maximum tensile load of 100 N or less. Failure of a specimen is considered where the failure region of a curve began, which was just after the linear region. It usually resulted in a slight change in slope of the linear region that resulted from a slight tear in the silicone, a slip in the cable tie, a slip of the end piece, or fibres slipping from the end piece or silicone. An abrupt down slope in a curve implied an end piece slipping out or a cable tie slipping while a slow, jagged, descent implied a tear in the silicone or a fibre slipping.

Most failures were attributed to factors related to the end fixtures. Section 3.3.8 discussed the issue with the braids elongating in the silicone and changing the geometry of the final composite, which had a large impact on how the composites failed. Figure 3.32 shows the main observed methods of failure for all the specimens.

Silicone tearing, shown in figure 3.32a, resulted mainly in the softer silicone rubbers when a secure fixation to the end piece was achieved. The silicone rubber would tear, which loosened the cable tie, and then the whole end piece would slip out. Cable ties slipping, shown in figure 3.32b, would usually occur when a proper fixation was not achieved between the cable tie and

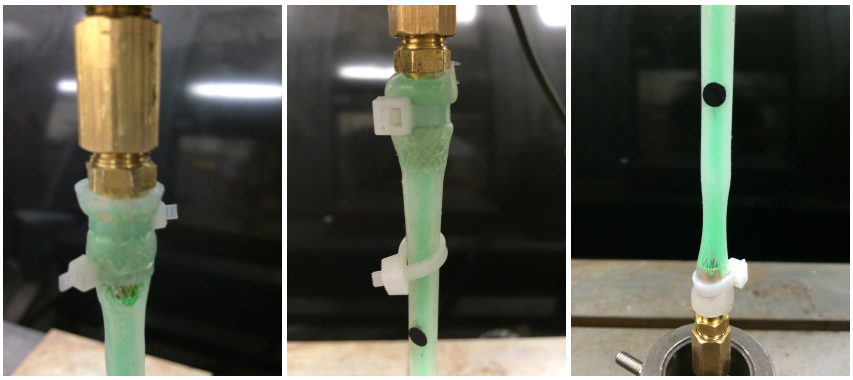

(a) Silicone tearing **(b)** Cable tie slip **(c)** Fibre pull-out

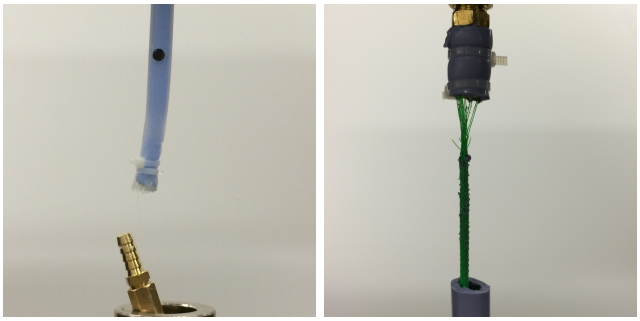

(d) End fixture pull-out **(e)** Catastrophic tear

Figure 3.32: Various failure methods for composite specimen tensile testing.

the silicone. Fibre pull-out, shown in figure 3.32c, mainly occurred in specimens made from soft silicones. In this case, the end fixations were held in place while the fibres were pulled through the silicone rubber. End fixture pull-outs, as seen in figure 3.32d, were the most common method of failure. This would occur if the specimen was not fitted correctly over the end fixture or, most of the time, the barbed connector would rip through the surrounding silicone and pull out. The final method of failure, shown in figure 3.32e, would only occur in the specimens made from the Oomoo silicone rubber. Due to its higher stiffness and Shore hardness, the Oomoo rubber was more susceptible to tearing than the other rubbers. It usually always snugly fit over the end pieces, but any inconsistency within the silicone would catastrophically fail. Most of the Oomoo specimens failed in this manner.

Chapter 4

Soft Composite Analytical Model

This chapter presents an analytical model that describes the tensile response of the SC. The SC was represented as a single continuum, and modeled using finite elasticity theory through a constitutive equation that relates the Cauchy stress to the Green's strain. Two distinct models were used and compared. The first was based on a structural strain energy function proposed by Holzapfel *et al.* [36], and the second was a phenominological strain energy function proposed by Fung *et al.* [33]. Boundary conditions were implemented to express the tensile force and internal wall pressure in terms of the axial stretch ratio and the external radius of the SC. Experimental data were collected using a modified version of the extension-inflation test. The analytical model was then fitted to the experimental data by optimizing specific material constants in the strain energy function. Finally, both analytical models were compared to experimental results.

4.1 General assumptions regarding the SC

Initial assumptions based on characteristics of the SC are outlined, in detail, in this section.

4.1.1 Thick walled tube

The SC specimens have a tubular geometry. Thick walled tubes are assumed to have an inner-radius-to-thickness ratio less than ten [58], or

$$\frac{r_i}{t} < 10, \tag{4.1}$$

where r_i represents the inner radius and t represents the thickness of the tube. The specimens fabricated in this study were molded with an inner radius of 3.57 mm and a wall thickness of 2.78 mm, which yields a ratio of 1.29. According to these results, the SC can be assumed as a thick walled tube.

4.1.2 Isochoric deformation

Assumptions of isochoric deformation are common throughout the studies of rubbers and fibrous soft tissue. For this research, the SC formed using incompressible PET fibres and an incompressible silicone matrix is assumed to maintain a constant volume during deformation.

4.1.3 Transversely isotropic behaviour

It is generally assumed that the PET fibres deform isotropically. Each silicone matrix used to fabricate the specimens was tested on the Cell Scale biaxial testing machine, and figure 3.19 illustrates the response. Each silicone demonstrated near identical curves for the horizontal and vertical deformation, thus confirming that each silicone behaves isotropically.

The anisotropy of a SC fabricated from isotropic fibres and an isotropic matrix is governed by the principal direction of the fibres. Fully anisotropic behaviour exists when the fibres are dispersed randomly, and transverse isotropy exists when the fibres prefer one principal direction, usually along the axis of the cylindrical composite. Figure 4.1 illustrates a magnification of the braiding style in one of the SC molds.

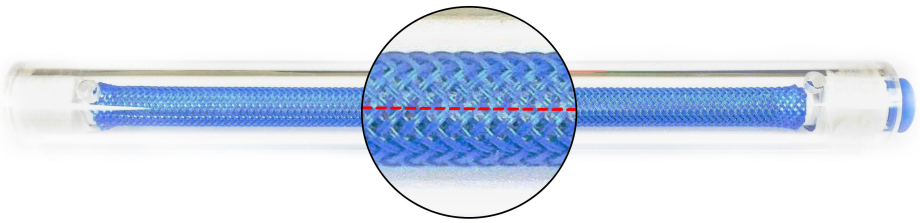

Figure 4.1: SC mold with a magnified segment to illustrate axisymmetrical, helical braiding style.

It can be seen that two distinct families of fibres were wound helically, and symmetrically, around the axis of the tube. This symmetry created an isotropy within the composite specimens, since each preferred direction created by one family of fibres was counteracted by another family of fibres

running in an equal but opposite direction. The fibre angle is assumed to be constant throughout the specimen, however, as the SC is elongated the fibres tend towards the axial direction. Hence the SC displays transversely isotropic behaviour.

4.1.4 Viscoelasticity

Viscous effects are caused by static or kinetic friction between the particles within the material. For elastic materials, viscous effects are apparent in a stress-strain, or force-elongation, graph by the energy loss between the loading and unloading cycle. This energy loss is known as a hysteresis, and it was seen during loading and unloading tests performed on a composite specimen in figure 3.20.

Viscous effects are inevitable in real life scenarios; however, they greatly complicate the analytical formulae involved in predicting the tensile response of the SC. Given the scope of this research, this model will focus on characterizing the most basic and critical aspect of the specimen's loading cycle, which is its initial tensile response. It was therefore decided that the SC was treated as if it behaved purely as a hyperelastic material, and that viscous effects would be neglected for this analysis.

4.1.5 Time dependency of the loading response

A multi-step elongation test, as seen in figure 3.22, illustrates the time independent force results of the SC. The peak axial force values at each data point, which were measured immediately after the SC was stretched, were compared to the axial force after a 30 min period where equilibrium has been reached. The energy lost in the composite material during this period was due to the uncoiling of material fibres, shifting between the fibres and the matrix, and other internal frictional forces. Since it was decided that viscous effects would be neglected in this analysis, only the peak forces at each point are going to be considered.

4.2 Analytical model

In this section, an analytical model is proposed that predicts both the axial force F and the internal pressure P of the SC specimen through a continuum mechanical model and associated boundary

conditions. Figure 4.2 illustrates a flow chart of the modelling approach.

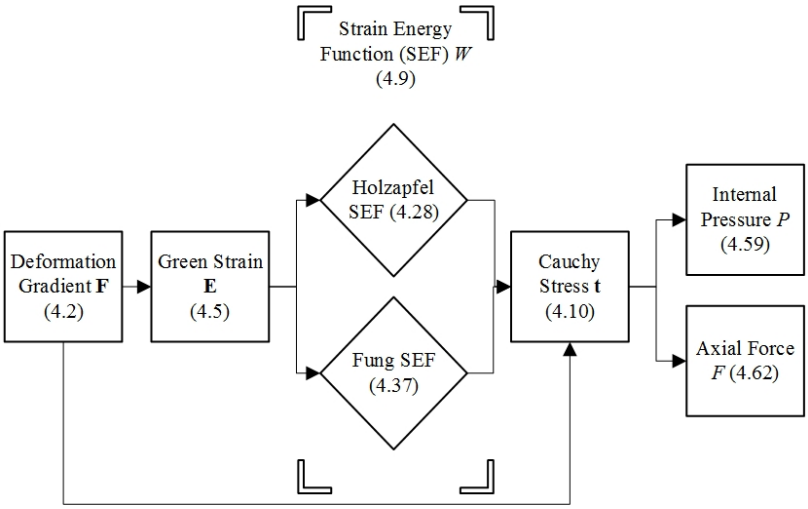

Figure 4.2: Flowchart outlining the methodology of the modelling approach to determine the predict the axial force F and the internal pressure P of the SC specimen for tensile loading conditions.

This section begins by describing the necessary kinematics needed to model the motion of the SC during deformation. A general form of the strain energy function is then declared and used to formulate a constitutive model that relates the Cauchy stress to the Green strain. Next, the strain energy function is given a more specific form as either Holzapfel's or Fung's type. Finally, boundary conditions are applied to the Cauchy stress tensor to derive the theoretical force and internal pressure.

4.2.1 General kinematics

Let Ω_0 represent the referential configuration of an arbitrary continuum, which is assumed to be completely stress free. Let $\boldsymbol{\chi} : \Omega_0 \to \mathbb{R}^3$ represent the linear transformation of a starting position $\mathbf{X} \in \Omega_0$ to a position $\mathbf{x} = \boldsymbol{\chi}(\mathbf{X}) \in \Omega$ in the deformed, spatial configuration Ω. The second order tensor $\mathbf{F}(\mathbf{X})$ is defined as the deformation gradient as

$$\mathbf{F}(\mathbf{X}) = \frac{\partial \boldsymbol{\chi}(\mathbf{X})}{\partial \mathbf{X}}, \tag{4.2}$$

where $\mathbf{F}(\mathbf{X})$ is a second order tensor. Let the Jacobian $J(\mathbf{X})$ represent the local volume ratio, where

$$J(\mathbf{X}) = \det \mathbf{F}(\mathbf{X}). \tag{4.3}$$

It is known that $J = 1$ for incompressible materials.

The right Cauchy-Green tensor $\mathbf{C}$ is a second order tensor that describes the deformation of the continuum from the referential configuration only, and is defined as

$$\mathbf{C} = \mathbf{F}^{\mathbf{T}} \cdot \mathbf{F}, \tag{4.4}$$

where "$\cdot$" is the scalar product. The tensor $\mathbf{C}$ can be further manipulated to yield the Green-Lagrange strain tensor $\mathbf{E}$, through

$$\mathbf{E} = \frac{1}{2}(\mathbf{C} - \mathbf{I}), \tag{4.5}$$

where $\mathbf{I}$ is the identity tensor.

4.2.2 Constitutive formulation

The Clausius-Duhem inequality is an expression of the second law of thermodynamics that predicts the existence of a Helmholtz free-energy function $\Psi(\mathbf{E})$. Assuming an isothermal process and no viscous effects, as stated in section 4.1.4, the material behaviour can be completely described by

$$\frac{\partial \Psi(\mathbf{E})}{\partial \mathbf{E}}. \tag{4.6}$$

From the Clausius-Duhem inequality, assuming isochoric deformation of the SC, standard arguments lead to the second Piola-Kirchoff stress tensor $\mathbf{S}$, which is expressed as

$$\mathbf{S} = \rho_0 \frac{\partial \Psi(\mathbf{E})}{\partial \mathbf{E}}, \tag{4.7}$$

a second order tensor with all of its components in the referential domain. A more useful measurement of stress for the SC is found through the Cauchy stress tensor $\mathbf{t}$, which is a symmetric, second order tensor with all of its elements in the spatial domain. It is expressed as

$$\mathbf{t} = -p\mathbf{I} + \mathbf{F} \cdot \rho_0 \frac{\partial \Psi(\mathbf{E})}{\partial \mathbf{E}} \cdot \mathbf{F}^{\mathbf{T}} \tag{4.8}$$

where p is an indeterminate *Lagrange multiplier* used to enforce incompressibility. Note that p physically represents a workless reaction to the kinematic constraint on the deformation field and

may only be determined from equilibrium and boundary conditions [59].

The Helmholtz free-energy function defined per unit-mass $W(\mathbf{E})$ is expressed as

$$W(\mathbf{E}) = \rho_0 \Psi(\mathbf{E}), \tag{4.9}$$

which is more commonly known as the strain energy function. The Cauchy stress can now conveniently be described as

$$\mathbf{t} = -p\mathbf{I} + \mathbf{F} \cdot \frac{\partial W(\mathbf{E})}{\partial \mathbf{E}} \cdot \mathbf{F}^{\mathbf{T}}. \tag{4.10}$$

This version of the Cauchy stress equation forms the basis for the remainder of the analysis. From here (4.10) will be tailored to represent the SC specimens by defining two separate strain energy functions based off of Holzapfel's structural model and Fung's phenomenological model. The theoretical axial force F and the theoretical internal pressure P will be determined from boundary conditions applied to the composite during experimental testing.

4.2.3 Specific forms of the strain energy function

The strain energy function provides information that uniquely classifies each material. In order to incorporate structural aspects such as initial fibre orientation within the formulation, a model proposed by Holzapfel *et al.* [36], which is based off of a strain energy model for composites created by Spencer *et al.* [60], was used for this analysis. The results from this model will be compared to a widely used phenomological function created by Fung *et al.* [33].

4.2.3.1 Strain energy function of Holzapfel's type

Holzapfel's strain energy function is expressed in an additive split [61] to highlight the defining features of the SC, which are the elastomeric matrix and the embedded, rigid fibres. The strain energy function is split into isotropic and anisotropic contributions from both the matrix and the fibres, respectively, to yield

$$W(\mathbf{C}, \mathbf{a_{01}}, \mathbf{a_{02}}) = W_{iso}(\mathbf{C}) + W_{aniso}(\mathbf{C}, \mathbf{a_{01}}, \mathbf{a_{02}}). \tag{4.11}$$

The vectors $\mathbf{a_{01}}$ and $\mathbf{a_{02}}$ are normalized reference direction vectors for the two families of fibres that are helically wound around the axis of the SC.

The integrity basis for the three symmetrical second order tensors $\mathbf{C}, \mathbf{A_1}, \mathbf{A_2}$, where

$$\mathbf{A_1} = \mathbf{a_{01}} \otimes \mathbf{a_{01}}, \tag{4.12}$$

$$\mathbf{A_2} = \mathbf{a_{02}} \otimes \mathbf{a_{02}} \tag{4.13}$$

consists of the invariants:

$$\begin{aligned}
&I_1(\mathbf{C}) = \operatorname{tr}\mathbf{C}, \quad I_2(\mathbf{C}) = \frac{1}{2}[(\operatorname{tr}\mathbf{C})^2 - \operatorname{tr}\mathbf{C}^2], \quad I_3(\mathbf{C}) = \det\mathbf{C} = 1,\\
&I_4(\mathbf{C}, \mathbf{A_1}) = \mathbf{C} : \mathbf{A_1}, \quad I_5(\mathbf{C}, \mathbf{A_1}) = \mathbf{C^2} : \mathbf{A_1}, \quad I_6(\mathbf{C}, \mathbf{A_2}) = \mathbf{C} : \mathbf{A_2},\\
&I_7(\mathbf{C}, \mathbf{A_2}) = \mathbf{C^2} : \mathbf{A_2}, \quad I_8(\mathbf{C}, \mathbf{a_{01}}, \mathbf{a_{02}}) = (\mathbf{a_{01}} \cdot \mathbf{a_{02}})\mathbf{a_{01}} \cdot \mathbf{C}\mathbf{a_{02}},\\
&I_9(\mathbf{a_{01}}, \mathbf{a_{02}}) = (\mathbf{a_{01}} \cdot \mathbf{a_{02}})^2.
\end{aligned} \tag{4.14}$$

The first three invariants $I_1(\mathbf{C})$, $I_2(\mathbf{C})$, and $I_3(\mathbf{C})$ are derived through the Cayley-Hamilton theorem, which specifies that a tensor will satisfy its own characteristic equation. The invariants $I_4(\mathbf{C}, \mathbf{A_1})$ and $I_6(\mathbf{C}, \mathbf{A_2})$ physically represent stretch measures of the two families of fibres $\mathbf{a_{01}}$ and $\mathbf{a_{02}}$, respectively, and they are equated as the squares of the stretches in these directions.

The invariants $I_3(\mathbf{C})$ and $I_9(\mathbf{a_{01}}, \mathbf{a_{02}})$ are constant meaning $W(\mathbf{C}, \mathbf{A_1}, \mathbf{A_2})$ can be expressed as a function of the remaining seven invariants. More specifically

$$W(\mathbf{C}, \mathbf{A_1}, \mathbf{A_2}) = W_{iso}(I_1, I_2) + W_{aniso}(I_1, I_2, I_4, \ldots, I_8). \tag{4.15}$$

The number of material parameters may be further minimized [36], for simplicity, to yield

$$W(\mathbf{C}, \mathbf{A_1}, \mathbf{A_2}) = W_{iso}(I_1) + W_{aniso}(I_4, I_6). \tag{4.16}$$

Equation (4.16) is a reduced version of the strain energy model presented in (4.15). This simplification still highlights the anisotropic features in the SC from the invariants $I_4(\mathbf{C}, \mathbf{A_1})$ and $I_6(\mathbf{C}, \mathbf{A_2})$, both of which physically correspond to the reaction of the embedded fibres.

Equation (4.16) must be particularized so as to fit the material parameters to the experimentally observed response of the SC. In order to classify the isotropic response $W_{iso}(I_1)$ the classical neo-Hookean model [40] was used to formulate

$$W_{iso}(I_1) = \frac{c_1}{2}(I_1 - 3), \tag{4.17}$$

where $c_1 > 0$ is a stress like material parameter representing features of the isotropic matrix. The strong stiffening effect that is exhibited in most materials with embedded fibres motivates the use of an exponential function to describe the strain energy stored within the fibre strands, $W_{aniso}(I_4, I_6)$. It is proposed, by Holzapfel *et al.* [36] that

$$W_{aniso}(I_4, I_6) = \frac{c_2}{2c_3} \sum_{i=4,6} \{\exp\left[c_3(I_i - 1)^2\right] - 1\}, \tag{4.18}$$

where $c_2 > 0$ is a stress-like material parameter and $c_3 > 0$ is a dimensionless parameter. Both parameters describe properties attributed to the stiff fibres.

Equations (4.17) and (4.18) describe W as a function of $\mathbf{C}$, $\mathbf{A_1}$, and $\mathbf{A_2}$ only. It is of interest to express $W(\mathbf{C}, \mathbf{A_1}, \mathbf{A_2})$ in terms of $\mathbf{E}$, instead of $\mathbf{C}$. This is achieved by rearranging (4.5) to yield

$$\mathbf{C} = 2\mathbf{E} + \mathbf{I}. \tag{4.19}$$

Some basic tensor manipulations are then used to rewrite invariants I_1, I_4, and I_6 as functions of $\mathbf{E}$, giving

$$I_1(\mathbf{E}) = \mathrm{tr}(2\mathbf{E} + \mathbf{I}) = 2E_{ii} + 3, \tag{4.20}$$

$$I_4(\mathbf{E}, \mathbf{A_1}, \mathbf{A_2}) = 2E_{ij}A_{1ij} + A_{1ii}, \tag{4.21}$$

$$I_6(\mathbf{E}, \mathbf{A_1}, \mathbf{A_2}) = 2E_{ij}A_{2ij} + A_{2ii}. \tag{4.22}$$

Please note that repeated indices indicate Einstein's summation notation of the tensor components, where $i, j = 1, 2, 3$.

For a cylindrical tube with axisymmetric, helically wound fibres, the principal directions are

expressed as

$$\{\mathbf{a_{01}}\} = \begin{Bmatrix} 0 \\ \cos\alpha \\ \sin\alpha \end{Bmatrix}, \quad \{\mathbf{a_{02}}\} = \begin{Bmatrix} 0 \\ \cos\alpha \\ -\sin\alpha \end{Bmatrix}. \tag{4.23}$$

Here, α represents the initial fibre angle measured between the fibres and the circumferential axis in the composite specimen. The resulting tensors $\mathbf{A_1}$ and $\mathbf{A_2}$ are calculated as

$$[\mathbf{A_1}] = \begin{bmatrix} 0 & 0 & 0 \\ 0 & \cos^2\alpha & \cos\alpha\sin\alpha \\ 0 & \cos\alpha\sin\alpha & \sin^2\alpha \end{bmatrix}, \quad [\mathbf{A_2}] = \begin{bmatrix} 0 & 0 & 0 \\ 0 & \cos^2\alpha & -\cos\alpha\sin\alpha \\ 0 & -\cos\alpha\sin\alpha & \sin^2\alpha \end{bmatrix}. \tag{4.24}$$

The invariants can be calculated, for a thick walled tube experiencing axial stretches, radial stretches, and a radial twist, as

$$I_1(\mathbf{E}) = 2(E_{RR} + E_{\theta\theta} + E_{ZZ}) + 3, \tag{4.25}$$

$$I_4(\mathbf{E}) = \cos^2\alpha(2E_{\theta\theta} + 1) + \sin^2\alpha(2E_{ZZ} + 1) + 4E_{\theta Z}\cos\alpha\sin\alpha, \tag{4.26}$$

$$I_6(\mathbf{E}) = \cos^2\alpha(2E_{\theta\theta} + 1) + \sin^2\alpha(2E_{ZZ} + 1) - 4E_{\theta Z}\cos\alpha\sin\alpha. \tag{4.27}$$

The strain energy function may now be expressed as

$$W(\mathbf{E}, \mathbf{A_1}, \mathbf{A_2}) = c_1(E_{RR} + E_{\theta\theta} + E_{ZZ}) + \frac{c_2}{2c_3}[\exp(c_3Q_1) + \exp(c_3Q_2) - 2], \tag{4.28}$$

where

$$Q_1 = (I_4 - 1)^2, \tag{4.29}$$

$$Q_2 = (I_6 - 1)^2. \tag{4.30}$$

Values for I_4 and I_6 can be determined from equations (4.26) and (4.27), respectively.

In general, W is expressed in terms of the strain components $E_{RR}, E_{\theta\theta}, E_{ZZ}, E_{R\theta}, E_{RZ}$, and $E_{\theta Z}$, but the extension-inflation test performed on the SC only deforms the material along its principal axes. This enables a simplification where W may be expressed as a function of only $E_{RR}, E_{\theta\theta}, E_{ZZ}$,

and $E_{\theta Z}$. This simplification, proposed by Vaishnav *et al.* [62], is referred to as a two-dimensional counterpart of W.

Available mechanical testing technology is unable to induce a radial twist onto the composite during elongation without adding additional costs and complexity [63]. The absence of an applied radial twist negates the significance of the strain component $E_{\theta Z}$. W is further reduced to a function of only the principal strain components $E_{RR}, E_{\theta\theta}$, and E_{ZZ}.

The Jacobian of $\mathbf{F}$, as seen in (4.3), can be rearranged to yield

$$\det \mathbf{C} = 1. \tag{4.31}$$

Equation 4.31, through further manipulations, expresses E_{RR} in terms of $E_{\theta\theta}$ and E_{ZZ}. The strain component E_{RR} can therefore be written as

$$E_{RR} = \frac{1}{2}\left[\frac{1}{\Delta} - 1\right], \tag{4.32}$$

where

$$\Delta = (2E_{\theta\theta} + 1)(2E_{ZZ} + 1). \tag{4.33}$$

The resulting strain energy function $W(E_{\theta\theta}, E_{ZZ})$ is more effective than physically measuring the strain difference in the radial direction during experimentation [64]. Such an assumption is generally not suitable for representing the anisotropy of a three dimensional, thick walled, hyperelastic cylinder but for the special case of combined inflation and axial extension that this model aims to achieve, the two dimensional counterpart is perfectly suitable for predicting the physical response for a transversely isotropic material such as the SC.

The partial derivatives of W with respect to $\mathbf{E}$ need to be determined in order to apply the strain energy function to (4.10). Firstly, differentiating E_{RR}, from (4.32), with respect to $E_{\theta\theta}$ and E_{ZZ} gives

$$\begin{aligned} \frac{\partial E_{RR}}{\partial E_{\theta\theta}} &= \frac{-1}{\Delta(2E_{\theta\theta} + 1)}, \\ \frac{\partial E_{RR}}{\partial E_{ZZ}} &= \frac{-1}{\Delta(2E_{ZZ} + 1)}. \end{aligned} \tag{4.34}$$

Differentiating Q_1, from (4.29), and Q_2, from (4.30), with respect to $\mathbf{E}$ yields

$$\begin{aligned}
&\frac{\partial Q_1}{\partial E_{RR}} = 0, \quad \frac{\partial Q_1}{\partial E_{\theta\theta}} = 4(I_4 - 1)\cos^2\alpha, \quad \frac{\partial Q_1}{\partial E_{ZZ}} = 4(I_4 - 1)\sin^2\alpha, \\
&\frac{\partial Q_2}{\partial E_{RR}} = 0, \quad \frac{\partial Q_2}{\partial E_{\theta\theta}} = 4(I_6 - 1)\cos^2\alpha, \quad \frac{\partial Q_2}{\partial E_{ZZ}} = 4(I_6 - 1)\sin^2\alpha.
\end{aligned} \tag{4.35}$$

The results from (4.34) and (4.35) are used express the derivation of (4.28) with respect to $\mathbf{E}$. The result, expressed in components of $\mathbf{E}$, is

$$\begin{aligned}
&\frac{\partial W}{\partial E_{RR}} = 0, \\
&\frac{\partial W}{\partial E_{\theta\theta}} = c_1\left(1 - \frac{1}{\Delta(2E_{\theta\theta}+1)}\right) + 2c_2\cos^2\alpha\left[(I_4 - 1)\exp(c_3Q_1) + (I_6 - 1)\exp(c_3Q_2)\right], \\
&\frac{\partial W}{\partial E_{ZZ}} = c_1\left(1 - \frac{1}{\Delta(2E_{zz}+1)}\right) + 2c_2\sin^2\alpha\left[(I_4 - 1)\exp(c_3Q_1) + (I_6 - 1)\exp(c_3Q_2)\right].
\end{aligned} \tag{4.36}$$

The partial derivatives of W presented in (4.36) may be substituted into (4.10) to determine the resulting Cauchy stress for a SC modelled with a strain energy function of Holzapfel's type.

4.2.3.2 Strain energy function of Fung's type

The strain energy function that is most extensively used in literature to model arteries, which are very similar in structure to the SC design proposed in this research, was created by Fung *et al.* in 1979 [33]. The full extension of Fung's model incorporates all shear stresses which creates a function with nine constants, however, a two dimensional formulation was sufficient for this research. Following the method in section 4.2.3.1, W may be expressed as a function of only $E_{RR}, E_{\theta\theta}, E_{ZZ}$, and $E_{\theta Z}$. Negating the applied radial twist reduces the strain energy function to $W(E_{\theta\theta}, E_{ZZ})$. Therefore, the strain energy function of Fung's type, in two dimensions, is expressed as

$$W = \frac{1}{2}c_1\left(\exp\left(c_2E_{\theta\theta}^2 + c_3E_{ZZ}^2 + 2c_4E_{\theta\theta}E_{ZZ}\right) - 1\right) \tag{4.37}$$

The material constants c_1, c_2, c_3, and c_4, which do not have a clear physical meaning, are optimized by fitting the strain energy function to experimental data.

The first partial derivatives of the strain energy function, with respect to the diagonal Green

strain elements, are

$$\frac{\partial W}{\partial E_{RR}} = 0,$$

$$\frac{\partial W}{\partial E_{\theta\theta}} = c_1 \left(c_2 E_{\theta\theta} + c_4 E_{ZZ}\right) \exp\left(Q\right) \tag{4.38}$$

$$\frac{\partial W}{\partial E_{ZZ}} = c_1 \left(c_4 E_{\theta\theta} + c_3 E_{ZZ}\right) \exp\left(Q\right)$$

where

$$Q = c_2 E_{\theta\theta}^2 + c_3 E_{ZZ}^2 + 2c_4 E_{\theta\theta} E_{ZZ}. \tag{4.39}$$

The partial derivatives of W presented in (4.38) may be substituted into (4.10) to determine the resulting Cauchy stress for a SC modelled with a strain energy function of Fung's type.

4.2.4 Application of the Cauchy stress model to the SC specimen

The following section employs the equations determined for the Cauchy stress in (4.10) with the partial derivatives of the strain energy function in (4.36) and (4.38) to the specific case involving the SC specimen in this work.

Let Ω_0 represent the reference configuration of a SC specimen, labelled as a cylindrical, thick-walled tube continuum, and is assumed to be completely stress free. Let Ω_{res} represent the reference configuration where the SC is unloaded but, due to residual stresses created by the fabrication process, is not completely stress free. Figure 4.3 illustrates these configuration states.

Let $\boldsymbol{\chi} : \Omega_0 \to \mathbb{R}^3$ represent the transformation of an arbitrary particle in the typical position $\mathbf{X} \in \Omega_0$ to a position $\mathbf{x} = \boldsymbol{\chi}(\mathbf{X}) \in \Omega$ in the deformed, or spatial configuration, Ω. For the considered problem, $\boldsymbol{\chi}$ will be composed of the linear transformations $\boldsymbol{\chi}_{res}$ and $\boldsymbol{\chi}_p$ so that $\boldsymbol{\chi} = \boldsymbol{\chi}_p \circ \boldsymbol{\chi}_{res}$ [36].

The stress free configuration of the specimen, introduced as Ω_0, can be achieved by inducing a stress-relieving cut within the composite tube [65, 66, 67]. According to Green [68], a material particle located at (R, Θ, Z) in domain Ω_0 in figure 4.3 can be linearly mapped to the location (ρ, ϑ, ζ) in the domain Ω_{res} by

$$\rho = \rho(R), \quad \vartheta = \frac{\pi}{\Theta_0}\Theta, \quad \zeta = \Lambda Z. \tag{4.40}$$

The variable Θ_0 is an opening angle as illustrated in figure 4.4, and Λ is an axial stress ratio

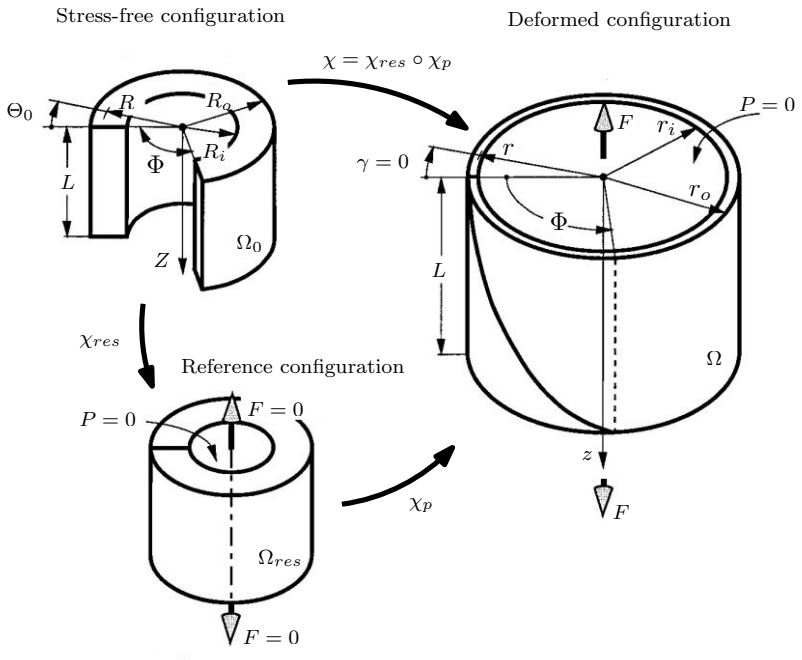

Figure 4.3: SC represented in its stress-free, reference, and deformed configurations [36].

associated with residual stress. An opening angle of $\Theta_0 = 180° = \pi$ implies that there is no residual stress stored in the cylinder. From (4.2) the gradient tensor $\mathbf{F_{res}}$ can now be expressed as

$$\mathbf{F_{res}} = \begin{bmatrix} \dfrac{\partial \rho}{\partial R} & \dfrac{1}{R}\dfrac{\partial \rho}{\partial \Theta} & \dfrac{\partial \rho}{\partial Z} \\ \rho\dfrac{\partial \vartheta}{\partial R} & \dfrac{\rho}{R}\dfrac{\partial \vartheta}{\partial \Theta} & \rho\dfrac{\partial \vartheta}{\partial Z} \\ \dfrac{\partial \zeta}{\partial R} & \dfrac{1}{R}\dfrac{\partial \zeta}{\partial \Theta} & \dfrac{\partial \zeta}{\partial Z} \end{bmatrix} = \begin{bmatrix} \dfrac{\partial \rho}{\partial R} & 0 & 0 \\ 0 & \dfrac{\pi \rho}{\Theta_0 R} & 0 \\ 0 & 0 & \Lambda \end{bmatrix}. \tag{4.41}$$

Similarly, a material particle can be linearly mapped from from its position in Ω_{res} at (ρ, ϑ, ζ)

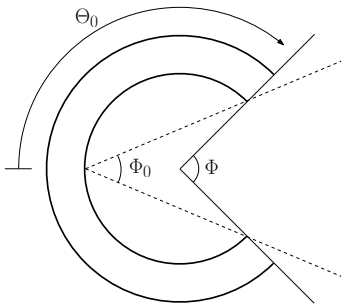

Figure 4.4: SC with stress relieving cut. The opening angle $\Theta_0 = \pi - \Phi_0$ [64].

to a position in a loaded configuration Ω at (r, θ, z) by

$$r = r(\rho), \quad \theta = \vartheta + \gamma\zeta, \quad z = \lambda\zeta \tag{4.42}$$

where γ is a twist per unit unloaded length which may be imposed through a torsion test, and λ is an axial load-induced stretch defined per unit unloaded length [64]. It was decided in section 4.2.3.1 that γ would be neglected, therefore, the linear mapping is now

$$r = r(\rho), \quad \theta = \vartheta, \quad z = \lambda\zeta \tag{4.43}$$

The transformation gradient tensor $\mathbf{F_p}$ for this linear map is given as

$$\mathbf{F_p} = \begin{bmatrix} \dfrac{\partial r}{\partial \rho} & \dfrac{1}{\rho}\dfrac{\partial r}{\partial \vartheta} & \dfrac{\partial r}{\partial \zeta} \\ r\dfrac{\partial \theta}{\partial \rho} & \dfrac{r}{\rho}\dfrac{\partial \theta}{\partial \vartheta} & r\dfrac{\partial \theta}{\partial \zeta} \\ \dfrac{\partial z}{\partial \rho} & \dfrac{1}{\rho}\dfrac{\partial z}{\partial \vartheta} & \dfrac{\partial z}{\partial \zeta} \end{bmatrix} = \begin{bmatrix} \dfrac{\partial r}{\partial \rho} & 0 & 0 \\ 0 & \dfrac{r}{\rho} & 0 \\ 0 & 0 & \lambda \end{bmatrix}. \tag{4.44}$$

The total deformation $\boldsymbol{\chi} : \Omega_0 \to \mathbb{R}^3$ can be achieved by equating

$$\mathbf{F} = \mathbf{F_p} \cdot \mathbf{F_{res}} \tag{4.45}$$

which produces the second order gradient tensor

$$\mathbf{F} = \begin{bmatrix} \dfrac{\partial r}{\partial R} & 0 & 0 \\ 0 & \dfrac{\pi r}{\Theta_0 R} & 0 \\ 0 & 0 & \lambda\Lambda \end{bmatrix}. \tag{4.46}$$

Incompressibility of the SC forces the Jacobian of $\mathbf{F}$ to equal one, which can be simplified to provide an expression for the first component of $\mathbf{F}$. This component is found to be

$$\frac{\partial r}{\partial R} = \frac{\Theta_0 R}{\pi r \lambda \Lambda}. \tag{4.47}$$

Solving this ordinary differential equation by separation of variables allows, depending on the chosen bounds of the integral,

$$r_o^2 - r_i^2 = \frac{\Theta_0}{\pi\lambda\Lambda}\left(R_o^2 - R_i^2\right), \tag{4.48}$$

$$r_o^2 - r^2 = \frac{\Theta_0}{\pi\lambda\Lambda}\left(R_o^2 - R^2\right), \tag{4.49}$$

$$r^2 - r_i^2 = \frac{\Theta_0}{\pi\lambda\Lambda}\left(R^2 - R_i^2\right), \tag{4.50}$$

where $r_i \leq r \leq r_o$ and $R_i \leq R \leq R_o$. It is common to see, in literature, the bounds be chosen to solve for the radius r and outer radius r_o based on experimentally found values of the inner radius r_i. In this research, however, measuring the outer radius was much more accessible and, therefore, these equations were used to solve for r and r_i from r_o instead.

The right Cauchy-Green tensor, from (4.4), is determined to be

$$\mathbf{C} = \begin{bmatrix} \left(\dfrac{\Theta_0 R}{\pi r\lambda\Lambda}\right)^2 & 0 & 0 \\ 0 & \left(\dfrac{\pi r}{\Theta_0 R}\right)^2 & 0 \\ 0 & 0 & (\Lambda\lambda)^2 \end{bmatrix}. \tag{4.51}$$

The Green strain $\mathbf{E}$ is easily found through (4.5). All of the equations: (4.36) for a Holzapfel model, or (4.38) for a Fung model, (4.46), and (4.51) were substituted into (4.10) to yield the Cauchy stress of the SC during extension-inflation tests. This allows the non-zero components of the Cauchy stress tensor to be expressed as

$$\begin{aligned} t_{rr} &= -p + \left(\frac{\Theta_0 R}{\pi r\lambda\Lambda}\right)^2 \frac{\partial W}{\partial E_{RR}}, \\ t_{\theta\theta} &= -p + \left(\frac{\pi r}{\Theta_0 R}\right)^2 \frac{\partial W}{\partial E_{\theta\theta}}, \\ t_{zz} &= -p + (\lambda\Lambda)^2 \frac{\partial W}{\partial E_{ZZ}}. \end{aligned} \tag{4.52}$$

4.2.4.1 Equilibrium and boundary conditions

Assuming axisymmetry, elementary tensor calculus was used to determine the only nontrivial solution to the equilibrium equation

$$\nabla \cdot \mathbf{t} = \mathbf{0} \tag{4.53}$$

as being

$$\frac{\partial t_{rr}}{\partial r} + \frac{t_{rr} - t_{\theta\theta}}{r} = 0. \tag{4.54}$$

It is useful to note that the total deformation $\mathbf{F}$ and p only vary with r [64]. Integration and further manipulations to (4.54) were performed to determine p as a function of r,

$$p(r) = \left(\frac{\Theta_0 R}{\pi r \lambda \Lambda}\right)^2 \frac{\partial W}{\partial E_{RR}} + P_i - \int_{r_i}^{r} (t_{\theta\theta} - t_{rr}) \frac{dr}{r}, \tag{4.55}$$

where

$$P_i = t_{rr}(r_i) \tag{4.56}$$

is the luminal pressure of the composite tube.

The Cauchy stress was assumed to be an additive split between an isochoric and volumetric component, where the volumetric component took the form of p to enforce incompressibility. It can be said that incompressibility can be enforced through (4.3), which would disregard the use for a Lagrange multiplier [69]. Section 4.2.3.1 clearly stated that incompressibility was upheld via a two-dimensional counterpart of W therefore p will henceforth be neglected.

Alternatively, if (4.54) is evaluated using the outer and inner radii as the integral bounds, the transmural pressure can be expressed as

$$t_{rr}(r) = P_i - P_o = \int_{r_i}^{r_o} (t_{\theta\theta} - t_{rr}) \frac{dr}{r}, \tag{4.57}$$

where

$$P_o = t_{rr}(r_o) \tag{4.58}$$

is another boundary condition of the system, and P_o is taken as the atmospheric pressure. This relation (4.57) is very important due to the nature of the experimental set up as it relates a

measurable pressure parameter to the strain in the radial direction.

The equations for the Cauchy stress components in (4.10) are substituted into (4.57), and reduced, to yield

$$P = \int_{r_i}^{r_o} \left[\left(\frac{\pi r}{\Theta_0 R} \right)^2 \frac{\partial W}{\partial E_{\theta\theta}} - \left(\frac{\Theta_0 R}{\pi r \lambda \Lambda} \right)^2 \frac{\partial W}{\partial E_{RR}} \right] \frac{dr}{r}, \tag{4.59}$$

where P is the internal pressure.

Similarly, tensile forces in the axial direction are measurable loads that relate to the strain along the axis of the tube. It is necessary to derive a relation that takes this knowledge into account. Consider the free body diagram in figure 4.5. It can be shown that, for an inflated, thick walled tube that

$$F = 2\pi \int_{r_i}^{r_o} t_{zz} r dr - \Gamma \pi r^2 P_i, \tag{4.60}$$

where $\Gamma = 1$ for a closed tube or $\Gamma = 0$ for an open tube. Performing a double integral, by parts,

Figure 4.5: Free body diagram of the SC in the axial direction.

on equation (4.60), and substituting in equation (4.57), gives

$$F = \pi \int_{r_i}^{r_o} \left(2t_{zz} - t_{rr} - t_{\theta\theta} \right) r dr + \left(1 - \Gamma \right) \pi r_i^2 P_i. \tag{4.61}$$

This expression for the axial force is very important as it gives a relation for the force and strains that are measured during experimentation in all three principal directions.

The equations for the Cauchy stress components in (4.10) are substituted into (4.61), and reduced, to yield

$$\begin{aligned} F = \pi \int_{r_i}^{r_o} \left[2 \left(\lambda \Lambda \right)^2 \frac{\partial W}{\partial E_{ZZ}} - \left(\frac{\Theta_0 R}{\pi r \lambda \Lambda} \right)^2 \frac{\partial W}{\partial E_{RR}} - \left(\frac{\pi r}{\Theta_0 R} \right)^2 \frac{\partial W}{\partial E_{\theta\theta}} \right] r dr \\ + \left(1 - \Gamma \right) \pi r_i^2 P_i. \end{aligned} \tag{4.62}$$

Equations (4.59) and (4.62) are fitted to the experimental results from the modified extension-

inflation tests through the optimization of several material constants present within the strain energy function.

4.3 Experimental data from a modified extension-inflation test

Planar biaxial tests are a common testing method used to characterize soft materials [70]. For cylindrical objects, extension-inflation tests are performed to obtain planar stress data much similar to the way biaxial testing does for flat samples. Typical extension-inflation tests involve pressurizing a cylinder made from a soft material while monitoring its internal pressure, axial force, internal radius, and axial elongation.

There is some criticism regarding the validity of using planar biaxial testing or extension-inflation tests to attempt to fully characterize anisotropic materials presented by Holzapfel and Ogden [71]. This statement is important for this research because, as stated in section 4.1.3, the SC specimens developed in this work are considered transversely isotropic materials due their helically wound, axisymmetric fibres and isotropic matrix. Even though the material cannot be fully characterized in this manner, many valuable attributes of the SC can still be modelled. Therefore, it was deemed acceptable to characterize the SC material through an extension-inflation test.

In this research, however, the extension-inflation test was modified. The SC was axially stretched, instead of being inflated, and the axial force and external radius were monitored. Since the main function of the SC was to act as a nonlinear spring, where it was only being elongated, it was more beneficial to analyse the material behaviour as it was strained to its axial limits as opposed to its radial limits. The fibre angles used in each specimen would not have allowed for the SC's full range of motion to be achieved if it were pressurized, since the increase in pressure would inhibit elongation. Therefore, the internal pressure was kept at 0 kPa for the entirety of the experiment and the theoretical pressure, from (4.59), will be forced to conform to an internal pressure of 0 kPa during the data fitting process.

4.3.1 Experimental procedure for raw data collection

Experimental data were collected from the results of a modified extension-inflation test performed on the SC specimen. A specimen was prepared using identical methods as those previously described

in section 3.1 to produce a SC as shown in figure 3.14. The specimen was then marked with two black dots as demonstrated in figure 4.6.

Figure 4.6: A SC specimen marked with black dots coated with charcoal.

The two black dots spaced 52 mm apart, while being centred with the middle of the specimen, were used to determine the elongation of the composite based on the increasing distance between the dots during elongation. The distance between the two dots was tracked by analysing a series of photos after the tests were completed. In order to assure that the dots were clearly visible in the photos, they were coated with black charcoal, and a white backdrop was placed behind the testing apparatus to highlight the contrasting colours. The dots were placed near the center of the specimen, away from the end fixtures, to help assure that the measured deformation was a result of the material properties, and not influenced by external factors.

A SC specimen that was marked with black dots was preconditioned for 15 cycles and then axially stretched using the Instron tensile testing machine. The experiment was performed in a dozen discrete steps starting from a resting position, without any slack, and ending at the maximum elongation length. At each step, data were manually recorded, and a photograph was taken of the markers. The recorded data included the peak axial force F_{exp}, the internal pressure P_{exp}, and the outer radius of the specimen r_{outexp}. For each step P_{exp} was assumed atmospheric, F_{exp} was measured from the peak value recorded by the 1 kN load cell, r_{outexp} was measured using a Vernier calliper, and the elongation was tracked by a snapshot incorporating the dual black dots on the composite.

4.3.2 Raw data post-processing

The raw data collected from the discrete steps were imported by a MATLAB function, shown in appendix D.1, and processed to yield experimental data. The first step was processing the images of the black dots to determine the distance between their centroids. The source code for the MATLAB function that accomplished this task is found in appendix D.2. The structure of the program was

inspired by a script written by Image Analyst [72].

The image was first converted into a grayscale format, as seen in figure 4.7a. This was to make the file based upon a 256 bit format that was then processed into a black and white image using a binary threshold just as in figure 4.7b. The holes were also filled using a MATLAB defined function

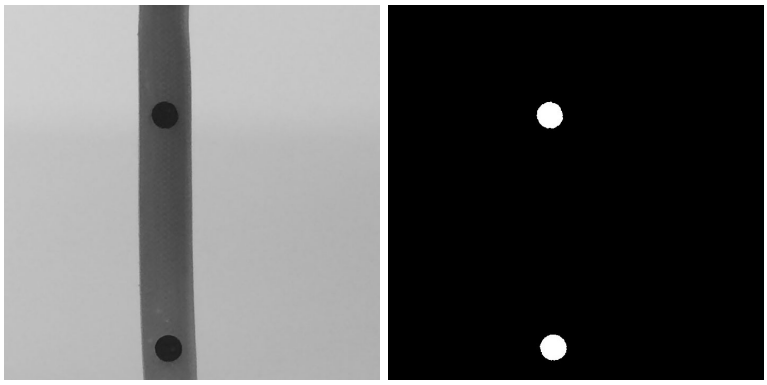

(a) Grayscale image **(b)** Binary threshold

Figure 4.7: A grayscale and binary threshold of the original SC with black dot markers.

to slightly increase the quality of the threshold.

Individual white dots were then differentiated based upon their connectivity. They were assigned different colors for visual purposes and displayed in figure 4.8a. The boundaries of each dot were plotted on the original grayscale image, in figure 4.8b, to assure that the entire marker was considered during the image processing function. Not every image was processed perfectly during

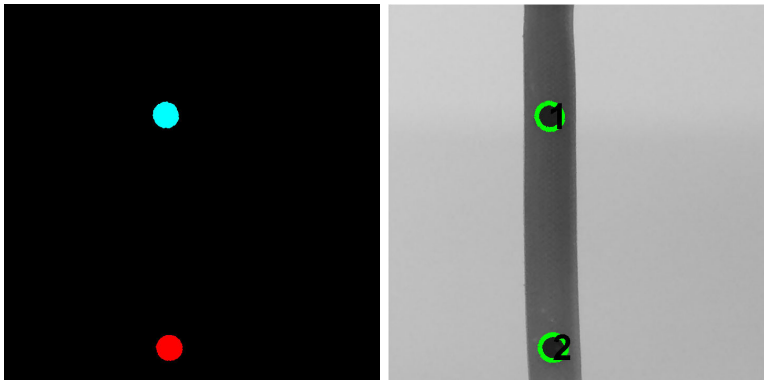

(a) Colored dots **(b)** Dot boundaries

Figure 4.8: A colored image used to differentiate between dot markers and labelled boundaries of black dot markers.

the binary threshold step and there was a risk of finding extra, smaller dots that did not pass the threshold. Subsequently, an algorithm was developed to cycle through all of the dots and select

the two largest, which corresponded to the markers, and only consider those for further analysis.

Once the dots were differentiated from each other, the location of their centroids were found through MATLAB, and the Pythagorean distance between both centroids was determined. Figure 4.9 illustrates the distance between the centroids of both dot markers by the blue line.

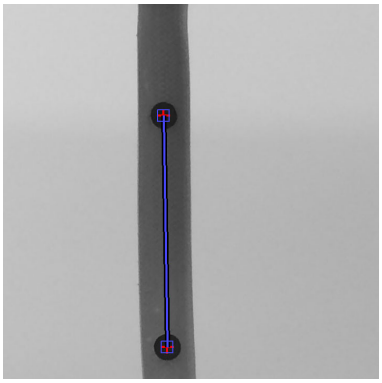

Figure 4.9: The Pythagorean distance between the centroids of the two black dot markers.

This process was iterated for the snapshot recorded during each of the dozen discrete steps in the experiment. Each Pythagorean distance was compared to the starting length between the dots to find the stretch ratio λ_{exp} for each of the dozen steps.

The processed raw data, at this point, consists of a dozen discrete values for F_{exp}, P_{exp}, r_{outexp}, and now λ_{exp}. A spline interpolation and a smoothing function were used from MATLAB, which can be referenced in appendix D.3, to create 76 data points from the original dozen.

4.4 Numerical methods used to optimize the theoretical results with experimental data

The equations for axial force (4.59) and internal pressure (4.62) were coded into a MATLAB script, which is found in appendix D.4. The results of the tests were analysed to determine the unknown material constants that most accurately predict the material behaviour. Figure 4.10 illustrates the algorithm used to optimize the material constants and fit the theoretical model to the experimental data in the means of a flow chart (pseudocode shown in appendix C).

The input variables to the model are the experimentally determined values for the peak axial force F, the internal pressure P, the outer radius of the specimen r_o, and the stretch ratio λ,

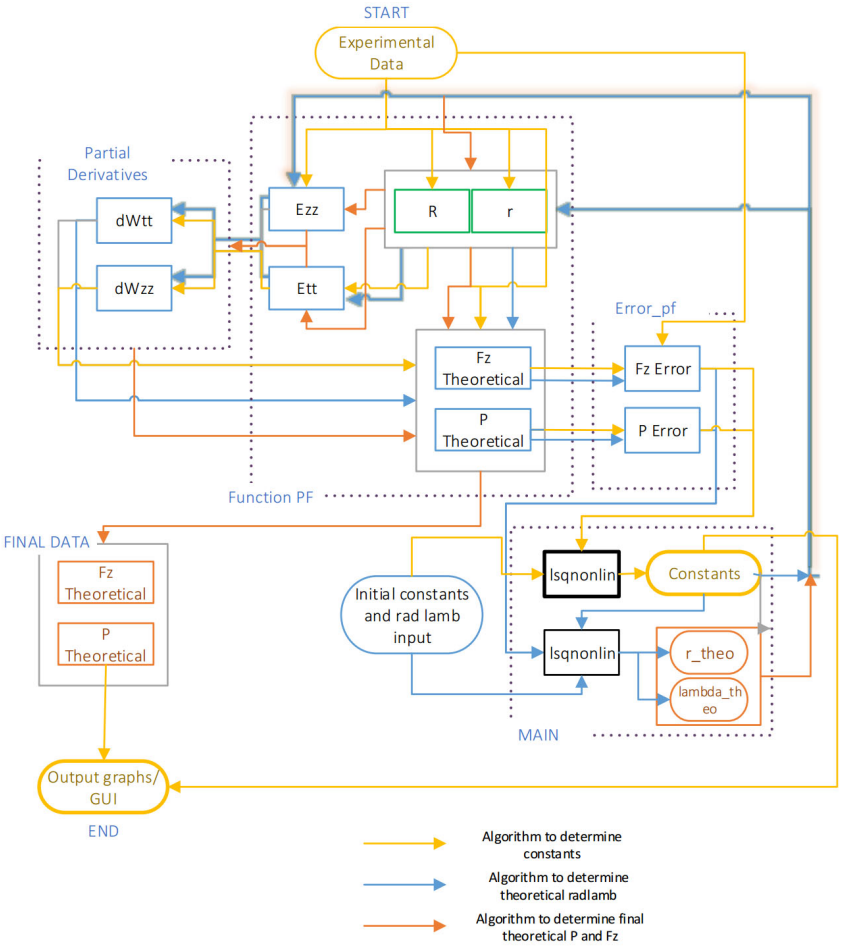

Figure 4.10: Flow chart illustrating the algorithm used to optimize the theoretical model by finding material constants that fit with the experimental data.

and were interpolated to yield 76 data points. The initial fibre angle α was measured before the impregnation process. The ratio Λ was set equal to one due to incompressibility constraints. The initial inner and outer radii, R_i and R_o, were measured during the referential state previous to the stretching of the composite. The opening angle revealed through a stress relieving cut Θ_0 was assumed to be 180° for each specimen. The SC, during testing, was assumed to be an open cylinder meaning $\Gamma = 0$.

The integrals developed in (4.59) and (4.62) were evaluated using the Gauss-Legendre method

$$\int_{r_i}^{r_o} f(r)dr = \frac{r_o - r_i}{2} \sum_{j=1}^{n} w_j f\left(\frac{r_o + r_i}{2} + \frac{r_o - r_i}{2}\xi_j\right) \tag{4.63}$$

with the six weighted points presented in table 4.1. The value of r_i was determined from the

experimentally derived r_o through (4.48). Evaluating these equations resulted in theoretical values of F and P that were compared to their experimental counterparts.

Table 4.1: Gauss points and their respective weights.

Gauss point	w_j	ξ_j
1	0.467913934572691	-0.238619186083197
2	0.360761573048139	-0.661209386466264
3	0.171324492379170	-0.932469514203152
4	0.467913934572691	0.238619186083197
5	0.360761573048139	0.661209386466264
6	0.171324492379170	0.932469514203152

The theoretical and experimental values for axial force and internal pressure were compared by equating an error value for m data points as

$$e = \sum_{k=1}^{m} \left(\varpi_1 \left(P_{theo} - P_{exp} \right)_k^2 + \varpi_2 \left(F_{theo} - F_{exp} \right)_k^2 \right). \tag{4.64}$$

Equation (4.64) is dependent on the material constants $\mathbf{c}$, which were introduced in the strain energy function W. The coefficients ϖ_1 and ϖ_2 are introduced as arbitrary weights used to optimize the error function. Table 4.2 illustrates the chosen weights for the Holzapfel and Fung error functions. While these weights provided optimal results, applying identical weights to both functions did not produce any convergence issues. This error value was minimized through the optimization of the material constants using MATLAB's Levenberg-Marquardt function (*"lsqnonlin"*).

Table 4.2: Weights chosen for the error function used in the Levenberg-Marquardt optimization.

	ϖ_1	ϖ_2
Holzapfel	0	R_o^2
Fung	R_o^2	0

4.5 Predicting SC behaviour with optimized material constants

The theoretical internal pressure P and axial force F derived in (4.59) and (4.62), respectively, were fitted to experimental data that were collected thorough a modified extension-inflation procedure described in section 4.3. The fitting process involved optimizing a set of material constants c_i

for each separate strain energy function W of Holzapfel and Fung types, given by (4.36) and (4.38), respectively. The fitting process used the MATLAB defined function, *lsqnonlin*, which is the nonlinear Levenberg-Marquardt optimizer described in (4.63). The results presented in this section only concern the tensile response of the SC and therefore only display the axial force versus the stretch ratio. Graphs displaying the axial force versus the external radius and the external radius versus the stretch ratio can be found in appendix B.

Specimens T1B4B_55, T1A4B_43, and R1B4C_56 were subjected to modified extension-inflation testing.

4.5.1 Specimen T1B4B_55

Results from the fitted curves for specimen T1B4B_55 are shown in figures 4.11 and 4.12. The optimized material constants are shown in table 4.3.

Table 4.3: Optimized material constants for specimen T1B4B_55.

Model type	c_1	c_2	c_3	c_4
Fung	0.002295	−69.265995	−35.365043	−58.892409
Holzapfel	−0.047320	−6.010873	−79.840948	–

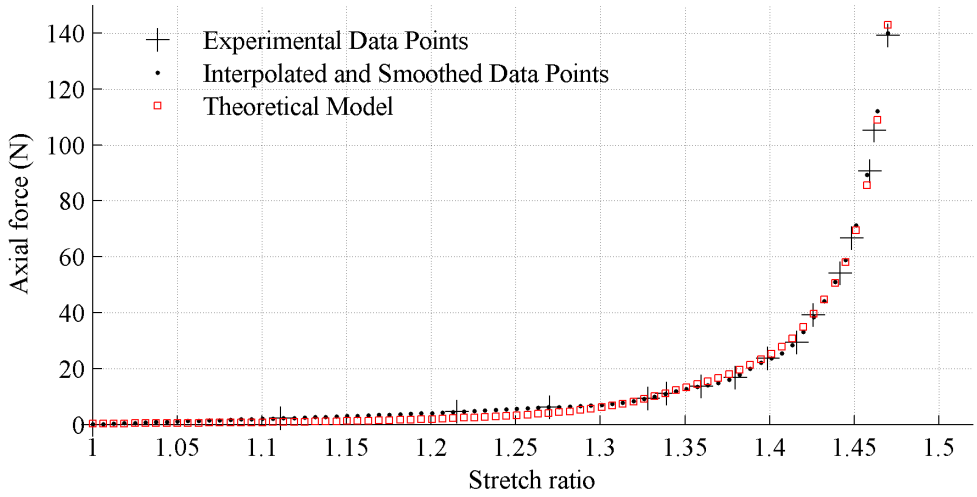

Figure 4.11: Axial force versus stretch ratio for Fung's model on specimen T1B4B_55.

With reference to figures 4.11 and 4.12, both graphs show theoretical curves that fit well to the experimental data. Figure 4.12 illustrates a break within the predicted Holzapfel data at a stretch

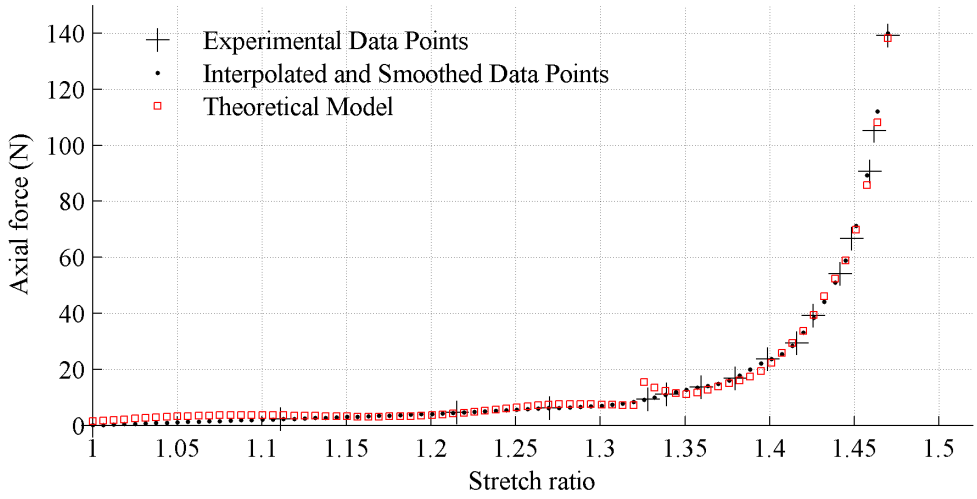

Figure 4.12: Axial force versus stretch ratio for Holzapfel's model on specimen T1B4B_55.

ratio of about 1.33. Figure B.1 illustrates an unnatural dip within the experimental data of the r_o versus λ curve at this same point, which implies that a mistake in measuring either r_o or λ influenced these results. Slight oscillations are also apparent in both theoretical curves in figures 4.11 and 4.12, more prominently so within the curves constructed from the Holzapfel strain energy function. Both the Holzapfel and Fung strain energy functions are purely exponential, meaning that there should not be any oscillations within the predicted results.

The oscillations and breaks within the curves are attributed to the formulation of imaginary values from calculating the experimental inner radius r_i during analysis. Rearranging (4.48) to calculate r_i, for every experimental data point, from the outer radius r_o, measured using a Vernier calliper, yields

$$r_i = \sqrt{r_o^2 - \frac{\Theta_0}{\pi\lambda\Lambda}\left(R_o^2 - R_i^2\right)}. \tag{4.65}$$

The initial inner and outer radii, R_i and R_o, were also measured using a Vernier calliper. Since the specimens were soft, it was very difficult to gauge the applied pressure of the calliper when making radial measurements. This created inconsistencies within measured radial values, including the measurements of the initial radii. Equation (4.65) output imaginary values for r_i when the specimen was near full elongation. These values were carried forward throughout the rest of the calculations, and they resulted in the oscillations and break seen in figures 4.12 and 4.11.

4.5.2 Specimen T1A4B_43

Specimen T1A4B_43 did not produce any imaginary radial values during the numerical calculations. Results from data fitting the curves for specimen T1A4B_43 are shown in figures 4.13 and 4.14. The optimized material constants are shown in table 4.4.

Table 4.4: Optimized material constants for specimen T1A4B_43.

Model type	c_1	c_2	c_3	c_4
Fung	0.002487	9.649096	28.376656	5.439776
Holzapfel	0.215498	0.001204	320.605184	–

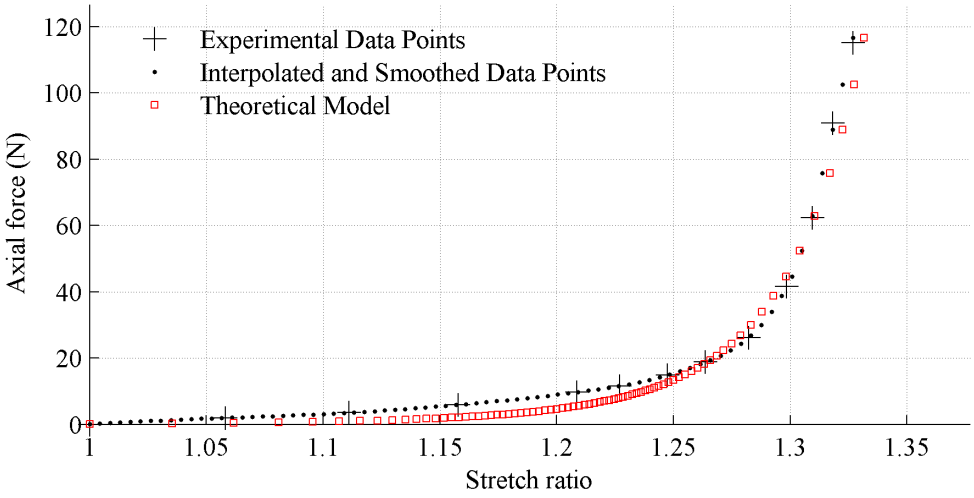

Figure 4.13: Axial force versus stretch ratio for Fung's model on specimen T1A4B_43.

There is a large difference with these material constants, being that for this specimen they are all positive, while for the specimen T1B4B_55 they were mostly negative. The resulting curves for both the Fung and Holzapfel models in figures 4.13 and 4.14 are pure exponential functions with no oscillations or discontinuities. This is true regardless of the experimental data involving the outer radius, as seen in figure B.2, not being completely smooth.

The Holzapfel model, as seen in figure 4.14, retraced the toe region of the exponential curves more accurately than the Fung model, however, the Fung model, in figure 4.13, far supersedes the Holzapfel model in tracing the exponential increase. The Holzapfel model underestimates the axial force when compared to the experimental data.

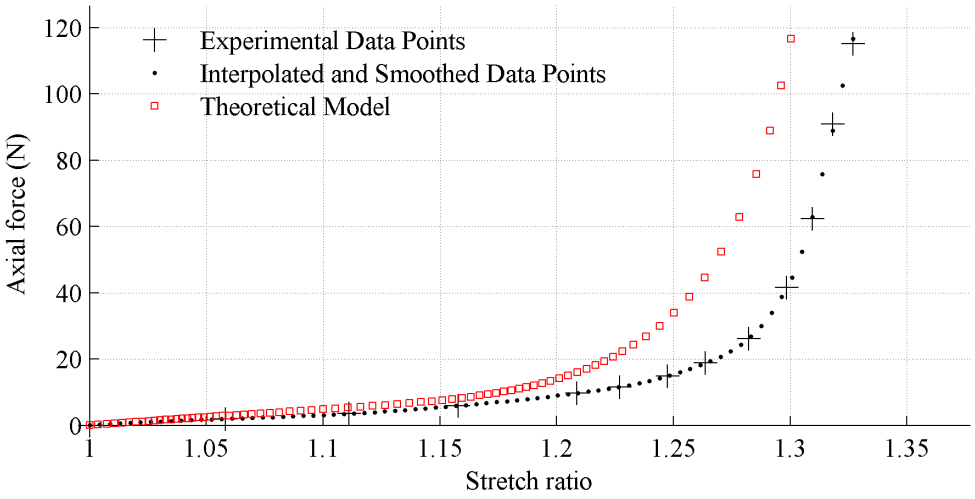

Figure 4.14: Axial force versus stretch ratio for Holzapfel's model on specimen T1A4B_43.

4.5.3 Specimen R1B4C_56

Results from data fitting the curves for specimen R1B4C_56 are shown in figures 4.15 and 4.16. The optimized material constants are shown in table 4.5.

Table 4.5: Optimized material constants for specimen R1B4C_56.

Model type	c_1	c_2	c_3	c_4
Fung	0.050627	2.644290	1.774586	0.926244
Holzapfel	0.109292	0.330281	43.539792	–

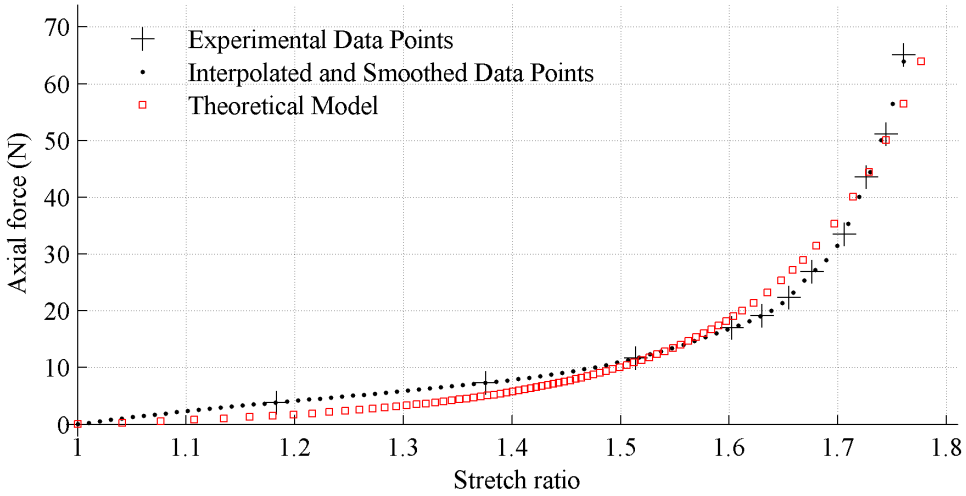

Figure 4.15: Axial force versus stretch ratio for Fung's model on specimen R1B4C_56.

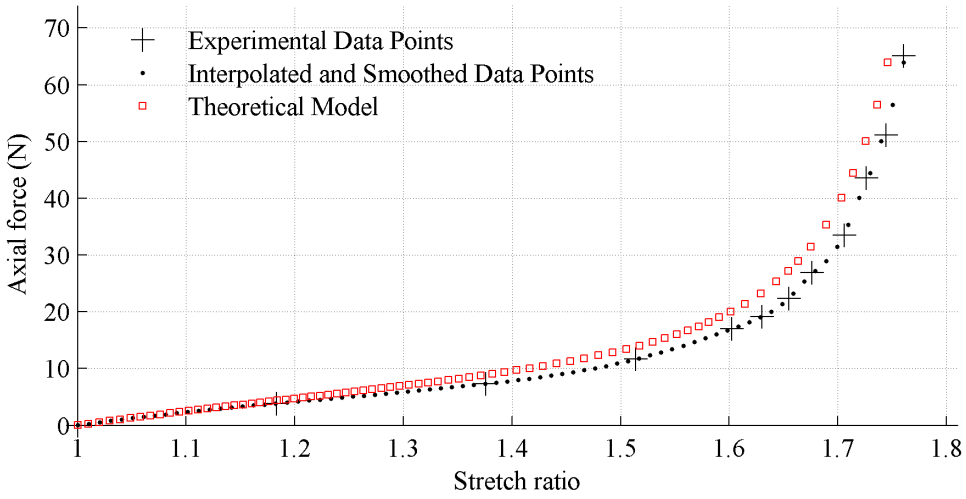

Figure 4.16: Axial force versus stretch ratio for Holzapfel's model on specimen R1B4C_56.

The resulting material constants, similarly to specimen T1A4B_43, are all positive. Both the Fung and Holzapfel models, shown in figures 4.15 and 4.16, fit the experimental response well. The Fung model underestimates the toe region of the response curve while the Holzapfel model fits it more accurately. Figures 4.15 and 4.16 show the exponential increase being more accurately traced by the Fung model while the Holzapfel model underestimates the axial force, just as it did for specimen T1A4B_43 in figure 4.14.

For both cases where the specimen data did not produce complex values, the Fung model provided results that fit to the experimental data better than the Holzapfel model did. The Holzapfel model fit the toe region of the curve better than the Fung model but underestimated the axial force response during the exponential increase. Overall, the Fung model more accurately described the tensile response of the SC.

4.6 Predicting SC behaviour using previous material constants

The Holzapfel strain energy function is intended to accurately predict the mechanical response of an entire group SCs, with equal initial design parameters but different initial fibre angles, after optimizing for the material constants of only a single specimen within that set. This is considered advantageous for designers since they may use only model to select the proper SC for passive actuation. This section compares the predictive capabilities of Holzapfel's model to Fung's model.

4.6.1 Specimen T1B4B_52 using material constants from T1A4B_43

The material constants presented in table 4.4, determined from fitting experimental data from the composite specimen T1A4B_43 to the Hofzapfel and Fung models, were used to formulate a prediction for the tensile response of specimen T1B4B_52. Both specimens were constructed from Moldstar silicone and a tight braid style. T1A4B_43 had an initial fibre angle of 43° and T1B4B_52 had an initial fibre angle of 52°. The results of these predictions are found in figures 4.17 and 4.18. Results illustrating the axial force versus the external radius or the external radius versus the stretch ratio are shown in figure B.4.

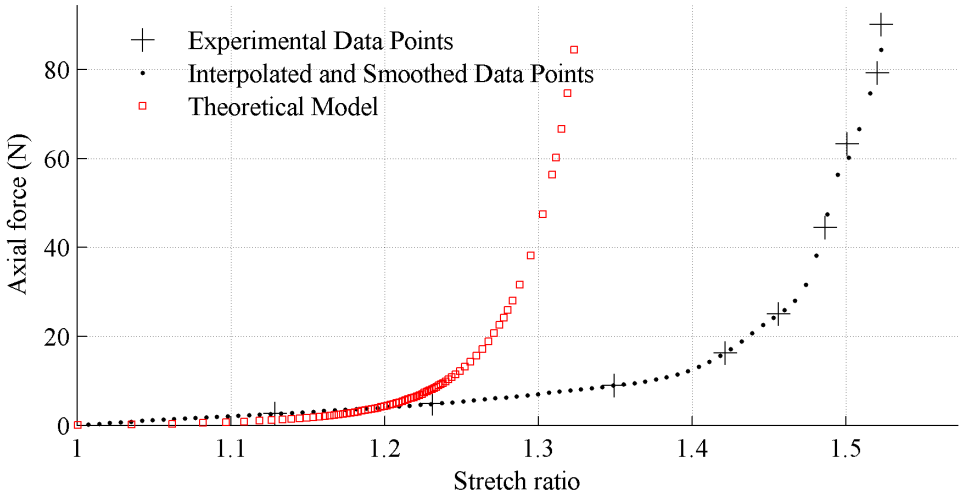

Figure 4.17: Axial force versus stretch ratio for Fung's model on specimen T1B4B_52 using material constants from fitting T1A4B_43.

It was seen that, in figure 4.17, the Fung model could not predict the tensile response of specimen T1B4B_52 using material constants determined from fitting T1A4B_43. Figure 4.17 shows that the predicted data grossly underestimated the axial response during the exponential increase. These results follow the hypothesis that Fung's model is purely phenomenological and cannot be used to predict other data sets without curve fitting those data first. Figure 4.18 shows that Holzapfel's model was also incapable of predicting the material response of T1B4B_52 using material constants derived from T1A4B_43. It did, however, trace the general shape of the experimental data, and underestimated it by an amount much less than Fung's model did.

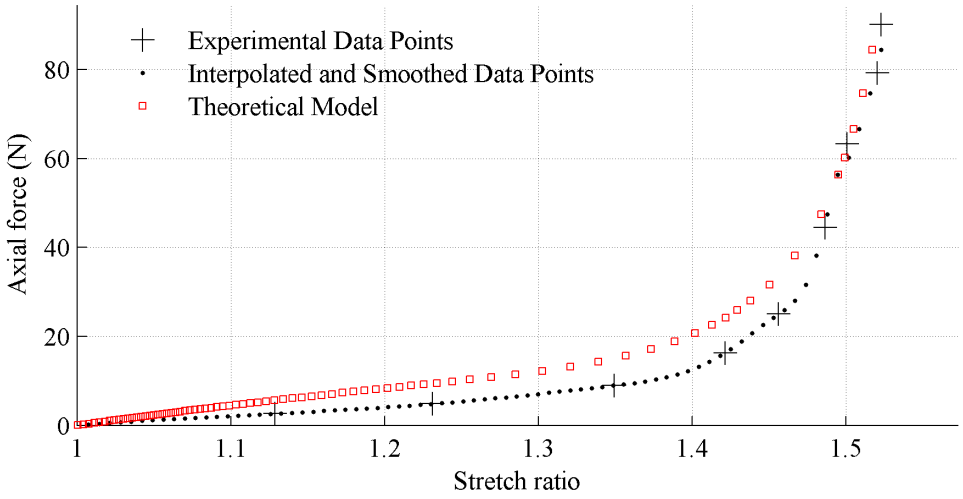

Figure 4.18: Axial force versus stretch ratio for Holzapfel's model on specimen T1B4B_52 using material constants from fitting T1A4B_43.

4.6.2 Specimen R1C4C_64 using material constants from R1B4C_56

The test was repeated using the material constants derived from specimen R1B4C_56, in table 4.5, to predict the mechanical response of R1C4C_64 under tensile strains. Both specimens were made from a regular braid style and Oomoo silicone rubber. R1B4C_56 had an initial fibre angle of 56° where R1C4C_64 had an initial fibre angle of 64°. Figures 4.19 and 4.20 illustrate these results. Results illustrating the axial force versus the external radius or the external radius versus

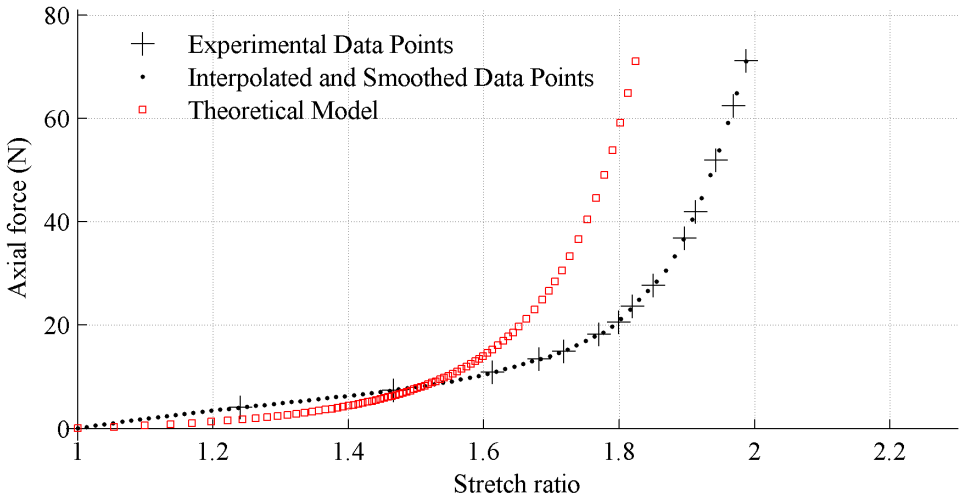

Figure 4.19: Axial force versus stretch ratio for Fung's model on specimen R1C4C_64 using material constants from fitting R1B4C_56.

the stretch ratio are shown in figure B.5, in appendix B.

Figure 4.19 illustrates that, again, Fung's model underestimated the axial force during the exponential increase in the curve. It was also shown, by figure 4.20, that Holzapfel's model did accurately trace the toe region. The slope of the linear region is the same between both the experimental and Holzapfel curves, although the Holzapfel model overestimated elongation at which the linear region would occur.

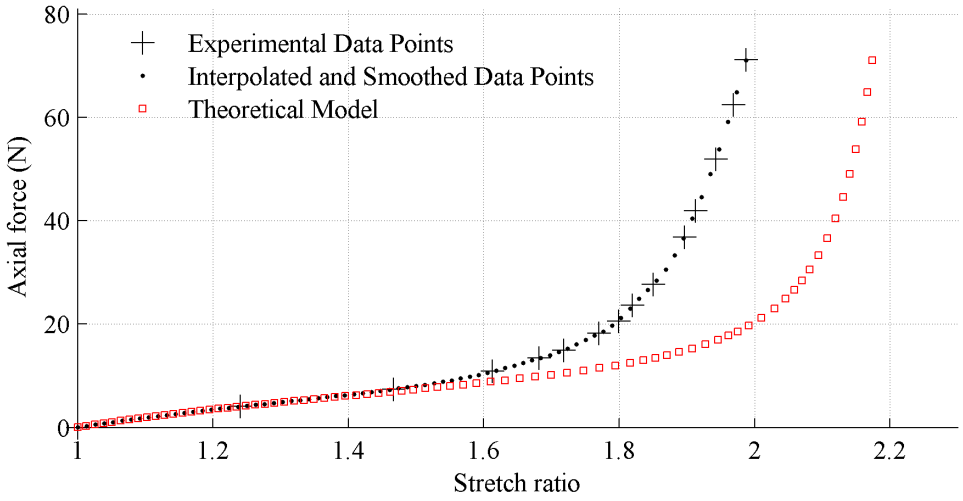

Figure 4.20: Axial force versus stretch ratio for Holzapfel's model on specimen R1C4C_64 using material constants from fitting R1B4C_56.

Chapter 5

Conclusions and Future Recommendations

The primary objective of this thesis was to design and develop a hyperelastic tubular soft composite that replicated the mechanical behaviour of the PAM without the need of internal pressurization. Moreover, it was desired to create the SC so that it may achieve a greater elongation potential than the PAM. Throughout this research, great emphasis was placed on experimentally and analytically characterizing the mechanical behaviour of the SC with the purpose of proposing a development method that would help designers select SCs that meet the actuation requirements of passive exoskeletons.

5.1 Conclusions

A literature survey was first conducted to identify and analyse previous research achievements. The survey was structured into sections that focused on alternative methods regarding hyperelastic braid solutions, the experimental characterization of tubular SCs, and the analytical models used to predict SC behaviour. In particular, to the knowledge of the author, it was noticed that there was no previous research that claimed to develop a tubular braided SC with an initial fibre angle greater than the 54.7° Magic Angle. This led to the development 18 SC specimens that were tested using an experimental setup to demonstrate their mechanical response to tensile loading conditions.

Experimentally, the tensile response of each specimen consisted of a toe and linear region similar

to the PAM and natural fibrous tissue. The majority of the SC specimens were able to achieve elongation potentials greater than, or equal to, the 30 % contraction distance of the PAM. In particular, specimens created with an initial fibre angle greater than the Magic Angle were able to be stretched up to 110 % of their original length, which is much larger than that of the PAM. The defining characteristics of the SC were able to be altered by three key control parameters: the initial fibre angle, the matrix stiffness, and the fibre braiding style.

It was determined, through experimentation, that the greatest influencing factor to the mechanical response of the SC was its initial fibre angle. It dictated the length of the toe region and, consequently, the elongation potential of the entire SC. The silicone matrix selection influenced the slope of the toe and linear region of the SC. It largely affected the transition between the toe and linear regions of the response, whereas the softer silicones yielded an abrupt transition while the stiffer silicones' transition was more gradual. This effect was largely attributed to the resistance of the silicone rubber to the compressive forces exerted by the fibres as they became aligned with the tensile load. Finally, the style of braid influenced the point at which the tensile jamming state would occur in the SC. The extra monofilament within the braid caused the jamming state to occur earlier than that of the specimens fabricated with a regular braid. This extra monofilament also increased the stiffness of the overall response of the SC.

The tensile response of the SC was modelled through a constitutive formula based on either a structural strain energy function of Holzapfel's type, or a phenomenological strain energy function of Fung's type. The process to form these models involved fitting the equations to experimental data, from a modified extension-inflation test, of a given specimen by optimizing material constants within the strain energy function. Both models were able to accurately predict the tensile response of the specimens that were used to determine the material constants. It could be seen that Holzapfel's model was able to more accurately model the toe region of the response curve while Fung's model more correctly resembled the exponential increase and linear region.

Each model was subsequently used to predict the tensile response of different specimen using the material constants found from fitting the previous SC with similar initial features but a different initial braiding angle. In this case, Holzapfel's model was much more suitable at recreating the experimental data than Fung's model. Fung's model was unable to recreate the toe or linear response. Holzapfel's model incorrectly estimated the point at which point the toe region would

transform into the linear region, however, it closely predicted the toe region and the slope of the linear region.

5.2 Recommendations for future work

The emphasis of this work was mainly on recreating the passive tensile response of a PAM and fibrous soft tissue. The SC was able to recreate the toe and linear regions of the PAM and fibrous tissue. Specific control parameters were identified and tested to observe their effects on the mechanical behaviour of the SC. The actual requirements for maximum tensile force of the SC, and other recommendations specific to passive exoskeletons, should be achieved through the proper selection of a matrix and fibre structure. The resulting selection should be tested on a functioning exoskeleton.

It is important to manufacture a reliable and robust SC that would survive many life cycles. This would require that attention be given to the end fixtures, which are currently fabricated from brass barbed connectors and cable ties. The current end fixtures are suitable for prototype tests involving low cycles, however, end fixtures should provide great strength for holding the SC without damaging the matrix over long cycling repetitions.

This research focused mainly on the initial response of the SC. In order to fully comprehend the behaviour of the SC its fatigue, creep, time dependent, and viscoelastic properties need to be examined. Testing should be performed on multiple specimens, with similar initial properties, so that a statistical analysis may be performed on each specimen. This will help further characterize the experimental response of the SC and provide reliability measurements for the lifetime of a specimen.

The SC should be assessed on a microscopic level to examine the interface between the PET fibres and the silicone matrix. The microscopic observations should then be used to determine if the PET fibres need to be treated with a bonding agent prior to impregnation.

With regards to the analytical testing, the model focused mainly on the initial tensile response of the SC. One of the main issues that occurred while collecting the experimental data was measuring the radius of the SC specimen. The pressure from the Vernier calliper on the SC specimen was difficult to retain consistent, resulting in a slight deviation of radial measurements for specimens

created with a softer matrix. It is suggested that, for future work, measurements of the radius be made from either an optical encoder or an image during the post-processing phase.

The models that were created in this research provide an excellent insight towards the behaviour of the SC material. However, future work is still needed in characterizing the SC in order to propose a model that would help designers select specific SCs to meet the actuation requirements of passive exoskeletons. In order to make the models in this research more general, it is suggested that multiple tests be completed on specimens with the same initial properties, and then their corresponding material constants acquired from the data fitting process be averaged. The resulting averaged model provides an excellent basis for further work regarding finite element analysis on the SC.

References

[1] S. Collins, M. Bruce Wiggin, and G. Sawicki, "Reducing the energy cost of human walking using an unpowered exoskeleton," *Nature*, vol. 522, no. 7555, pp. 212–215, 2015. cited By 38.

[2] J. Leclair, M. Doumit, and G. McAllister, "Analytical stiffness modeling and experimental validation for a pneumatic artificial muscle," *ASME 2014 International Mechanical Engineering Congress and Exposition*, pp. V009T12A089–V009T12A089, 2014.

[3] M. Doumit, J. Murillo, A. Lawrynczyk, and N. Baddour, "Design and evaluation of pneumatic artificial muscle for powered transfemoral prostheses," *Journal of Medical and Biological Engineering*, vol. 34, no. 5, pp. 439–447, 2014.

[4] M. Doumit, A. Fahim, and M. Munro, "Analytical modeling and experimental validation of the braided pneumatic muscle," *IEEE Transactions on Robotics*, vol. 25, no. 6, pp. 1282–1291, 2009.

[5] J. W. Freeman, M. D. Woods, and C. T. Laurencin, "Tissue engineering of the anterior cruciate ligament using a braid–twist scaffold design," *Journal of biomechanics*, vol. 40, no. 9, pp. 2029–2036, 2007.

[6] H. Saraswat, A. Rawal, and R. Singh, "Tensile behaviour of multi-layered braided structures," *Journal of Materials Science*, vol. 49, no. 18, pp. 6427–6436, 2014.

[7] A. Rawal, H. Saraswat, and R. Kumar, "Tensile response of tubular braids with an elastic core," *Composites Part A: Applied Science and Manufacturing*, vol. 47, no. 1, pp. 150–155, 2013.

[8] S. Phoenix, "Mechanical response of a tubular braided cable with an elastic core.," *Textile Research Journal*, vol. 48, no. 2, pp. 81–91, 1978.

[9] R. H. Hopper Jr., J. Grant, and P. Popper, "Mechanics of a hybrid circular braid with an elastic core," *Textile Research Journal*, vol. 65, no. 12, pp. 709–722, 1995.

[10] J. Bach, M. Cherkaoui, L. Corté, S. Cantournet, and D. Ku, "Design considerations for a prosthetic anterior cruciate ligament," *Journal of Medical Devices, Transactions of the ASME*, vol. 6, no. 4, 2012.

[11] J. S. Bach, F. Detrez, M. Cherkaoui, S. Cantournet, D. N. Ku, and L. Corte, "Hydrogel fibers for acl prosthesis: design and mechanical evaluation of pva and pva/uhmwpe fiber constructs," *Journal of biomechanics*, vol. 46, no. 8, pp. 1463–1470, 2013.

[12] J. Cruz, S. Rana, R. Fangueiro, and R. Guedes, "Designing artificial anterior cruciate ligaments based on novel fibrous structures," *Fibers and Polymers*, vol. 15, no. 1, pp. 181–186, 2014.

[13] P. Potluri and S. Nawaz, *Developments in braided fabrics*. 2011.

[14] C. Laurent, D. Durville, D. Mainard, J.-F. Ganghoffer, and R. Rahouadj, "A multilayer braided scaffold for anterior cruciate ligament: Mechanical modeling at the fiber scale," *Journal of the Mechanical Behavior of Biomedical Materials*, vol. 12, pp. 184–196, 2012.

[15] K. Hristov, E. Armstrong-Carroll, M. Dunn, C. Pastore, and Y. Gowayed, "Mechanical behavior of circular hybrid braids under tensile loads," *Textile Research Journal*, vol. 74, no. 1, pp. 20–26, 2004.

[16] S. Nawaz, "Braided cords in flexible composites for aerospace and automotive applications," 2014.

[17] S. Iannace, G. Sabatini, L. Ambrosio, and L. Nicolais, "Mechanical behaviour of composite artificial tendons and ligaments," *Biomaterials*, vol. 16, no. 9, pp. 675–680, 1995.

[18] L. Ambrosio, R. De Santis, and L. Nicolais, "Composite hydrogels for implants," *Proceedings of the Institution of Mechanical Engineers, Part H: Journal of Engineering in Medicine*, vol. 212, no. 2, pp. 93–99, 1998.

[19] L. Ambrosio, R. De Santis, S. Lannace, P. Netti, and L. Nicolais, "Viscoelastic behavior of composite ligament prostheses," *Journal of Biomedical Materials Research*, vol. 42, no. 1, pp. 6–12, 1998.

[20] D. Iliadis, D. Bourlos, D. Mastrokalos, E. Chronopoulos, and G. Babis, "Lars artificial ligament versus abc purely polyester ligament for anterior cruciate ligament reconstruction," *Orthopaedic Journal of Sports Medicine*, vol. 4, no. 6, 2016.

[21] P. S. Thayer, A. F. Dimling, D. S. Plessl, M. R. Hahn, S. A. Guelcher, L. A. Dahlgren, and A. S. Goldstein, "Cellularized cylindrical fiber/hydrogel composites for ligament tissue engineering," *Biomacromolecules*, vol. 15, no. 1, pp. 75–83, 2013.

[22] C. Lou, P. Lu, J. Hu, and J. Lin, "Manufacturing technique and property evaluations of pet/gelatin composite tubular braids," *Advanced Materials Research*, vol. 910, pp. 157–160, 2014.

[23] R. De Santis, F. Sarracino, F. Mollica, P. Netti, L. Ambrosio, and L. Nicolais, "Continuous fibre reinforced polymers as connective tissue replacement," *Composites Science and Technology*, vol. 64, no. 6, pp. 861–871, 2004. cited By 32.

[24] F. Mollica, M. Ventre, F. Sarracino, L. Ambrosio, and L. Nicolais, "Mechanical properties and modelling of a hydrophilic composite used as a biomaterial," *Composites Science and Technology*, vol. 66, no. 1, pp. 92–101, 2006.

[25] E. Roche, R. Wohlfarth, J. Overvelde, N. Vasilyev, F. Pigula, D. Mooney, K. Bertoldi, and C. Walsh, "A bioinspired soft actuated material," *Advanced Materials*, vol. 26, no. 8, pp. 1200–1206, 2014.

[26] A. Faudzi, M. Razif, I. Nordin, K. Suzumori, S. Wakimoto, and D. Hirooka, "Development of bending soft actuator with different braided angles," pp. 1093–1098, 2012.

[27] S. Obiajulu, E. Roche, F. Pigula, and C. Walsh, "Soft pneumatic artificial muscles with low threshold pressures for a cardiac compression device," vol. 6 A, 2013.

[28] A. Rawal, H. Saraswat, and A. Sibal, "Tensile response of braided structures: a review," *Textile Research Journal*, vol. 85, no. 19, pp. 2083–2096, 2015.

[29] B. Gershon, D. Cohn, and G. Marom, "Utilization of composite laminate theory in the design of synthetic soft tissues for biomedical prostheses," *Biomaterials*, vol. 11, no. 8, pp. 548–552, 1990.

[30] B. Boonstra, "Stress-strain properties of natural rubber under biaxial strain," *Journal of Applied Physics*, vol. 21, no. 11, pp. 1098–1104, 1950.

[31] H. Vangerko and L. Treloar, "The inflation and extension of rubber tube for biaxial strain studies," *Journal of Physics D: Applied Physics*, vol. 11, no. 14, pp. 1969–1978, 1978.

[32] M. Latorre and F. J. Montáns, "Material-symmetries congruency in transversely isotropic and orthotropic hyperelastic materials," *European Journal of Mechanics-A/Solids*, vol. 53, pp. 99–106, 2015.

[33] Y. Fung, K. Fronek, and P. Patitucci, "Pseudoelasticity of arteries and the choice of its mathematical expression.," *The American journal of physiology*, vol. 237, no. 5, pp. H620–631, 1979.

[34] W. Sun, M. Sacks, T. Sellaro, W. Slaughter, and M. Scott, "Biaxial mechanical response of bioprosthetic heart valve biomaterials to high in-plane shear," *Journal of Biomechanical Engineering*, vol. 125, no. 3, pp. 372–380, 2003.

[35] M. Sacks, "A method for planar biaxial mechanical testing that includes in-plane shear," *Journal of biomechanical engineering*, vol. 121, no. 5, pp. 551–555, 1999.

[36] G. Holzapfel, T. Gasser, and R. Ogden, "A new constitutive framework for arterial wall mechanics and a comparative study of material models," *Journal of Elasticity*, vol. 61, no. 1-3, pp. 1–48, 2000. cited By 1213.

[37] P. Vena, R. Contro, R. Pietrabissa, and L. Ambrosio, "Design of materials subject to biomechanical compatibility constraints," in *IUTAM Symposium on Synthesis in Bio Solid Mechanics*, pp. 67–78, Springer, 1999.

[38] Y. Lanir, "Constitutive equations for fibrous connective tissues," *Journal of biomechanics*, vol. 16, no. 1, pp. 1–12, 1983.

[39] M. Mooney, "A theory of large elastic deformation," *Journal of Applied Physics*, vol. 11, no. 9, pp. 582–592, 1940.

[40] R. Rivlin, "Large elastic deformations of isotropic materials. iv. further developments of the general theory," *Philosophical Transactions of the Royal Society of London A: Mathematical, Physical and Engineering Sciences*, vol. 241, no. 835, pp. 379–397, 1948.

[41] S. Hirokawa and R. Tsuruno, "Three-dimensional deformation and stress distribution in an analytical/computational model of the anterior cruciate ligament," *Journal of Biomechanics*, vol. 33, no. 9, pp. 1069–1077, 2000.

[42] G. Limbert and M. Taylor, "On the constitutive modeling of biological soft connective tissues: a general theoretical framework and explicit forms of the tensors of elasticity for strongly anisotropic continuum fiber-reinforced composites at finite strain," *International Journal of Solids and Structures*, vol. 39, no. 8, pp. 2343–2358, 2002.

[43] C. Chuong and Y. Fung, "Three-dimensional stress distribution in arteries," *Journal of biomechanical engineering*, vol. 105, no. 3, pp. 268–274, 1983.

[44] M. Zulliger, P. Fridez, K. Hayashi, and N. Stergiopulos, "A strain energy function for arteries accounting for wall composition and structure," *Journal of Biomechanics*, vol. 37, no. 7, pp. 989–1000, 2004.

[45] P. Fridez, M. Zulliger, F. Bobard, G. Montorzi, H. Miyazaki, K. Hayashi, and N. Stergiopulos, "Geometrical, functional, and histomorphometric adaptation of rat carotid artery in induced hypertension," *Journal of biomechanics*, vol. 36, no. 5, pp. 671–680, 2003.

[46] P. Fridez, A. Makino, H. Miyazaki, J.-J. Meister, K. Hayashi, and N. Stergiopulos, "Short-term biomechanical adaptation of the rat carotid to acute hypertension: contribution of smooth muscle," *Annals of biomedical engineering*, vol. 29, no. 1, pp. 26–34, 2001.

[47] T. Gasser, R. Ogden, and G. Holzapfel, "Hyperelastic modelling of arterial layers with distributed collagen fibre orientations," *Journal of the Royal Society Interface*, vol. 3, no. 6, pp. 15–35, 2006.

[48] M. Doumit, *Characterization, Modeling and Design of the Braided Pneumatic Muscle*. PhD thesis, University of Ottawa, Ottawa, Ontario, Canada, KN1 6N5, September 2009.

[49] Smooth-On Inc., "Smooth-on, inc.." https://www.smooth-on.com/, 2016.

[50] Smooth-On Inc., "Ecoflex series: super-soft, addition cure silicone rubbers (technical specifications)," 2015. Original document from Smooth-On Inc.

[51] Smooth-On Inc., "Mold star 20t: 1a:1b mix by volume platinum silicone rubber (technical specifications)," 2015. Original document from Smooth-On Inc.

[52] Smooth-On Inc., "Oomoo series: 1a:1b mix by volume platinum silicone rubber (technical specifications)," 2015. Original document from Smooth-On Inc.

[53] Smooth-On Inc., "Durometer shore hardness scale." https://www.smooth-on.com/page/durometer-shore-hardness-scale/, 2016. Original image from Smooth-On Inc.

[54] Techflex Inc., "Techflex braided sleeving solutions." https://www.techflex.com, 2015.

[55] Wirecare.com Cable Managment Superstore, "Ptn0.13ng - flexo pet - 1/8" - neon green." https://www.wirecare.com/braided-sleeving.asp, 2016. Original image from Wirecare.com.

[56] Wirecare.com Cable Managment Superstore, "Ptn0.25nb - pet tightweave - 1/4" - neon blue." https://www.wirecare.com/braided-sleeving.asp, 2016. Original image from Wirecare.com.

[57] M. Hossain, D. Vu, and P. Steinmann, "Experimental study and numerical modelling of vhb 4910 polymer," *Computational Materials Science*, vol. 59, pp. 65–74, 2012.

[58] R. Hibbeler, *Mechanics of Materials*. Pearson Education, 2016.

[59] G. Holzapfel, *Nonlinear Solid Mechanics: A Continuum Approach for Engineering*. Wiley, 2000.

[60] A. J. M. Spencer, *Continuum Theory of the Mechanics of Fibre-Reinforced Composites*. Vienna: Springer Vienna, 1984.

[61] G. A. Holzapfel and H. W. Weizsäcker, "Biomechanical behavior of the arterial wall and its numerical characterization," *Computers in biology and medicine*, vol. 28, no. 4, pp. 377–392, 1998.

[62] R. Vaishnav, J. Young, and D. Patel, "Distribution of stresses and of strain energy density through the wall thickness in a canine aortic segment," *Circulation Research*, vol. 32, no. 5, pp. 577–583, 1973.

[63] M. S. Sacks and W. Sun, "Multiaxial mechanical behavior of biological materials," *Annual review of biomedical engineering*, vol. 5, no. 1, pp. 251–284, 2003.

[64] J. Humphrey, *Cardiovascular Solid Mechanics: Cells, Tissues, and Organs*. Springer, 2002.

[65] R. N. Vaishnav and J. Vossoughi, "Estimation of residual strains in aortic segments.," pp. 330–333, 1983.

[66] C. Chuong and Y. Fung, "On residual stresses in arteries.," *Journal of Biomechanical Engineering*, vol. 108, no. 2, pp. 189–192, 1986.

[67] J. Humphrey, R. Strumpf, and F. Yin, "A theoretically-based experimental approach for identifying vascular constitutive relations.," *Biorheology*, vol. 26, no. 4, pp. 687–702, 1988.

[68] A. Green and J. Adkins, *Large elastic deformations*. Clarendon Press, 1970.

[69] J. Humphrey, "Mechanics of the arterial wall: Review and directions," *Critical Reviews in Biomedical Engineering*, vol. 23, no. 1-2, pp. 1–162, 1995.

[70] G. Holzapfel and R. Ogden, "Constitutive modelling of arteries," *Proceedings of the Royal Society A: Mathematical, Physical and Engineering Sciences*, vol. 466, no. 2118, pp. 1551–1597, 2010.

[71] G. Holzapfel and R. Ogden, "On planar biaxial tests for anisotropic nonlinearly elastic solids. a continuum mechanical framework," *Mathematics and Mechanics of Solids*, vol. 14, no. 5, pp. 474–489, 2009.

[72] Image Analyst, "Image segmentation tutorial." http://www.mathworks.com/matlabcentral/fileexchange/25157-image-segmentation-tutorial/content/BlobsDemo.m, 2009 updated in 2015. Source code.

Appendices

Appendix A

Assembly Drawing of the Mold

With reference to figure A.1, parts 1 through 4 illustrate the components used to create the mold.

Part 1: flanged end cap - This piece is one of the 3D printed end caps used to create a seal for the mold. It is flanged so that it can easily be removed with pliers during the demolding process.

Part 2: flat end cap - This piece is one of the 3D printed endcaps used to create a seal for the mold. It is flat so that the inner rod will maintain alignment with input and exhaust holes when the end cap is flush with the outer tube.

Part 3: inner brass rod - This part is intended to create the inner radius of the final tubular composite.

Part 4: outer acrylic tube - This part is intended to create the outer radius of the final tubular composite.

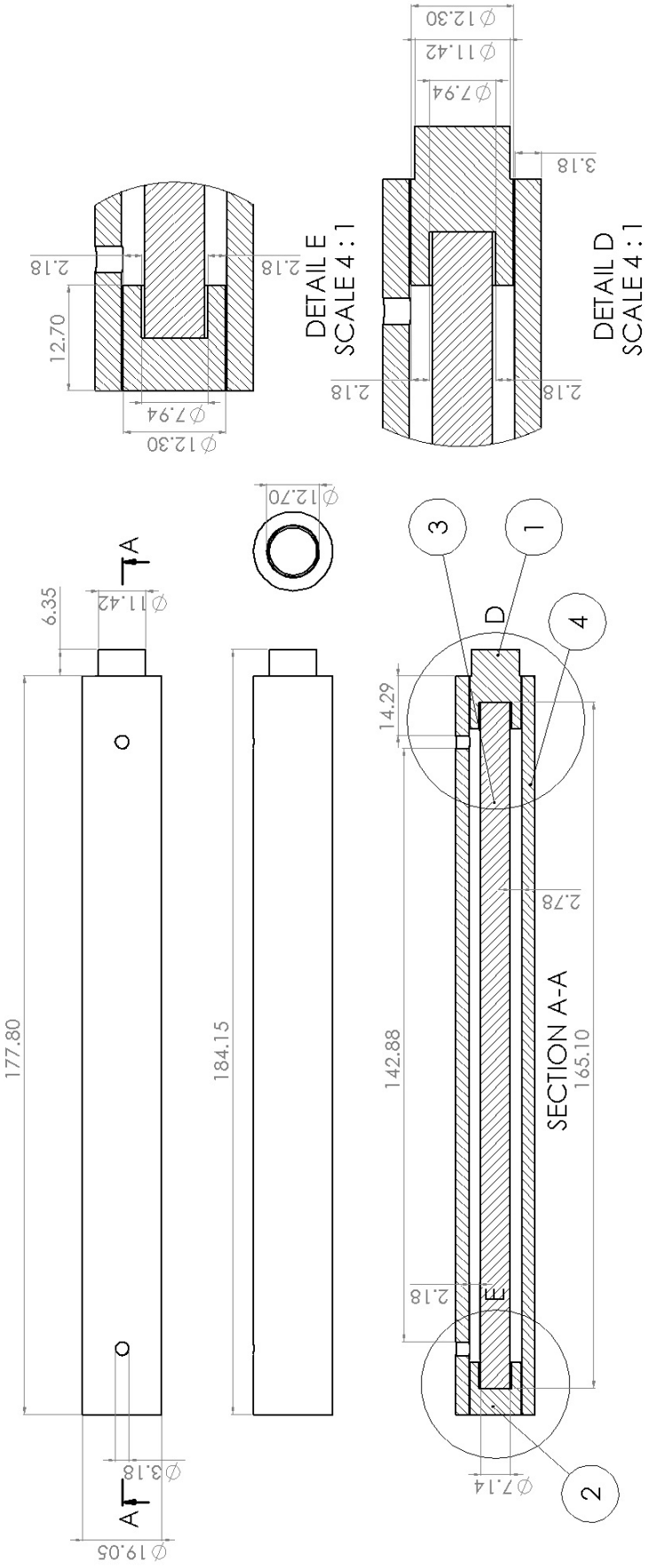

Figure A.1: Assembly drawing of the full mold created on SolidWorks 2016.

Appendix B

Comparison of Results, Continued

In order to give a more in-depth view as to how the material behaves, this section will expand upon section 4.5 by illustrating the relation between the axial force F, and external radius r_o, as well as the external radius r_o, and stretch ratio λ.

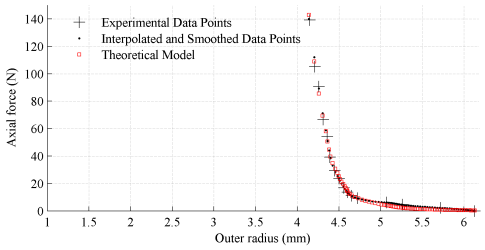

(a) F vs. r_o, Fung

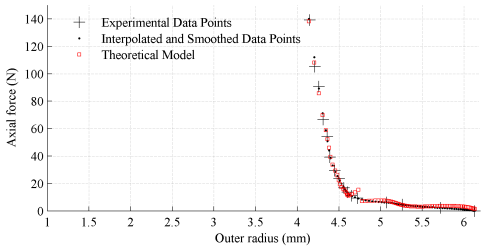

(b) F vs. r_o, Holzapfel

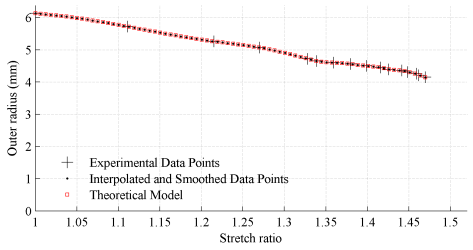

(c) r_o vs. λ, Fung

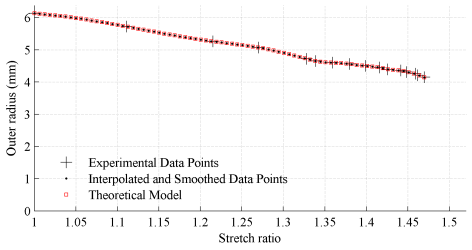

(d) r_o vs. λ, Holzapfel

Figure B.1: Resulting data plots for Fung and Holzapfel strain energy models on specimen T1B4B_55.

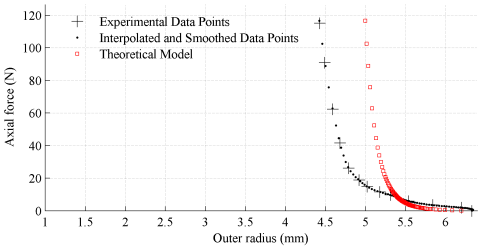

(a) F vs. r_o, Fung

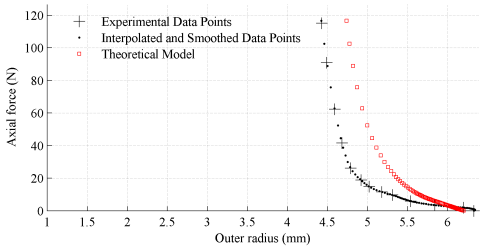

(b) F vs. r_o, Holzapfel

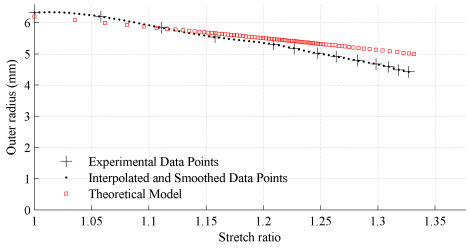

(c) r_o vs. λ, Fung

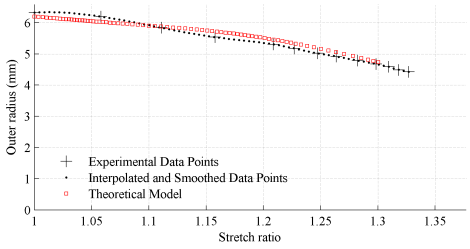

(d) r_o vs. λ, Holzapfel

Figure B.2: Resulting data plots for Fung and Holzapfel strain energy models on specimen T1A4B_43.

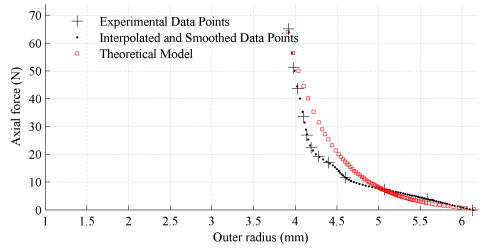

(a) F vs. r_o, Fung

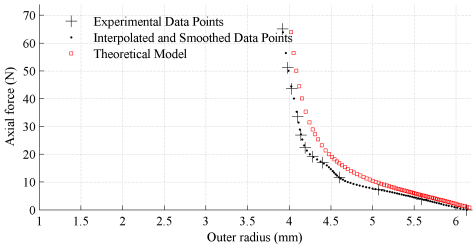

(b) F vs. r_o, Holzapfel

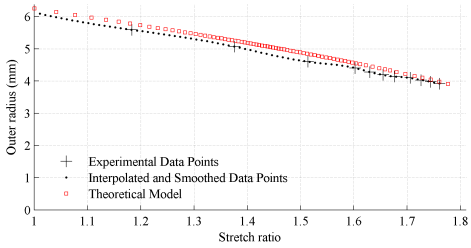

(c) r_o vs. λ, Fung

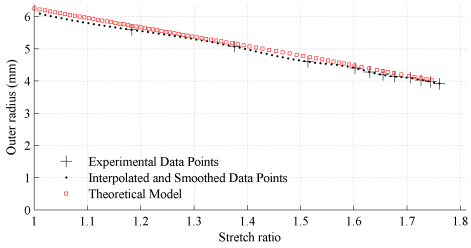

(d) r_o vs. λ, Holzapfel

Figure B.3: Resulting data plots for Fung and Holzapfel strain energy models on specimen R1B4C_56.

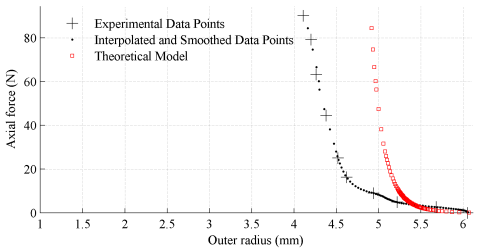

(a) F vs. r_o, Fung

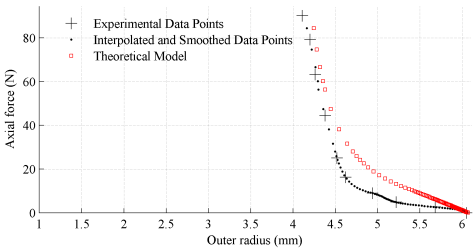

(b) F vs. r_o, Holzapfel

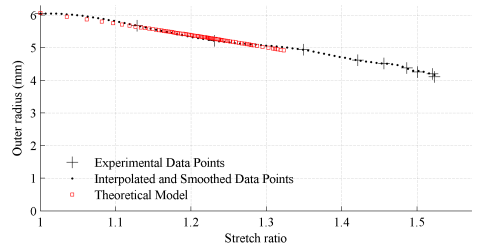

(c) r_o vs. λ, Fung

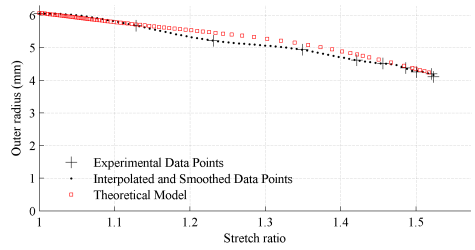

(d) r_o vs. λ, Holzapfel

Figure B.4: Resulting data plots for Fung and Holzapfel strain energy models on specimen T1B4B_52 using material constants from fitting T1A4B_43.

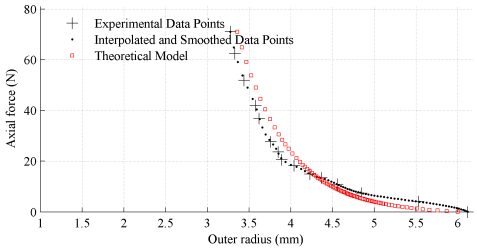

(a) F vs. r_o, Fung

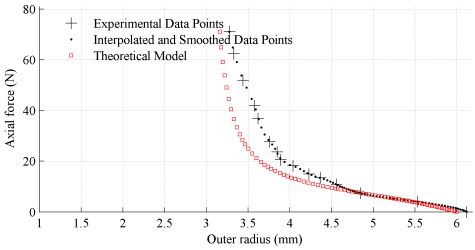

(b) F vs. r_o, Holzapfel

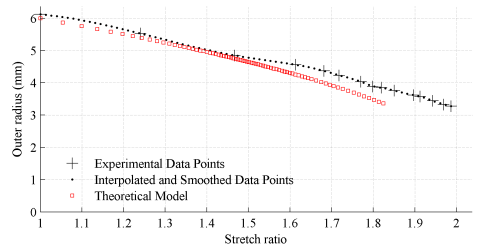

(c) r_o vs. λ, Fung

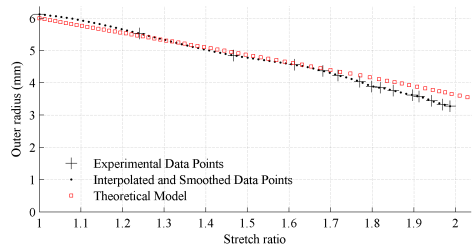

(d) r_o vs. λ, Holzapfel

Figure B.5: Resulting data plots for Fung and Holzapfel strain energy models on specimen R1C4C_64 using material constants from fitting R1B4C_56.

Appendix C

Determining Theoretical Results: Pseudocode

This section illustrates the general algorithms used to determine the material constants of the any of the two strain energy functions, as well as the theoretical values produced by (4.59) and (4.62). The function *materialconstants* is called by a main function that passes parameters regarding experimental data and arbitrary starting material constants for the strain energy function.

Algorithm 1 Determine optimized material constants and theoretical values.

function MATERIALCONSTANTS($c_i, R_i, R_o, \Theta_0, \alpha, P_{exp}, r_{outexp}, \lambda_{exp}, F_{exp}$)
  options $\leftarrow$ *options set for lsqnonlin*
  $w \leftarrow$ [*6 Gauss weights*] ▷ from table 4.1
  $\xi \leftarrow$ [*6 Gauss nodes*] ▷ from table 4.1
  $c_{arb} \leftarrow c_i$ ▷ $c_{arb} = c_i$ are arbitrary initial constants
  $r\lambda_{exp} \leftarrow [r_{outexp}, \lambda_{exp}]$
  $c \leftarrow$ *lsqnonlin*(*@x*, ERRORPF($x, r\lambda_{exp}, R_o, R_i, \Theta_0, \alpha, w, \xi, P_{exp}, F_{exp}$), c_{arb}, *options*)
  $r\lambda_{initial} \leftarrow [r_{outexp}, \lambda_{exp}]$
  $r\lambda_{theo} \leftarrow$ *lsqnonlin*(*@x*, ERRORPF($c, x, R_o, R_i, \Theta_0, \alpha, w, \xi, P_{exp}, F_{exp}$), $r\lambda_{initial}$, *options*)
  $[P_{theo}, F_{theo}] \leftarrow \mathrm{PF}(r\lambda_{theo}, R_o, R_i, \Theta_0, \alpha, w, \xi, c)$
  return P_{theo}, F_{theo}, c
end function

Algorithm 2 Calculate error between theoretical and experimental values.

function ERRORPF($c, r\lambda_{exp}, R_o, R_i, \Theta_0, \alpha, w, \xi, P_{exp}, F_{exp}$)
  $[P_{theo}, F_{theo}] \leftarrow \mathrm{PF}(r\lambda_{exp}, R_o, R_i, \Theta_0, \alpha, w, \xi, c)$
  if *Holzapfel's SEF* **then**
    $e_{pressure} \leftarrow (P_{theo} - P_{exp})$
    $e_{force} \leftarrow (F_{theo} - F_{exp})(R_o^2)$
  else if *Fung's SEF* **then**
    $e_{pressure} \leftarrow (P_{theo} - P_{exp})(R_o^2)$
    $e_{force} \leftarrow (F_{theo} - F_{exp})$
  end if
  $e \leftarrow [e_{pressure}; e_{force}]$ ▷ e is the total error vector
  return e
end function

Algorithm 3 Calculate the theoretical internal pressure and axial force.

function PF($r\lambda_{exp}, R_o, R_i, \Theta_0, \alpha, w, \xi, c$)
  $r_o \leftarrow r\lambda_{exp}[:, 1]$
  $\lambda \leftarrow r\lambda_{exp}[:, 2]$
  $r_i \leftarrow \sqrt{r_o^2 - \frac{\Theta_0}{\pi\lambda}\left(R_o^2 - R_i^2\right)}$
  for $g \leq length(\xi)$ **do**
    $r \leftarrow \frac{r_i + r_o}{2} + \frac{\xi[g]}{2}(r_o - r_i)$
    $R \leftarrow \sqrt{R_i^2 + \frac{\pi\lambda}{\Theta_0}\left(r^2 - r_i^2\right)}$
    $E_{\theta\theta} \leftarrow \frac{1}{2}\left(\left(\frac{\pi r}{\Theta_0 R}\right)^2 - 1\right)$
    $E_{ZZ} \leftarrow \frac{1}{2}\left(\lambda^2 - 1\right)$
    if *Holzapfel's SEF* **then**
      $\left[\frac{\partial W}{\partial E_{\theta\theta}}, \frac{\partial W}{\partial E_{ZZ}}\right] \leftarrow$ HolzapfelPDE$(c, E_{\theta\theta}, E_{ZZ}, \alpha)$
    else if *Fung's SEF* **then**
      $\left[\frac{\partial W}{\partial E_{\theta\theta}}, \frac{\partial W}{\partial E_{ZZ}}\right] \leftarrow$ FungPDE$(c, E_{\theta\theta}, E_{ZZ})$
    end if
    $P_{theo} \leftarrow P_{theo} + \left(\frac{w[g]}{r}\right)\left(\frac{\pi r}{\Theta_0 R}\right)^2\left(\frac{\partial W}{\partial E_{\theta\theta}}\right)$
    $F_{theo} \leftarrow F_{theo} + (w[g]r)\left(\left(2\lambda^2\frac{\partial W}{\partial E_{ZZ}}\right) - \left(\frac{\pi r}{\Theta_0 R}\right)^2\left(\frac{\partial W}{\partial E_{\theta\theta}}\right)\right)$
  end for
  $P_{theo} \leftarrow P_{theo}\left(\frac{r_o - r_i}{2}\right)$
  $F_{theo} \leftarrow \pi F_{theo}\left(\frac{r_o - r_i}{2}\right)$
  return P_{theo}, F_{theo}
end function

Algorithm 4 Partial derivative calculators for both Holzapfel's and Fung's strain energy functions.

function HolzapfelPDE$(c, E_{\theta\theta}, E_{ZZ}, \alpha)$
  $I_4(\mathbf{E}) \leftarrow \cos^2\alpha(2E_{\theta\theta} + 1) + \sin^2\alpha(2E_{ZZ} + 1)$
  $I_6(\mathbf{E}) \leftarrow \cos^2\alpha(2E_{\theta\theta} + 1) + \sin^2\alpha(2E_{ZZ} + 1)$
  $Q_1 \leftarrow (I_4 - 1)^2$
  $Q_2 \leftarrow (I_6 - 1)^2$
  $\Delta \leftarrow (2E_{\theta\theta} + 1)(2E_{ZZ} + 1)$
  $\frac{\partial W}{\partial E_{\theta\theta}} \leftarrow c_1\left(1 - \frac{1}{\Delta(2E_{\theta\theta}+1)}\right) + 2c_2\cos^2\alpha\left((I_4 - 1)\exp(c_3Q_1) + (I_6 - 1)\exp(c_3Q_2)\right)$
  $\frac{\partial W}{\partial E_{ZZ}} \leftarrow c_1\left(1 - \frac{1}{\Delta(2E_{zz}+1)}\right) + 2c_2\sin^2\alpha\left((I_4 - 1)\exp(c_3Q_1) + (I_6 - 1)\exp(c_3Q_2)\right)$
  return $\frac{\partial W}{\partial E_{\theta\theta}}, \frac{\partial W}{\partial E_{ZZ}}$
end function

function FungPDE$(c, E_{\theta\theta}, E_{ZZ})$
  $\frac{\partial W}{\partial E_{\theta\theta}} \leftarrow c_1\left(c_2E_{\theta\theta} + c_4E_{ZZ}\right)\exp\left(c_2E_{\theta\theta}^2 + c_3E_{ZZ}^2 + 2c_4E_{\theta\theta}E_{ZZ}.\right)$
  $\frac{\partial W}{\partial E_{ZZ}} \leftarrow c_1\left(c_4E_{\theta\theta} + c_3E_{ZZ}\right)\exp\left(c_2E_{\theta\theta}^2 + c_3E_{ZZ}^2 + 2c_4E_{\theta\theta}E_{ZZ}.\right)$
  return $\frac{\partial W}{\partial E_{\theta\theta}}, \frac{\partial W}{\partial E_{ZZ}}$
end function

Appendix D

MATLAB Script

D.1 Main function

```
% ------------------------------------------------------------------------
% This is the main body of the code used for the analysis of my thesis
% Robert Shaheen (5273205)
% Summer 2016
% ------------------------------------------------------------------------

function main_analysis()
clc; % Clears command window each re-run
clear all; % Clears everything on re-run
format longg; % Sets the number of decimal places in the output
format compact; % Format for output window

% Number of specimens that will be fit.
% Anything > 1 will only compare the latter specimens to the constants
% fitted with the first specimen.
numberFits = 2;
% Number of Strain Energy Functions
numberSEF = 2;
% Initial constants for holzapfel and fung model.
holzapfelConstants = [1 0.1 0.1];
fungConstants = [1 0.1 0.1 0.1];
for k = 1:1:numberFits
    % ------------------------------------------------------------------------
    % Open the user-specified specimen raw data by requesting the user
    % input.
    % ------------------------------------------------------------------------
    flag = 0;
    while flag == 0
        prompt = ...
            'Please identify which specimen you would like to analyze:\n';
        containmentFolder = ['D:\MASc mechanical engineering'...
            ,'\.MCG 7999 Thesis\analysis\raw specimen data\'];
        specimenSelection = input(prompt, 's');
        baseFileName = '\raw_data.txt';
```

```
    fullFileName = sprintf('%s%s%s',containmentFolder,...
        specimenSelection,baseFileName); % Location of the raw_data
    % Make sure that the file exists, otherwise abort program
    if ~exist(fullFileName, 'file')
        % Check if the specified file exists
        warningMessage = ...
            sprintf('Error: the input file\n%s\nwas not found',...
            fullFileName);
        uiwait(warndlg(warningMessage));
    else
        flag = 1;
    end
end
tic;
rawDataFile = fopen(fullFileName, 'rt'); % Open the chosen file
baseFileNameOutput = '\output_data.txt';
fullFileNameOutput = sprintf('%s%s%s',containmentFolder,...
    specimenSelection,baseFileNameOutput);
% Create an output file
outputDataFile = fopen(fullFileNameOutput,'w');
% Assign the text file numbers to variable/variable arrays
cellArray = textscan(rawDataFile, '%f %f %f %f %f %f', 1);
RadiusOut = cellArray{1}(1); % Initial outer radius (mm)
fprintf(outputDataFile,'Initial Outer Radius = %f(mm)\r\n',RadiusOut);
RadiusIn = cellArray{2}(1); % Initial inner radius (mm)
fprintf(outputDataFile,'Initial Inner Radius = %f(mm)\r\n',RadiusIn);
theta0 = cellArray{3}(1); % Stress relief angle (deg)
fprintf(outputDataFile,'Opening Angle = %f(deg)\r\n',theta0);
theta0 = theta0*pi/180; % Stress relief angle (rad)
% % Original leng between markers (mm)
% initialDotLength = cellArray{5}(1);
alpha = 90 - cellArray{4}(1);  % Initial braid angle (deg)
% initialFullLength = cellArray{6}(1);
% Initial full length:  end->end (mm)/hopefully is not used
% 90 - alpha because for doumit the angle is
% measured from the axial axis but the analysis uses
% the angle measured from the tangential axis.
fprintf(outputDataFile,...
    'Braiding Angle = %f(deg), from horizon\r\n',alpha);
fprintf(outputDataFile,'\r\n');
alpha = alpha*pi/180; % Initial braid angle (rad)
% Scan the rest of the file and assign to variable, then close
cellArray = textscan(rawDataFile, '%f %f %f %f');
fclose(rawDataFile);
% Import the data points for the raw data measurements
pressureExpRaw = cellArray{1};  % Experimental pressure (MPa)
radiusOutExpRaw = cellArray{2};
% Experimental inner rad in current reference frame (mm)
axialForceExpRaw = cellArray{3}; % Expermimental z-force (N)
% % The elongalation measured from the instron (mm)
% fullElongation = cellArray{4};

% ------------------------------------------------------------------
% Determine the axial stretch, lambda, using the image recogonition
% software function and the 12 images taken during testing for the
% selected specimen.
% ------------------------------------------------------------------
fprintf('Determining stretch ratio through image analysis...\n');
pythagoreanDistance = zeros(numel(axialForceExpRaw),1);
```

```
for i = 1:1:numel(pythagoreanDistance)
    % Will be from 1 to n when I have n images to sort through
    fprintf(outputDataFile,...
        'Picture number %d/%d:\r\n',i,numel(pythagoreanDistance));
    baseFileName = sprintf('\\elongation_%d.JPG',i);
    % Location of the elongation image
    fullFileName = sprintf('%s%s%s',containmentFolder,...
        specimenSelection,baseFileName);
    pythagoreanDistance(i,1) = image_processing(fullFileName,...
        outputDataFile,i,numel(pythagoreanDistance));
end
% Determine the experimental stretch ratis from the returned values
% from the image analysis function.
lambdaExpRaw = pythagoreanDistance(:,1)./pythagoreanDistance(1,1);
fprintf(outputDataFile,...
    '\r\nPythagorean distance (pixels)\tStretch Ratio (lambda)\r\n');
for i = 1:1:numel(pythagoreanDistance)
    fprintf(outputDataFile,'%f\t\t\t', pythagoreanDistance(i,1));
    fprintf(outputDataFile,'%f\r\n', lambdaExpRaw(i,1));
end
fprintf(outputDataFile,'————————————————————————————————————————\r\n');

% ————————————————————————————————————————————————————————————————————
% pressureExpRaw,radiusInExpRaw,axialForceExpRaw,lambdaExpRaw, only
% have about 12 data points.  They will be interpolated to yield about
% 75 data points using a spline interpolation.
% ————————————————————————————————————————————————————————————————————
fprintf('Finished image analysis.\n');
fprintf('Interpolating data points...\n');
[pressureExp radiusOutExp lambdaExp axialForceExp] = ...
    spline_interpolation(pressureExpRaw, radiusOutExpRaw,...
    lambdaExpRaw, axialForceExpRaw);
% Print for debug purpose, may edit out later
fprintf(outputDataFile,['\r\nThere are %d interpolated pressure '...
    ,'points\r\n'],numel(pressureExp));
fprintf(outputDataFile,['\r\nThere are %d interpolated radiusOut '...
    ,'points\r\n'],numel(radiusOutExp));
fprintf(outputDataFile,['\r\nThere are %d interpolated lambda '...
    ,'points\r\n'],numel(lambdaExp));
fprintf(outputDataFile,['\r\nThere are %d interpolated axialForce '...
    ,'points\r\n'],numel(axialForceExp));
fprintf(outputDataFile,'————————————————————————————————————————\r\n');
% Make sure all of the arrays are column vectors
pressureExp = pressureExp';
lambdaExp = lambdaExp';
% %%%%%%%%%%%%%%%%%%%%%%%%% IF NO SMOOTHING IS APPLIED UNCOMMENT BELOW
%  axialForceExp = axialForceExp';
%  radiusOutExp = radiusOutExp';
% %%%%%%%%%%%%%%%%%%%%%%%%%%%%%%%%%%%%%%%%%%%%%%%%%%%%%%%%%%%%%%%%%%%%%%%
% Plot the results of the experimental interpolation values in the
% output document.
fprintf(outputDataFile,'Pressure\tRadius\t\tLambda\t\tForce\r\n');
for i = 1:1:numel(pressureExp)
    fprintf(outputDataFile,'%f\t%f\t%f\t%f\r\n', pressureExp(i,1),...
        radiusOutExp(i,1),lambdaExp(i,1),axialForceExp(i,1));
end
fprintf(outputDataFile,'————————————————————————————————————————\r\n');
% For plotting purposes, find the max force, radius, and lambda
maxForce = 0;
```

```
maxRadius = 0;
maxLambda = 0;
for i = 1:1:numel(axialForceExp)
    if maxForce < axialForceExp(i,1)
        maxForce = axialForceExp(i,1);
    end
    if maxRadius < radiusOutExp(i,1)
        maxRadius = radiusOutExp(i,1);
    end
    if maxLambda < lambdaExp(i,1)
        maxLambda = lambdaExp(i,1);
    end
end
% ------------------------------------------------------------------------
% Determine the material constants of the specimen and output them to
% the document.
% ------------------------------------------------------------------------
fprintf('Finished interpolating.\n');
fprintf('Optimizing material constants...\n');
for i = 1:1:numberSEF
    if i == 1
        modelSelection = 'holzapfel';
    elseif i == 2
        modelSelection = 'fung';
    end
    [holzapfelConstants,fungConstants,radLambTheo,axialForceTheo]...
        = material_constants(holzapfelConstants,fungConstants,...
        RadiusOut,RadiusIn,theta0,alpha,pressureExp,radiusOutExp,...
        lambdaExp,axialForceExp,modelSelection,k);
    fprintf(outputDataFile,...
        '\r\nThe material constants for %s are:\r\n',modelSelection);
    if i == 1
        materialConstants = holzapfelConstants;
    elseif i == 2
        materialConstants = fungConstants;
    end
    for j = 1:1:numel(materialConstants)
        fprintf(outputDataFile,'c%d = %f\r\n', j,...
            materialConstants(1,j));
    end
    % ------------------------------------------------------------------
    % Graphing interpolated and theoretcial results and saving
    % the files.  Stretch ratio vs. Axial force
    theoForceElongation = figure();
    if strcmp(specimenSelection,'R1c4c_64') == 1 && k == 2
        xAxisLimit = 2.3;
    else
        xAxisLimit = maxLambda + 0.05;
    end
    yAxisLimit = maxForce + 10;
    labelXAxis = 'Stretch ratio';
    labelYAxis = 'Axial force (N)';
    % Call the plot function to ensure consitency
    % within graphing format
    plot_this_for_me(theoForceElongation,xAxisLimit,yAxisLimit,...
        labelXAxis,labelYAxis)
    % Plot the results
    hold on;
    plot(lambdaExpRaw,axialForceExpRaw,'k+','Linewidth',0.5,...
```

```
    'MarkerSize',9);
plot(lambdaExp,axialForceExp,'k.','MarkerSize',5);
plot(radLambTheo(:,2),axialForceTheo,'rs','MarkerSize',3);
hold off;
% Apply a legend to the graph
legend('Experimental Data Points',...
    'Interpolated and Smoothed Data Points',...
    'Theoretical Model','Location','NorthWest');
% Turn the box around the legend off
legend boxoff;
% Save the figure to use for the latex file document.
fileLocation = ['D:\MASc mechanical engineering\.MCG 7999'...
    ,' Thesis\written\images\graphs'];
if k == 1
    nameForFile = sprintf('%s_%s_theo_force_lambda_fitted',...
        specimenSelection,modelSelection);
else
    nameForFile = sprintf('%s_%s_theo_force_lambda',...
        specimenSelection,modelSelection);
end
save_this_for_me(fileLocation,nameForFile,theoForceElongation);
% ------------------------------------------------------------------
% Graphing experimental and theoretcial results and saving
% the files.  Stretch ratio vs. Radius
theoRadiusElongation = figure();
xAxisLimit = maxLambda + 0.05;
yAxisLimit = maxRadius + 0.25;
labelXAxis = 'Stretch ratio';
labelYAxis = 'Outer radius (mm)';
% Call the plot function to ensure consitency within graphing
% format
plot_this_for_me(theoRadiusElongation,xAxisLimit,yAxisLimit,...
    labelXAxis,labelYAxis)
% Plot the results
hold on;
plot(lambdaExpRaw,radiusOutExpRaw,'k+','Linewidth',0.5,...
    'MarkerSize',9);
plot(lambdaExp,radiusOutExp,'k.','MarkerSize',5);
plot(radLambTheo(:,2),radLambTheo(:,1),'rs','MarkerSize',3);
hold off;
% Apply a legend to the graph
legend('Experimental Data Points',...
    'Interpolated and Smoothed Data Points',...
    'Theoretical Model','Location','SouthWest');
% Turn the box around the legend off
legend boxoff;
% Save the figure to use for the latex file document.
fileLocation = ['D:\MASc mechanical engineering\.MCG 7999'...
    ,' Thesis\written\images\graphs'];
if k == 1
    nameForFile = sprintf('%s_%s_theo_lambda_radius_fitted',...
        specimenSelection,modelSelection);
else
    nameForFile = sprintf('%s_%s_theo_lambda_radius',...
        specimenSelection,modelSelection);
end
save_this_for_me(fileLocation,nameForFile,theoRadiusElongation);
% ------------------------------------------------------------------
% Graphing experimental and theoretcial results and saving
```

```
        % the files.  Radius vs. Axial force
        theoForceRadius = figure();
        xAxisLimit = maxRadius + 0.05;
        yAxisLimit = maxForce + 10;
        labelXAxis = 'Outer radius (mm)';
        labelYAxis = 'Axial force (N)';
        % Call the plot function to ensure consitency within graphing
        % format
        plot_this_for_me(theoForceRadius,xAxisLimit,yAxisLimit,...
            labelXAxis,labelYAxis)
        % Plot the results
        hold on;
        plot(radiusOutExpRaw,axialForceExpRaw,'k+','Linewidth',0.5,...
            'MarkerSize',9);
        plot(radiusOutExp,axialForceExp,'k.','MarkerSize',5);
        plot(radLambTheo(:,1),axialForceTheo,'rs','MarkerSize',3);
        hold off;
        % Apply a legend to the graph
        legend('Experimental Data Points',...
            'Interpolated and Smoothed Data Points',...
            'Theoretical Model','Location','NorthWest');
        % Turn the box around the legend off
        legend boxoff;
        % Save the figure to use for the latex file document.
        fileLocation = ['D:\MASc mechanical engineering\.MCG 7999'...
            ,' Thesis\written\images\graphs'];
        if k == 1
            nameForFile = sprintf('%s_%s_theo_force_radius_fitted',...
                specimenSelection,modelSelection);
        else
            nameForFile = sprintf('%s_%s_theo_force_radius',...
                specimenSelection,modelSelection);
        end
        save_this_for_me(fileLocation,nameForFile,theoForceRadius);
    end
    % Close the output file
    fclose(outputDataFile);
end
beep on; beep;
fprintf('DONE!  Time to stand :P\n');
toc;
end
```

D.2 Image processing function

```
% ------------------------------------------------------------------------
% The purpose of this function is to analyze photos of the composite that
% track its elongation.  The function will output the pythagorean distance,
% in pixels, between the centroids of two markers that are put onto the
% tendon.  This function will be called 12 times per tendon, and each
% distance will be divided by the original distance to determine the
% stretch ratio.
% ------------------------------------------------------------------------

function pythagoreanDistance = image_processing(fullFileName,...
    outputDataFile,iterationNumber,numIterationsTotal)
 fileLocation = ['D:\MASc mechanical engineering\.MCG 7999'...
```

```
            ,' Thesis\written\images\'];
% Font size for captions
captionFontSize = 10;
% Read the image file that is passed from main().
originalImage = imread(fullFileName);
originalImage = rgb2gray(originalImage); % Convert to grayscale
% ------------------------------------------------------------------------
% Plot the grayscale image
if iterationNumber <= numIterationsTotal && iterationNumber >= 1
    % Can change conditions to isolate figures that show up during
    % iterations
    imageProcessingExample = figure();
    set(imageProcessingExample,'visible','off');
end
subplot(2, 2, 1);
set(gcf,'visible','off')
imshow(originalImage);
% Force it to display RIGHT NOW.
drawnow;
caption = sprintf('Original tendon image made grayscale.');
title(caption, 'FontSize', captionFontSize);
% ------------------------------------------------------------------------
% Threshold the grayscale image to get a binary
% image using a logical operation
thresholdValue = 43; % This value was hand picked.  It may change
% The < symbol turns all dark pixels white and makes the background black
binaryImage = originalImage < thresholdValue;
% Cleanup the image by filling any holes in the binary image
binaryImage = imfill(binaryImage, 'holes');
% ------------------------------------------------------------------------
% Display the binary image
subplot(2, 2, 2);
set(gcf,'visible','off')
imshow(binaryImage);
title('Binary Image, obtained by thresholding',...
    'FontSize', captionFontSize);

% ------------------------------------------------------------------------
% This function looks at the connected pixels and seperates the blobs from
% the background by creating a matrix the same size as the image matrix
% with a number n for the blobs and 0 for the background
labeledImage = bwlabel(binaryImage, 8);
% note that bwconncomp does the same function but uses less memory.
% Assign each blob a different color to visually show the user the distinct
% blobs.
coloredLabels = label2rgb (labeledImage, 'hsv', 'k', 'shuffle');
% pseudo random color labels
% ------------------------------------------------------------------------
subplot(2, 2, 3);
set(gcf,'visible','off')
imshow(coloredLabels);
axis image; % Make sure image is not artificially stretched
% because of screen's aspect ratio.
caption = sprintf('Pseudo colored labels.');
title(caption, 'FontSize', captionFontSize);

% ------------------------------------------------------------------------
% Get all the blob properties.
blobMeasurements = regionprops(labeledImage, originalImage, 'all');
```

```
numberOfBlobs = size(blobMeasurements, 1);
% ------------------------------------------------------------------------
% bwboundaries() returns a cell array, where each cell
% contains the row/column coordinates for an object in the image.
% Plot the borders of all the coins on the original grayscale
% image using the coordinates returned by bwboundaries.
subplot(2, 2, 4);
set(gcf,'visible','off')
imshow(originalImage);
title('Outlines, from bwboundaries()', 'FontSize', captionFontSize);
axis image; % Make sure image is not artificially
% stretched because of screen's aspect ratio.
hold on;
boundaries = bwboundaries(binaryImage);
numberOfBoundaries = size(boundaries, 1);
for k = 1 : numberOfBoundaries
    thisBoundary = boundaries{k};
    plot(thisBoundary(:,2), thisBoundary(:,1), 'g', 'LineWidth', 2);
end
hold off;

% ------------------------------------------------------------------------
% Used to control size of "blob number" labels put atop the image.
textFontSize = 14;
% Used to align the labels in the centers of the coins.
labelShiftX = -7;
blobECD = zeros(1, numberOfBlobs);
% Print header line in the command window.
stringHeadPt1 = 'Blob #    Area   ';
stringHeadPt2 = '   Centroid(x,y)    Diameter';
fprintf(outputDataFile,'%s%s\r\n',stringHeadPt1,stringHeadPt2);
% Loop over all blobs printing their measurements to the command window.
for k = 1 : numberOfBlobs           % Loop through all blobs.
    blobArea = blobMeasurements(k).Area;
    % Get area.
    blobCentroid = blobMeasurements(k).Centroid;
    % Get centroid one at a time
    blobECD(k) = sqrt(4 * blobArea / pi);
    % Compute ECD - Equivalent Circular Diameter.
    fprintf(outputDataFile,...
        '#%2d %11.1f %8.1f %8.1f % 8.1f\r\n',...
        k, blobArea, blobCentroid, blobECD(k));
    % Put the "blob number" labels on the "boundaries" grayscale image.
    text(blobCentroid(1) + labelShiftX, blobCentroid(2),...
        num2str(k), 'FontSize', textFontSize, 'FontWeight', 'Bold');
end
% Algorithm to find the largest 2 areas.  This is used to get rid of any
% extra blobs that may have been found due to improper image editing.
allBlobAreas = [blobMeasurements.Area]';
largest = 0;
largest2 = 0;
for k = 1 : numberOfBlobs
    if largest < allBlobAreas(k)
        largest = allBlobAreas(k);
        flag = k;
    end
end
for k = 1 : numberOfBlobs
    if (largest2 < allBlobAreas(k)) && (k ~= flag)
```

```
        largest2 = allBlobAreas(k);
    end
end
% Reduce the original blobMeasurements array to only useful blobs
% determined by the 2 largest areas.
usefulCentroid = zeros(2,2);
lineTag = 0;
for k = 1 : numberOfBlobs
    if (blobMeasurements(k).Area == largest)...
            || (blobMeasurements(k).Area == largest2)
        lineTag = lineTag + 1;
        usefulCentroid(lineTag,:) = blobMeasurements(k).Centroid;
    end
end
fprintf(outputDataFile,...
    '\r\nCentroid(x,y) of useful blobs (in pixels):\r\n');
for i = 1:1:2
    fprintf(outputDataFile,...
        '%8.1f\t%8.1f\r\n', usefulCentroid(i,1),usefulCentroid(i,2));
end
fprintf(outputDataFile,'-------------------------------------------------\r\n');
subplot(2, 2, 1);
set(gcf,'visible','off')
hold on; % Don't blow away image.
for k = 1 : 2 % Loop through all keeper blobs.
    plot(usefulCentroid(k,1),usefulCentroid(k,2),...
            'r+', 'MarkerSize', 5, 'LineWidth', 1);
end
h = imline(gca,[usefulCentroid(1,1),usefulCentroid(2,1)],...
    [usefulCentroid(1,2),usefulCentroid(2,2)]);
% Determine the pythagorean distance between the 2 useful centroids.
% This value is meant to be passed back to the main script to be used
% for the strecth ratio value.
pythagoreanDistance = sqrt((usefulCentroid(2,1)-...
    usefulCentroid(1,1))^2 + (usefulCentroid(2,2)-usefulCentroid(1,2))^2);
% For file saving purposes to put into the report
if iterationNumber == 1
    nameForFile = 'image_processing_example';
    save_this_for_me(fileLocation,nameForFile,imageProcessingExample);
end
end
```

D.3 Spline interpolation function

```
% ------------------------------------------------------------------------
% This function interpolates 12 data points into 100 data
% points for a force, radius, and stretch ratio for certain data pairs.
% P will be held at zero.  This data set is held as 2 seperate 2d spline
% interpolation functions.  If this works it is not neccessary to involve
% tensor product splines, which dabbles in mathematical knot theory.
% ------------------------------------------------------------------------

function [pressureExp,radiusOutExp,lambdaExp,axialForceExp] = ...
    spline_interpolation(pressureExpRaw,radiusOutExpRaw,...
    lambdaExpRaw,axialForceExpRaw)
% The number of points that I want to interpolate to
numInterpolatePoints = 75;
```

```
% Determine the bounds of the extension array, and then the step size
% based on the number of interpolation points that I want.
minLambda = lambdaExpRaw(1,1);
maxLambda = lambdaExpRaw(numel(lambdaExpRaw),1);
stepSizeLambda = (maxLambda - minLambda)/numInterpolatePoints;
% Size the inputs to ensure they match in size for failsafe
sizeLambdaExpRaw = numel(lambdaExpRaw);
sizeRadiusOutExpRaw = numel(radiusOutExpRaw);
% Generate the data points for the new force array
lambdaExp = minLambda:stepSizeLambda:maxLambda;
sizeLambdaExp = numel(lambdaExp);
% 2D Spline interpolation Lambda vs Radius
if sizeLambdaExpRaw == sizeRadiusOutExpRaw
    radiusOutExp = spline...
        (lambdaExpRaw,radiusOutExpRaw,lambdaExp);
    radiusOutExp = smooth(radiusOutExp,0.1,'loess');
else
    warningMessage = ...
    sprintf('Error: sizing of variable inputs does not match (Radius)');
    uiwait(warndlg(warningMessage));
    quit force;
end
% Let's do the same thing with the force, F, using the same stretch ratio
% values.
sizeAxialForceExpRaw = numel(axialForceExpRaw);
if sizeLambdaExpRaw == sizeAxialForceExpRaw
    axialForceExp = spline...
         (lambdaExpRaw,axialForceExpRaw,lambdaExp);
    axialForceExp = smooth(axialForceExp,0.1,'loess');
else
    warningMessage = ...
    sprintf('Error: sizing of variable inputs does not match (Force)');
    uiwait(warndlg(warningMessage));
    quit force;
end

% lambdaExp = smooth(lambdaExp,0.10,'loess');
% Create an array with zeros for the pressure that is the size of the new
% values.
sumPressure = 0;
for i = 1:1:numel(pressureExpRaw)
    sumPressure = sumPressure + pressureExpRaw(i,1);
end
if sumPressure == 0
    pressureExp = zeros(1,sizeLambdaExp);
else
    warningMessage = ...
    sprintf('Error: Pressure matrix is not 0');
    uiwait(warndlg(warningMessage));
    quit force;
end
end
```

D.4 Material constants and theoretical results

```
% ------------------------------------------------------------------------
% The purpose of this function is to input the initial data from the
```

```
% spline interpolation function, as well as the initial data from the
% stress free and referential configuration, and output material constants
% that describe the specimen.  The code will use a nonlinear error
% reduction method, the levenberg marquardt method (lsqnonlin) to fit the
% theoretical curves to the experimental results.
%
% This function will also reevaluate the radius and strech ratio to
% determine the theoretical force and pressure values.
% ------------------------------------------------------------------------

function [holzapfelConstants,fungConstants,radLambTheo,axialForceTheo]...
    = material_constants(holzapfelConstants,fungConstants,RadiusOut,...
    RadiusIn,theta0,alpha,pressureExp,radiusOutExp,lambdaExp,...
    axialForceExp,modelSelection,k)
% Optimize material constants using optimset function for the lsqnonlin fxn
options = optimset('largescale','off','MaxFunEvals',1e100,'tolFun'...
    ,1e-30,'TolX',1e-30,'MaxIter',5e6,'Algorithm',...
    'levenberg-marquardt','Display','iter-detailed');
% For Gaussian integration:
% Define nodes and weights for gauss constants for n = 6.
weight = [0.4679139345726910 0.3607615730481386 0.1713244923791704 ...
    0.4679139345726910 0.3607615730481386 0.1713244923791704]';
ksi = [-0.2386191860831969 -0.6612093864662645 -0.9324695142031521 ...
    0.2386191860831969 0.6612093864662645 0.9324695142031521]';
% Determine constants and re-examination for holzapfel model-------------
if strcmp(modelSelection,'holzapfel') == 1
    if k == 1
        % Arbitrary initial constant guesses
        initialConstants = holzapfelConstants;
        % Group the radius and the stretch ratio into one variable so that
        % the lsqnonlin function will optimize them simultaneously
        radLambExp = [radiusOutExp, lambdaExp];
            holzapfelConstants = lsqnonlin(@(x) errorPF(x,radLambExp,...
                RadiusOut,RadiusIn,theta0,alpha,weight,ksi,...
                modelSelection,pressureExp,axialForceExp),...
                initialConstants,[],[],options);
        % Optimize for the new RadLamb using lsqnonlin again
        initialRadLamb = [radiusOutExp lambdaExp];
        radLambTheo = lsqnonlin(@(x) errorPF(holzapfelConstants,x,...
            RadiusOut,RadiusIn,theta0,alpha,weight,ksi,...
            modelSelection,pressureExp,axialForceExp),initialRadLamb,...
            [],[],options);
    else
        % Setting the radlamb Theo equal to the experimental values from
        % the second specimen trials
        initialRadLamb = [radiusOutExp lambdaExp];
        radLambTheo = lsqnonlin(@(x) errorPF(holzapfelConstants,x,...
            RadiusOut,RadiusIn,theta0,alpha,weight,ksi,...
            modelSelection,pressureExp,axialForceExp),initialRadLamb,...
            [],[],options);
    end
    % Re-evalute the Pt and Ft using the new constants and radlamb
    [pressureTheo, axialForceTheo] = PF(radLambTheo,RadiusOut,...
    RadiusIn,theta0,alpha,weight,ksi,modelSelection,...
    holzapfelConstants);
% Determine constants and re-examination for fung model-----------------
elseif strcmp(modelSelection,'fung') == 1
    if k == 1
        % Arbitrary initial constant guesses
```

```
        initialConstants = fungConstants;
        % Group the radius and the stretch ratio into one variable so that
        % the lsqnonlin function will optimize them simultaneously
        radLambExp = [radiusOutExp lambdaExp];
        fungConstants = lsqnonlin(@(x) errorPF(x,radLambExp,...
            RadiusOut,RadiusIn,theta0,alpha,weight,ksi,...
            modelSelection,pressureExp,axialForceExp),initialConstants,...
            [],[],options);
        % Optimize for the new RadLamb using lsqnonlin again
        initialRadLamb = [radiusOutExp lambdaExp];
        radLambTheo = lsqnonlin(@(x) errorPF(fungConstants, x,...
            RadiusOut, RadiusIn, theta0, alpha, weight, ksi,...
            modelSelection, pressureExp, axialForceExp), initialRadLamb,...
            [],[],options);
    else
        % Setting the radlamb Theo equal to the experimental values from
        % the second specimen trials
        initialRadLamb = [radiusOutExp lambdaExp];
        radLambTheo = lsqnonlin(@(x) errorPF(fungConstants, x,...
            RadiusOut, RadiusIn, theta0, alpha, weight, ksi,...
            modelSelection, pressureExp, axialForceExp), initialRadLamb,...
            [],[],options);
    end
    % Re-evalute the Pt and Ft using the new constants and radlamb
    [pressureTheo, axialForceTheo] = PF(radLambTheo, RadiusOut,...
    RadiusIn, theta0, alpha, weight, ksi, modelSelection,...
    fungConstants);
end
end

% -------------------------------------------------------------------------
% Determine the error between the fit and experimental pressures and forces
% -------------------------------------------------------------------------
function error = errorPF(c,radLambExp,RadiusOut,RadiusIn,theta0, ...
    alpha,weight,ksi,modelSelection,pressureExp,axialForceExp)
% Call the function to determine the theoretical pressure and zforce
[pressureTheo, axialForceTheo] = PF(radLambExp,RadiusOut,RadiusIn, ...
    theta0,alpha,weight,ksi,modelSelection,c);
% Error between the theo and exp values, this value is passed back to the
% lsqnonlin function and it is the value error that will be minimized.
% The constants will be based off of the results from this function.
if strcmp(modelSelection, 'holzapfel') == 1
    errorPressure = (pressureTheo - pressureExp);
    errorAxialForce = (axialForceTheo - axialForceExp)*RadiusOut^2;
elseif strcmp(modelSelection, 'fung') == 1
    errorPressure = (pressureTheo - pressureExp)*RadiusOut^2;
    errorAxialForce = (axialForceTheo - axialForceExp);
end
error = [errorPressure; errorAxialForce];
end

% -------------------------------------------------------------------------
% Calculate the theoretical pressure and axial force.  This is integrating
% the final functions for force and pressure derived in the methodology.
% The integration is non-elementary therefore it will be performed
% numerically using a Gauss-Legnedre method with 6 weighing points.
% -------------------------------------------------------------------------
function [pressureTheo, axialForceTheo] = PF(radLambExp,RadiusOut,...
    RadiusIn,theta0,alpha,weight,ksi,modelSelection,c)
```

```
radiusOut = radLambExp(:,1);
lambda = radLambExp(:,2);
pressureTheo = zeros(length(radiusOut), 1);
axialForceTheo = zeros(length(radiusOut), 1);
% Calculate the inner radius of the current frame (outer radius is
% measured)
radiusIn = sqrt(radiusOut.^2 - (theta0./(pi*lambda)).*...
    (RadiusOut^2 - RadiusIn^2));
for g = 1:length(weight)
    % Calculate the radius used for the gauss function
    radius = (radiusIn + radiusOut)./2 + ...
        ((ksi(g,1)/2).*(radiusOut - radiusIn));
    % Calculate the Radius used for the gauss function
    Radius = sqrt(RadiusIn.^2+(pi.*lambda./(theta0)).*...
        (radius.^2-radiusIn.^2));
    % Green Strains, Ethetatheta, Ezz
    Ett = 0.5.*(((pi.*radius)./(theta0.*Radius)).^2 - 1);
    Ezz = 0.5.*((lambda).^2 - 1);
    % Call the partial derivative function to calculate the partial
    % derivative functions (based off of modelSelection).
    partialdercalc = str2func(modelSelection);
    if strcmp(modelSelection, 'holzapfel') == 1
        [dWtt, dWzz] =  partialdercalc(c,Ett,Ezz,alpha);
    else
        [dWtt, dWzz] =  partialdercalc(c,Ett,Ezz);
    end
    % Pt and Ft iterations with different gauss points
    pressureTheo = pressureTheo + (weight(g,1)./radius).*...
        ((((pi*radius)./(theta0*Radius)).^2).*dWtt);
    axialForceTheo = axialForceTheo + (weight(g,1)*radius).*...
        ((2*lambda.^2.*dWzz) - ((pi.*radius)./(theta0.*Radius)).^2.*dWtt);
end
% full value for Pt and Ft after gauss-legendre integration
pressureTheo = pressureTheo.*(radiusOut-radiusIn)./2;
axialForceTheo = pi.*axialForceTheo.*(radiusOut-radiusIn)./2;
end

% ------------------------------------------------------------------------
% Partial derviative functions
% ------------------------------------------------------------------------
function [dWtt,dWzz] = holzapfel(c,Ett,Ezz,alpha)
invariantFour = (cos(alpha).^2).*(2.*Ett + 1) +...
    (sin(alpha).^2).*(2.*Ezz + 1);
invariantSix = (cos(alpha).^2).*(2.*Ett + 1) +...
    (sin(alpha).^2).*(2.*Ezz + 1);
firstQ = (invariantFour - 1).^2;
secondQ = (invariantSix - 1).^2;
delta = (1 + 2.*Ett).*(1 + 2.*Ezz);
dWtt = c(1,1).*(1 - 1./(delta.*(2.*Ett + 1))) ...
    + 2.*c(1,2).*cos(alpha)^2.*((invariantFour - 1).*exp(c(1,3).*firstQ)...
    + (invariantSix - 1).*exp(c(1,3).*secondQ));
dWzz = c(1,1).*(1 - 1./(delta.*(2.*Ezz + 1))) ...
    + 2.*c(1,2).*sin(alpha)^2.*((invariantFour - 1).*exp(c(1,3).*firstQ)...
    + (invariantSix - 1).*exp(c(1,3).*secondQ));
end

function [dWtt,dWzz] = fung(c,Ett,Ezz)
dWtt = c(1,1).*(c(1,2).*Ett + c(1,4).*Ezz).*...
    exp((c(1,2).*Ett.^2) + (c(1,3).*Ezz.^2) + (2.*c(1,4).*Ett.*Ezz));
```

```
dWzz = c(1,1).*(c(1,4).*Ett + c(1,3).*Ezz).*...
    exp((c(1,2).*Ett.^2) + (c(1,3).*Ezz.^2) + (2.*c(1,4).*Ett.*Ezz));
end
```

D.5 Plotting function for the experimental results

```
% ------------------------------------------------------------------------
% This function will plot the graphs of the instron testing data and put
% them into a format that presents the data in the most appealing way.
% ------------------------------------------------------------------------

function graphing_instron_data()
clc; % Clears command window each re-run
clear all; % Clears everything on re-run
format longg; % Sets the number of decimal places in the output
format compact; % Format for output window
tic;
% ------------------------------------------------------------------------
% Open data files for the instron data tests.  Divide the elongation by
% the original length and then smooth the curve.  These results will later
% be plotted in various formats.
% ------------------------------------------------------------------------
% Set the folder paths in char lengths less than the page width
disp('and.... GO!');
firstFileName = 'D:\MASc mechanical engineering\.MCG 7999 Thesis';
secondFileName = '\analysis\raw specimen data\';
middleFileName = char('ecoflex','moldstar','oomoo','blue braid',...
    'green braid','cyclic2mmsec','cyclic4mmsec','cyclic6mmsec',...
    'cyclic8mmsec','R1a4a_47','R1a4b_46','R1a4b_49','R1a4c_47',...
    'R1a4c_48','R1b4a_54','R1b4b_53','R1b4b_55','R1b4c_50',...
    'R1b4c_56','R1c4a_61','R1c4b_62','R1c4b_63',...
    'R1c4c_59','R1c4c_64','T1a4a_40','T1a4b_43','T1a4c_49',...
    'T1b4a_48','T1b4b_52','T1b4c_50','T1c4a_60','T1c4b_57',...
    'T1a4c_45','T1b4c_56','T1c4c_65','T1b4b_56','green braid strained',...
    'blue braid strained','T1c4b_63','T1b4a_51',...
    'hyst_1','hyst_2','hyst_3','hyst_4','hyst_5','hyst_6','hyst_7',...
    'hyst_8','hyst_9','hyst_10','R1a4a_45','T1b4a_53','T1a4c_45_fail',...
    'R1a4b_49_fail','R1a4c_47_fail','R1b4b_53_fail','R1b4c_50_fail',...
    'T1a4b_43_fail','T1b4c_50_fail','T1a4a_40_fail','R1c4c_64_fail');
lastFileName = '\instron_data.txt';
for i = 1:1:size(middleFileName,1)
    % Choose all data files in a loop to assign the columns to
    % appropriate arrays.  The middleFileName is the separator that chooses
    % which instron data file will be opened.
    % Elimintate any trailing white space set by char() in each cell.
    tempMiddleFileName = strcat(middleFileName(i,:));
    % Concate the file name into 1 horizontal array.
    fullFileName = sprintf('%s%s%s%s',firstFileName,secondFileName,...
        tempMiddleFileName,lastFileName);
    % Open the chosen file
    rawDataFile = fopen(fullFileName, 'rt');
    % Transfer data into a matrix named cell array
    cellArray = textscan(rawDataFile, '%f %f %f');
    fclose(rawDataFile);
    % Assign the instron data to temporary variables.
    tempElongation = cellArray{1};
    tempAxialForceExp = cellArray{2};
```

```
    originalLength = cellArray{3}(1);
    % Divide the elongation by the original length to get the Stretch ratio
    % of the tendons.
    tempStretchRatio = (tempElongation + originalLength)./originalLength;
    % Smooth the curves for force versus stretch ratio
    tempAxialForceExpSmoothed = smooth(tempStretchRatio,...
        tempAxialForceExp,0.1,'loess');
    % Determine stiffness for stiffness plots, under a load of threshload
    if (strcmp(tempMiddleFileName,'R1c4a_61') == 1) ||...
            (strcmp(tempMiddleFileName,'R1c4b_62') == 1) ||...
            (strcmp(tempMiddleFileName,'R1c4c_64') == 1) ||...
            (strcmp(tempMiddleFileName,'T1c4a_60') == 1) ||...
            (strcmp(tempMiddleFileName,'T1c4b_63') == 1) ||...
            (strcmp(tempMiddleFileName,'T1c4c_65') == 1)
        disp(tempMiddleFileName)
        % Assign the temp columns to a permanent matrix
        threshload = 69; % For max 70N force
        % Smooth the stiffness force value with elongation.
        tempAxialForceSmoothedStiffness = smooth(tempElongation,...
                tempAxialForceExp,0.10,'loess');
        for j = 1:1:numel(tempAxialForceSmoothedStiffness)
            countThresh = j;
            if tempAxialForceSmoothedStiffness(j,1) >= threshload
                break
            end
        end
        countThresh = countThresh - 1;
        % Process to select only every nth value of the matrix.  This is
        % done for "smoothing" purposes cause the force values are so all
        % over the place.
        skipValue = 3;
        countCondense = 0;
        numElementsCondensed = fix(countThresh/skipValue);
        condensedAxialForce = zeros(numElementsCondensed,1);
        condensedElongation = zeros(numElementsCondensed,1);
        for n = 1:skipValue:countThresh
            countCondense = countCondense + 1;
            condensedAxialForce(countCondense,1) = ...
                tempAxialForceSmoothedStiffness(n,1);
            condensedElongation(countCondense,1) = tempElongation(n,1);
        end
        tempMaterialStiffness = zeros(countCondense-1,1);
        for k = 1:1:(countCondense-1)
            tempMaterialStiffness(k,1) = ...
                (condensedAxialForce(k+1,1)-...
                condensedAxialForce(k,1))/...
                (condensedElongation(k+1,1)-condensedElongation(k,1));
        end
%         for k = 1:1:(countCondense)
%             tempMaterialStiffness(k,1) = ...
%                 (condensedAxialForce(k,1)/...
%                 condensedElongation(k,1));
%         end
        % Make the elongation the same length as the stiffness vector
        % rather than the force vector, which is n-1
        condensedElongation = condensedElongation(1:end-1,1);
        tempMaterialStiffness = smooth(condensedElongation,...
                tempMaterialStiffness,0.20,'loess');
    end
```

```
% ------------------------------------------------------------------------
% Silicone rubbers only
% ------------------------------------------------------------------------
    if (strcmp(strcat(middleFileName(i,:)),'ecoflex')) == 1
        elongationEcoflex = tempStretchRatio;
        axialForceEcoflex = tempAxialForceExpSmoothed;
    elseif (strcmp(strcat(middleFileName(i,:)),'moldstar')) == 1
        elongationMoldstar = tempStretchRatio;
        axialForceMoldstar = tempAxialForceExpSmoothed;
    elseif (strcmp(strcat(middleFileName(i,:)),'oomoo')) == 1
        elongationOomoo = tempStretchRatio;
        axialForceOomoo = tempAxialForceExpSmoothed;
% ------------------------------------------------------------------------
% Braids only
% ------------------------------------------------------------------------
    elseif (strcmp(strcat(middleFileName(i,:)),'blue braid')) == 1
        elongationBlueBraid = tempStretchRatio;
        axialForceBlueBraid = tempAxialForceExpSmoothed;
    elseif (strcmp(strcat(middleFileName(i,:)),'green braid')) == 1
        elongationGreenBraid = tempStretchRatio;
        axialForceGreenBraid = tempAxialForceExpSmoothed;
    elseif (strcmp(strcat(middleFileName(i,:)),...
                'green braid strained')) == 1
        elongationGreenStrained = tempStretchRatio;
        axialForceGreenStrained = tempAxialForceExpSmoothed;
    elseif (strcmp(strcat(middleFileName(i,:)),...
                'blue braid strained')) == 1
        elongationBlueStrained = tempStretchRatio;
        axialForceBlueStrained = tempAxialForceExpSmoothed;
% ------------------------------------------------------------------------
% Cyclical testing and hysteresis
% ------------------------------------------------------------------------
    elseif (strcmp(strcat(middleFileName(i,:)),'cyclic2mmsec')) == 1
        elongationCyclic2mmsec = tempStretchRatio;
        axialForceCyclic2mmsec = tempAxialForceExp;
    elseif (strcmp(strcat(middleFileName(i,:)),'cyclic4mmsec')) == 1
        elongationCyclic4mmsec = tempStretchRatio;
        axialForceCyclic4mmsec = tempAxialForceExp;
    elseif (strcmp(strcat(middleFileName(i,:)),'cyclic6mmsec')) == 1
        elongationCyclic6mmsec = tempStretchRatio;
        axialForceCyclic6mmsec = tempAxialForceExp;
    elseif (strcmp(strcat(middleFileName(i,:)),'cyclic8mmsec')) == 1
        elongationCyclic8mmsec = tempStretchRatio;
        axialForceCyclic8mmsec = tempAxialForceExp;
    elseif (strcmp(strcat(middleFileName(i,:)),'hyst_1')) == 1
        elongationHyst1 = tempStretchRatio;
        axialForceHyst1 = tempAxialForceExp;
    elseif (strcmp(strcat(middleFileName(i,:)),'hyst_2')) == 1
        elongationHyst2 = tempStretchRatio;
        axialForceHyst2 = tempAxialForceExp;
    elseif (strcmp(strcat(middleFileName(i,:)),'hyst_3')) == 1
        elongationHyst3 = tempStretchRatio;
        axialForceHyst3 = tempAxialForceExp;
    elseif (strcmp(strcat(middleFileName(i,:)),'hyst_4')) == 1
        elongationHyst4 = tempStretchRatio;
        axialForceHyst4 = tempAxialForceExp;
    elseif (strcmp(strcat(middleFileName(i,:)),'hyst_5')) == 1
        elongationHyst5 = tempStretchRatio;
        axialForceHyst5 = tempAxialForceExp;
```

```
    elseif (strcmp(strcat(middleFileName(i,:)),'hyst_6')) == 1
        elongationHyst6 = tempStretchRatio;
        axialForceHyst6 = tempAxialForceExp;
    elseif (strcmp(strcat(middleFileName(i,:)),'hyst_7')) == 1
        elongationHyst7 = tempStretchRatio;
        axialForceHyst7 = tempAxialForceExp;
    elseif (strcmp(strcat(middleFileName(i,:)),'hyst_8')) == 1
        elongationHyst8 = tempStretchRatio;
        axialForceHyst8 = tempAxialForceExp;
    elseif (strcmp(strcat(middleFileName(i,:)),'hyst_9')) == 1
        elongationHyst9 = tempStretchRatio;
        axialForceHyst9 = tempAxialForceExp;
    elseif (strcmp(strcat(middleFileName(i,:)),'hyst_10')) == 1
        elongationHyst10 = tempStretchRatio;
        axialForceHyst10 = tempAxialForceExp;
% ------------------------------------------------------------------------
% "Small" braiding angles, any rubber, any braid pattern.
% ------------------------------------------------------------------------
    elseif (strcmp(strcat(middleFileName(i,:)),'R1a4a_45')) == 1
        elongationR1a4a_45 = tempStretchRatio;
        axialForceR1a4a_45 = tempAxialForceExpSmoothed;
    elseif (strcmp(strcat(middleFileName(i,:)),'R1a4a_47')) == 1
        elongationR1a4a_47 = tempStretchRatio;
        axialForceR1a4a_47 = tempAxialForceExpSmoothed;
    elseif (strcmp(strcat(middleFileName(i,:)),'R1a4b_46')) == 1
        elongationR1a4b_46 = tempStretchRatio;
        axialForceR1a4b_46 = tempAxialForceExpSmoothed;
    elseif (strcmp(strcat(middleFileName(i,:)),'R1a4b_49')) == 1
        elongationR1a4b_49 = tempStretchRatio;
        axialForceR1a4b_49 = tempAxialForceExpSmoothed;
    elseif (strcmp(strcat(middleFileName(i,:)),'R1a4c_47')) == 1
        elongationR1a4c_47 = tempStretchRatio;
        axialForceR1a4c_47 = tempAxialForceExpSmoothed;
    elseif (strcmp(strcat(middleFileName(i,:)),'R1a4c_48')) == 1
        elongationR1a4c_48 = tempStretchRatio;
        axialForceR1a4c_48 = tempAxialForceExpSmoothed;
    elseif (strcmp(strcat(middleFileName(i,:)),'T1a4a_40')) == 1
        elongationT1a4a_40 = tempStretchRatio;
        axialForceT1a4a_40 = tempAxialForceExpSmoothed;
    elseif (strcmp(strcat(middleFileName(i,:)),'T1a4b_43')) == 1
        elongationT1a4b_43 = tempStretchRatio;
        axialForceT1a4b_43 = tempAxialForceExpSmoothed;
    elseif (strcmp(strcat(middleFileName(i,:)),'T1a4c_45')) == 1
        elongationT1a4c_45 = tempStretchRatio;
        axialForceT1a4c_45 = tempAxialForceExpSmoothed;
    elseif (strcmp(strcat(middleFileName(i,:)),'T1a4c_49')) == 1
        elongationT1a4c_49 = tempStretchRatio;
        axialForceT1a4c_49 = tempAxialForceExpSmoothed;
% ------------------------------------------------------------------------
% "Medium" braiding angles, any rubber, any braid pattern.
% ------------------------------------------------------------------------
    elseif (strcmp(strcat(middleFileName(i,:)),'R1b4a_54')) == 1
        elongationR1b4a_54 = tempStretchRatio;
        axialForceR1b4a_54 = tempAxialForceExpSmoothed;
    elseif (strcmp(strcat(middleFileName(i,:)),'R1b4b_53')) == 1
        elongationR1b4b_53 = tempStretchRatio;
        axialForceR1b4b_53 = tempAxialForceExpSmoothed;
    elseif (strcmp(strcat(middleFileName(i,:)),'R1b4b_55')) == 1
        elongationR1b4b_55 = tempStretchRatio;
```

```
        axialForceR1b4b_55 = tempAxialForceExpSmoothed;
    elseif (strcmp(strcat(middleFileName(i,:)),'R1b4c_50')) == 1
        elongationR1b4c_50 = tempStretchRatio;
        axialForceR1b4c_50 = tempAxialForceExpSmoothed;
    elseif (strcmp(strcat(middleFileName(i,:)),'R1b4c_56')) == 1
        elongationR1b4c_56 = tempStretchRatio;
        axialForceR1b4c_56 = tempAxialForceExpSmoothed;
    elseif (strcmp(strcat(middleFileName(i,:)),'T1b4a_48')) == 1
        elongationT1b4a_48 = tempStretchRatio;
        axialForceT1b4a_48 = tempAxialForceExpSmoothed;
    elseif (strcmp(strcat(middleFileName(i,:)),'T1b4a_51')) == 1
        elongationT1b4a_51 = tempStretchRatio;
        axialForceT1b4a_51 = tempAxialForceExpSmoothed;
    elseif (strcmp(strcat(middleFileName(i,:)),'T1b4a_53')) == 1
        elongationT1b4a_53 = tempStretchRatio;
        axialForceT1b4a_53 = tempAxialForceExpSmoothed;
    elseif (strcmp(strcat(middleFileName(i,:)),'T1b4b_52')) == 1
        elongationT1b4b_52 = tempStretchRatio;
        axialForceT1b4b_52 = tempAxialForceExpSmoothed;
    elseif (strcmp(strcat(middleFileName(i,:)),'T1b4b_56')) == 1
        elongationT1b4b_56 = tempStretchRatio;
        axialForceT1b4b_56 = tempAxialForceExpSmoothed;
    elseif (strcmp(strcat(middleFileName(i,:)),'T1b4c_50')) == 1
        elongationT1b4c_50 = tempStretchRatio;
        axialForceT1b4c_50 = tempAxialForceExpSmoothed;
% ------------------------------------------------------------------------
% "Large" braiding angles, any rubber, any braid pattern.
% ------------------------------------------------------------------------
    elseif (strcmp(strcat(middleFileName(i,:)),'R1c4a_61')) == 1
        elongationR1c4a_61 = tempStretchRatio;
        axialForceR1c4a_61 = tempAxialForceExpSmoothed;
        instronElongationR1c4a_61 = condensedElongation;
        stiffnessR1c4a_61 = tempMaterialStiffness;
    elseif (strcmp(strcat(middleFileName(i,:)),'R1c4b_62')) == 1
        elongationR1c4b_62 = tempStretchRatio;
        axialForceR1c4b_62 = tempAxialForceExpSmoothed;
        instronElongationR1c4b_62 = condensedElongation;
        stiffnessR1c4b_62 = tempMaterialStiffness;
    elseif (strcmp(strcat(middleFileName(i,:)),'R1c4b_63')) == 1
        elongationR1c4b_63 = tempStretchRatio;
        axialForceR1c4b_63 = tempAxialForceExpSmoothed;
    elseif (strcmp(strcat(middleFileName(i,:)),'R1c4c_59')) == 1
        elongationR1c4c_59 = tempStretchRatio;
        axialForceR1c4c_59 = tempAxialForceExpSmoothed;
    elseif (strcmp(strcat(middleFileName(i,:)),'R1c4c_64')) == 1
        elongationR1c4c_64 = tempStretchRatio;
        axialForceR1c4c_64 = tempAxialForceExpSmoothed;
        instronElongationR1c4c_64 = condensedElongation;
        stiffnessR1c4c_64 = tempMaterialStiffness;
    elseif (strcmp(strcat(middleFileName(i,:)),'T1c4a_60')) == 1
        elongationT1c4a_60 = tempStretchRatio;
        axialForceT1c4a_60 = tempAxialForceExpSmoothed;
        instronElongationT1c4a_60 = condensedElongation;
        stiffnessT1c4a_60 = tempMaterialStiffness;
    elseif (strcmp(strcat(middleFileName(i,:)),'T1c4b_57')) == 1
        elongationT1c4b_57 = tempStretchRatio;
        axialForceT1c4b_57 = tempAxialForceExpSmoothed;
    elseif (strcmp(strcat(middleFileName(i,:)),'T1c4b_63')) == 1
        elongationT1c4b_63 = tempStretchRatio;
```

```
        axialForceT1c4b_63 = tempAxialForceExpSmoothed;
        instronElongationT1c4b_63 = condensedElongation;
        stiffnessT1c4b_63 = tempMaterialStiffness;
    elseif (strcmp(strcat(middleFileName(i,:)),'T1b4c_56')) == 1
        elongationT1b4c_56 = tempStretchRatio;
        axialForceT1b4c_56 = tempAxialForceExpSmoothed;
    elseif (strcmp(strcat(middleFileName(i,:)),'T1c4c_65')) == 1
        elongationT1c4c_65 = tempStretchRatio;
        axialForceT1c4c_65 = tempAxialForceExpSmoothed;
        instronElongationT1c4c_65 = condensedElongation;
        stiffnessT1c4c_65 = tempMaterialStiffness;

% ------------------------------------------------------------------------
% Tests until failure
% ------------------------------------------------------------------------
    elseif (strcmp(strcat(middleFileName(i,:)),'R1a4b_49_fail')) == 1
        elongationR1a4b_49_fail = tempStretchRatio;
        axialForceR1a4b_49_fail = tempAxialForceExpSmoothed;
    elseif (strcmp(strcat(middleFileName(i,:)),'R1a4c_47_fail')) == 1
        elongationR1a4c_47_fail = tempStretchRatio;
        axialForceR1a4c_47_fail = tempAxialForceExpSmoothed;
    elseif (strcmp(strcat(middleFileName(i,:)),'R1b4b_53_fail')) == 1
        elongationR1b4b_53_fail = tempStretchRatio;
        axialForceR1b4b_53_fail= tempAxialForceExpSmoothed;
    elseif (strcmp(strcat(middleFileName(i,:)),'R1b4c_50_fail')) == 1
        elongationR1b4c_50_fail = tempStretchRatio;
        axialForceR1b4c_50_fail = tempAxialForceExpSmoothed;
    elseif (strcmp(strcat(middleFileName(i,:)),'R1c4c_64_fail')) == 1
        elongationR1c4c_64_fail = tempStretchRatio;
        axialForceR1c4c_64_fail = tempAxialForceExpSmoothed;
    elseif (strcmp(strcat(middleFileName(i,:)),'T1a4a_40_fail')) == 1
        elongationT1a4a_40_fail = tempStretchRatio;
        axialForceT1a4a_40_fail = tempAxialForceExpSmoothed;
    elseif (strcmp(strcat(middleFileName(i,:)),'T1a4c_45_fail')) == 1
        elongationT1a4c_45_fail = tempStretchRatio;
        axialForceT1a4c_45_fail = tempAxialForceExpSmoothed;
    elseif (strcmp(strcat(middleFileName(i,:)),'T1a4b_43_fail')) == 1
        elongationT1a4b_43_fail = tempStretchRatio;
        axialForceT1a4b_43_fail = tempAxialForceExpSmoothed;
    elseif (strcmp(strcat(middleFileName(i,:)),'T1b4c_50_fail')) == 1
        elongationT1b4c_50_fail = tempStretchRatio;
        axialForceT1b4c_50_fail = tempAxialForceExpSmoothed;
    end
end
% ------------------------------------------------------------------------
% Open data files for the biaxial data tests.  These results will later
% be plotted in various formats.
% ------------------------------------------------------------------------
% Set the folder paths in char lengths less than the page width
firstFileName = 'D:\MASc mechanical engineering\.MCG 7999 Thesis';
secondFileName = '\analysis\raw specimen data\';
middleFileName = char('biaxial_ecoflex','biaxial_moldstar',...
    'biaxial_oomoo');
lastFileName = '\biaxial_data.txt';
for i = 1:1:size(middleFileName,1)
    % Choose all data files in a loop to assign the columns to
    % appropriate arrays.  The middleFileName is the separator that chooses
    % which instron data file will be opened.
    % Elimintate any trailing white space set by char() in each cell.
```

```
    tempMiddleFileName = strcat(middleFileName(i,:));
    % Concate the file name into 1 horizontal array.
    fullFileName = sprintf('%s%s%s%s',firstFileName,secondFileName,...
        tempMiddleFileName,lastFileName);
    % Open the chosen file
    rawDataFile = fopen(fullFileName, 'rt');
    % Transfer data into a matrix named cell array
    cellArray = textscan(rawDataFile, '%f %f %f %f');
    fclose(rawDataFile);
    % Assign the instron data to temporary variables.
    tempXElongation = (cellArray{1}+12000)/12000;
    tempYElongation = (cellArray{2}+12000)/12000;
    tempXForce = cellArray{3};
    tempYForce = cellArray{4};
    % Smooth the curves.
    tempXForceSmoothed = smooth(tempXElongation,...
            tempXForce,0.00001,'loess');
    tempYForceSmoothed = smooth(tempYElongation,...
            tempYForce,0.00001,'loess');
    % Assign the temp columns to a permanent matrix
    if (strcmp(strcat(middleFileName(i,:)),'biaxial_ecoflex')) == 1
        elongationEcoflexX = tempXElongation;
        elongationEcoflexY = tempYElongation;
        axialForceEcoflexX = tempXForceSmoothed;
        axialForceEcoflexY = tempYForceSmoothed;
    elseif (strcmp(strcat(middleFileName(i,:)),'biaxial_moldstar')) == 1
        elongationMoldstarX = tempXElongation;
        elongationMoldstarY = tempYElongation;
        axialForceMoldstarX = tempXForceSmoothed;
        axialForceMoldstarY = tempYForceSmoothed;
    elseif (strcmp(strcat(middleFileName(i,:)),'biaxial_oomoo')) == 1
        elongationOomooX = tempXElongation;
        elongationOomooY = tempYElongation;
        axialForceOomooX = tempXForceSmoothed;
        axialForceOomooY = tempYForceSmoothed;
    end
end
% ------------------------------------------------------------------------
% ------------------------------- PLOTS ----------------------------------
% ------------------------------------------------------------------------
disp('Starting to plot now...');
% Instron experimental pure silicone plots:
instronPureSilicone = figure();
xAxisLimit = 4.5;
yAxisLimit = 30;
labelXAxis = 'Stretch ratio';
labelYAxis = 'Axial force (N)';
% Call the plot function to ensure consitency within graphing format
plot_this_for_me(instronPureSilicone,xAxisLimit,yAxisLimit,labelXAxis,...
    labelYAxis)
% Plot the silicone tensile results
hold on;
plot(elongationEcoflex,axialForceEcoflex,'k-','Linewidth',1);
plot(elongationMoldstar,axialForceMoldstar,'k--','Linewidth',0.5);
plot(elongationOomoo,axialForceOomoo,'k-.','Linewidth',1.5);
hold off;
% Apply a legend to the graph.
legend('Ecoflex','Moldstar','Oomoo');
% Turn the box around the legend off
```

```
legend boxoff;
% Save the figure to use for the latex file document.
fileLocation = ['D:\MASc mechanical engineering\.MCG 7999'...
    ,' Thesis\written\images\graphs'];
nameForFile = 'instron_pure_silicone';
save_this_for_me(fileLocation,nameForFile,instronPureSilicone);
% ------------------------------------------------------------------------
% Instron experimental braid only plots:
instronBraidOnly = figure();
xAxisLimit = 2;
yAxisLimit = 100;
labelXAxis = 'Stretch ratio';
labelYAxis = 'Axial force (N)';
% Call the plot function to ensure consitency within graphing format
plot_this_for_me(instronBraidOnly,xAxisLimit,yAxisLimit,labelXAxis,...
    labelYAxis)
% Plot the silicone tensile results
hold on;
plot(elongationGreenStrained,axialForceGreenStrained,'k-','Linewidth',1);
plot(elongationBlueStrained,axialForceBlueStrained,'k--','Linewidth',1);
hold off;
% Apply a legend to the graph.
legend('Regular Braid','Tight Braid');
% Turn the box around the legend off
legend boxoff;
% Save the figure to use for the latex file document.
fileLocation = ['D:\MASc mechanical engineering\.MCG 7999'...
    ,' Thesis\written\images\graphs'];
nameForFile = 'instron_braid_only';
save_this_for_me(fileLocation,nameForFile,instronBraidOnly);
% ------------------------------------------------------------------------
% Instron experimental cyclic tests:
instronCyclicTests = figure();
xAxisLimit = 1.45;
yAxisLimit = 70;
labelXAxis = 'Stretch ratio';
labelYAxis = 'Axial force (N)';
% Call the plot function to ensure consitency within graphing format
plot_this_for_me(instronCyclicTests,xAxisLimit,yAxisLimit,...
    labelXAxis,labelYAxis)
% Plot the silicone tensile results
hold on;
plot(elongationCyclic2mmsec,axialForceCyclic2mmsec,'k-','Linewidth',1);
plot(elongationCyclic4mmsec,axialForceCyclic4mmsec,'k--','Linewidth',1);
%plot(elongationCyclic6mmsec,axialForceCyclic6mmsec,'k--','Linewidth',1);
%plot(elongationCyclic8mmsec,axialForceCyclic8mmsec,'k--','Linewidth',1);
hold off;
% Apply a legend to the graph.
legend('2mm/sec','4mm/sec','Location','NorthWest');
% Turn the box around the legend off
legend boxoff;
% Save the figure to use for the latex file document.
fileLocation = ['D:\MASc mechanical engineering\.MCG 7999'...
    ,' Thesis\written\images\graphs'];
nameForFile = 'instron_cyclic_tests';
save_this_for_me(fileLocation,nameForFile,instronCyclicTests);
% ------------------------------------------------------------------------
% Instron experimental hysteresis tests:
instronHystTests = figure();
```

```
xAxisLimit = 1.45;
yAxisLimit = 70;
labelXAxis = 'Stretch ratio';
labelYAxis = 'Axial force (N)';
% Call the plot function to ensure consitency within graphing format
plot_this_for_me(instronHystTests,xAxisLimit,yAxisLimit,...
    labelXAxis,labelYAxis)
% Plot the silicone tensile results
hold on;
plot(elongationHyst1,axialForceHyst1,'k-','Linewidth',1);
plot(elongationHyst5,axialForceHyst5,'k:','Linewidth',1);
plot(elongationHyst10,axialForceHyst10,'k--','Linewidth',1);
hold off;
% Apply a legend to the graph.
legend('Cycle 1','Cycle 5','Cycle 10','Location','NorthWest');
% Turn the box around the legend off
legend boxoff;
% Save the figure to use for the latex file document.
fileLocation = ['D:\MASc mechanical engineering\.MCG 7999'...
    ,' Thesis\written\images\graphs'];
nameForFile = 'instron_hyst_tests';
save_this_for_me(fileLocation,nameForFile,instronHystTests);
% ------------------------------------------------------------------------
% Instron experimental ecoflex with regular braid:
instronEcoflexRegular = figure();
xAxisLimit = 1.95;
yAxisLimit = 70;
labelXAxis = 'Stretch ratio';
labelYAxis = 'Axial force (N)';
% Call the plot function to ensure consitency within graphing format
plot_this_for_me(instronEcoflexRegular,xAxisLimit,yAxisLimit,labelXAxis,...
    labelYAxis)
% Plot the silicone tensile results
hold on;
plot(elongationR1a4a_45,axialForceR1a4a_45,'k-','Linewidth',1);
plot(elongationR1b4a_54,axialForceR1b4a_54,'k--','Linewidth',0.5);
plot(elongationR1c4a_61,axialForceR1c4a_61,'k-.','Linewidth',1.5);
hold off;
% Apply a legend to the graph.
sOne = sprintf('45%c', char(176));
sTwo = sprintf('54%c', char(176));
sThree = sprintf('61%c', char(176));
legend(sOne,sTwo,sThree,'Location','NorthEast');
% Turn the box around the legend off
legend boxoff;
% Save the figure to use for the latex file document.
fileLocation = ['D:\MASc mechanical engineering\.MCG 7999'...
    ,' Thesis\written\images\graphs'];
nameForFile = 'instron_ecoflex_regular';
save_this_for_me(fileLocation,nameForFile,instronEcoflexRegular);
% ------------------------------------------------------------------------
% Instron experimental ecoflex with tight braid:
instronEcoflexTight = figure();
xAxisLimit = 1.95;
yAxisLimit = 70;
labelXAxis = 'Stretch ratio';
labelYAxis = 'Axial force (N)';
% Call the plot function to ensure consitency within graphing format
plot_this_for_me(instronEcoflexTight,xAxisLimit,yAxisLimit,labelXAxis,...
```

```
    labelYAxis)
% Plot the silicone tensile results
hold on;
plot(elongationT1a4a_40,axialForceT1a4a_40,'k-','Linewidth',1);
plot(elongationT1b4a_53,axialForceT1b4a_53,'k--','Linewidth',0.5);
plot(elongationT1c4a_60,axialForceT1c4a_60,'k-.','Linewidth',1.5);
hold off;
% Apply a legend to the graph.
sOne = sprintf('40%c', char(176));
sTwo = sprintf('53%c', char(176));
sThree = sprintf('60%c', char(176));
legend(sOne,sTwo,sThree,'Location','North');
% Turn the box around the legend off
legend boxoff;
% Save the figure to use for the latex file document.
fileLocation = ['D:\MASc mechanical engineering\.MCG 7999'...
    ,' Thesis\written\images\graphs'];
nameForFile = 'instron_ecoflex_tight';
save_this_for_me(fileLocation,nameForFile,instronEcoflexTight);
% ------------------------------------------------------------------------
% Instron experimental moldstar with regular braid:
instronMoldstarRegular = figure();
xAxisLimit = 1.95;
yAxisLimit = 70;
labelXAxis = 'Stretch ratio';
labelYAxis = 'Axial force (N)';
% Call the plot function to ensure consitency within graphing format
plot_this_for_me(instronMoldstarRegular,xAxisLimit,yAxisLimit,...
    labelXAxis,labelYAxis)
% Plot the silicone tensile results
hold on;
plot(elongationR1a4b_49,axialForceR1a4b_49,'k-','Linewidth',1);
plot(elongationR1b4b_55,axialForceR1b4b_55,'k--','Linewidth',0.5);
plot(elongationR1c4b_62,axialForceR1c4b_62,'k-.','Linewidth',1.5);
hold off;
% Apply a legend to the graph.
sOne = sprintf('49%c', char(176));
sTwo = sprintf('55%c', char(176));
sThree = sprintf('62%c', char(176));
legend(sOne,sTwo,sThree,'Location','NorthWest');
% Turn the box around the legend off
legend boxoff;
% Save the figure to use for the latex file document.
fileLocation = ['D:\MASc mechanical engineering\.MCG 7999'...
    ,' Thesis\written\images\graphs'];
nameForFile = 'instron_moldstar_regular';
save_this_for_me(fileLocation,nameForFile,instronMoldstarRegular);
% ------------------------------------------------------------------------
% Instron experimental moldstar with tight braid:
instronMoldstarTight = figure();
xAxisLimit = 1.95;
yAxisLimit = 70;
labelXAxis = 'Stretch ratio';
labelYAxis = 'Axial force (N)';
% Call the plot function to ensure consitency within graphing format
plot_this_for_me(instronMoldstarTight,xAxisLimit,yAxisLimit,...
    labelXAxis,labelYAxis)
% Plot the silicone tensile results
hold on;
```

```
plot(elongationT1a4b_43,axialForceT1a4b_43,'k-','Linewidth',1);
plot(elongationT1b4b_52,axialForceT1b4b_52,'k--','Linewidth',0.5);
plot(elongationT1c4b_63,axialForceT1c4b_63,'k-.','Linewidth',1.5);
hold off;
% Apply a legend to the graph.
sOne = sprintf('43%c', char(176));
sTwo = sprintf('52%c', char(176));
sThree = sprintf('63%c', char(176));
legend(sOne,sTwo,sThree,'Location','NorthWest');
% Turn the box around the legend off
legend boxoff;
% Save the figure to use for the latex file document.
fileLocation = ['D:\MASc mechanical engineering\.MCG 7999'...
    ,' Thesis\written\images\graphs'];
nameForFile = 'instron_moldstar_tight';
save_this_for_me(fileLocation,nameForFile,instronMoldstarTight);
% ------------------------------------------------------------------------
% Instron experimental oomoo with regular braid:
instronOomooRegular = figure();
xAxisLimit = 2.15;
yAxisLimit = 70;
labelXAxis = 'Stretch ratio';
labelYAxis = 'Axial force (N)';
% Call the plot function to ensure consitency within graphing format
plot_this_for_me(instronOomooRegular,xAxisLimit,yAxisLimit,...
    labelXAxis,labelYAxis)
% Plot the silicone tensile results
hold on;
plot(elongationR1a4c_48,axialForceR1a4c_48,'k-','Linewidth',1);
plot(elongationR1b4c_56,axialForceR1b4c_56,'k--','Linewidth',0.5);
plot(elongationR1c4c_64,axialForceR1c4c_64,'k-.','Linewidth',1.5);
hold off;
% Apply a legend to the graph.
sOne = sprintf('48%c', char(176));
sTwo = sprintf('56%c', char(176));
sThree = sprintf('64%c', char(176));
legend(sOne,sTwo,sThree,'Location','NorthWest');
% Turn the box around the legend off
legend boxoff;
% Save the figure to use for the latex file document.
fileLocation = ['D:\MASc mechanical engineering\.MCG 7999'...
    ,' Thesis\written\images\graphs'];
nameForFile = 'instron_oomoo_regular';
save_this_for_me(fileLocation,nameForFile,instronOomooRegular);
% ------------------------------------------------------------------------
% Instron experimental oomoo with tight braid:
instronOomooTight = figure();
xAxisLimit = 1.95;
yAxisLimit = 70;
labelXAxis = 'Stretch ratio';
labelYAxis = 'Axial force (N)';
% Call the plot function to ensure consitency within graphing format
plot_this_for_me(instronOomooTight,xAxisLimit,yAxisLimit,...
    labelXAxis,labelYAxis)
% Plot the silicone tensile results
hold on;
plot(elongationT1a4c_45,axialForceT1a4c_45,'k-','Linewidth',1);
plot(elongationT1b4c_56,axialForceT1b4c_56,'k--','Linewidth',0.5);
plot(elongationT1c4c_65,axialForceT1c4c_65,'k-.','Linewidth',1.5);
```

```
hold off;
% Apply a legend to the graph.
sOne = sprintf('45%c', char(176));
sTwo = sprintf('56%c', char(176));
sThree = sprintf('65%c', char(176));
legend(sOne,sTwo,sThree,'Location','NorthWest');
% Turn the box around the legend off
legend boxoff;
% Save the figure to use for the latex file document.
fileLocation = ['D:\MASc mechanical engineering\.MCG 7999'...
    ,' Thesis\written\images\graphs'];
nameForFile = 'instron_oomoo_tight';
save_this_for_me(fileLocation,nameForFile,instronOomooTight);
% ------------------------------------------------------------------------
% Instron experimental small braid angle with regular braid:
instronSmallAngleRegular = figure();
xAxisLimit = 1.95;
yAxisLimit = 70;
labelXAxis = 'Stretch ratio';
labelYAxis = 'Axial force (N)';
% Call the plot function to ensure consitency within graphing format
plot_this_for_me(instronSmallAngleRegular,xAxisLimit,yAxisLimit,...
    labelXAxis,labelYAxis)
% Plot the silicone tensile results
hold on;
plot(elongationR1a4a_45,axialForceR1a4a_45,'k-','Linewidth',1);
plot(elongationR1a4b_49,axialForceR1a4b_49,'k--','Linewidth',0.5);
plot(elongationR1a4c_48,axialForceR1a4c_48,'k-.','Linewidth',1.5);
hold off;
% Apply a legend to the graph.
sOne = sprintf('45%c Ecoflex', char(176));
sTwo = sprintf('49%c Moldstar', char(176));
sThree = sprintf('48%c Oomoo', char(176));
legend(sOne,sTwo,sThree,'Location','NorthEast');
% Turn the box around the legend off
legend boxoff;
% Save the figure to use for the latex file document.
fileLocation = ['D:\MASc mechanical engineering\.MCG 7999'...
    ,' Thesis\written\images\graphs'];
nameForFile = 'instron_small_angle_regular';
save_this_for_me(fileLocation,nameForFile,instronSmallAngleRegular);
% ------------------------------------------------------------------------
% Instron experimental small braid angle with tight braid:
instronSmallAngleTight = figure();
xAxisLimit = 1.95;
yAxisLimit = 70;
labelXAxis = 'Stretch ratio';
labelYAxis = 'Axial force (N)';
% Call the plot function to ensure consitency within graphing format
plot_this_for_me(instronSmallAngleTight,xAxisLimit,yAxisLimit,...
    labelXAxis,labelYAxis)
% Plot the silicone tensile results
hold on;
plot(elongationT1a4a_40,axialForceT1a4a_40,'k-','Linewidth',1);
plot(elongationT1a4b_43,axialForceT1a4b_43,'k--','Linewidth',0.5);
plot(elongationT1a4c_45,axialForceT1a4c_45,'k-.','Linewidth',1.5);
hold off;
% Apply a legend to the graph.
sOne = sprintf('40%c Ecoflex', char(176));
```

```
sTwo = sprintf('43%c Moldstar', char(176));
sThree = sprintf('45%c Oomoo', char(176));
legend(sOne,sTwo,sThree,'Location','NorthEast');
% Turn the box around the legend off
legend boxoff;
% Save the figure to use for the latex file document.
fileLocation = ['D:\MASc mechanical engineering\.MCG 7999'...
    ,' Thesis\written\images\graphs'];
nameForFile = 'instron_small_angle_tight';
save_this_for_me(fileLocation,nameForFile,instronSmallAngleTight);
% ------------------------------------------------------------------------
% Instron experimental medium braid angle with regular braid:
instronMediumAngleRegular = figure();
xAxisLimit = 1.95;
yAxisLimit = 70;
labelXAxis = 'Stretch ratio';
labelYAxis = 'Axial force (N)';
% Call the plot function to ensure consitency within graphing format
plot_this_for_me(instronMediumAngleRegular,xAxisLimit,yAxisLimit,...
    labelXAxis,labelYAxis)
% Plot the silicone tensile results
hold on;
plot(elongationR1b4a_54,axialForceR1b4a_54,'k-','Linewidth',1);
plot(elongationR1b4b_55,axialForceR1b4b_55,'k--','Linewidth',0.5);
plot(elongationR1b4c_56,axialForceR1b4c_56,'k-.','Linewidth',1.5);
hold off;
% Apply a legend to the graph.
sOne = sprintf('54%c Ecoflex', char(176));
sTwo = sprintf('55%c Moldstar', char(176));
sThree = sprintf('56%c Oomoo', char(176));
legend(sOne,sTwo,sThree,'Location','NorthWest');
% Turn the box around the legend off
legend boxoff;
% Save the figure to use for the latex file document.
fileLocation = ['D:\MASc mechanical engineering\.MCG 7999'...
    ,' Thesis\written\images\graphs'];
nameForFile = 'instron_medium_angle_regular';
save_this_for_me(fileLocation,nameForFile,instronMediumAngleRegular);
% ------------------------------------------------------------------------
% Instron experimental medium braid angle with tight braid:
instronMediumAngleTight = figure();
xAxisLimit = 1.95;
yAxisLimit = 70;
labelXAxis = 'Stretch ratio';
labelYAxis = 'Axial force (N)';
% Call the plot function to ensure consitency within graphing format
plot_this_for_me(instronMediumAngleTight,xAxisLimit,yAxisLimit,...
    labelXAxis,labelYAxis)
% Plot the silicone tensile results
hold on;
plot(elongationT1b4a_53,axialForceT1b4a_53,'k-','Linewidth',1);
plot(elongationT1b4b_52,axialForceT1b4b_52,'k--','Linewidth',0.5);
plot(elongationT1b4c_56,axialForceT1b4c_56,'k-.','Linewidth',1.5);
hold off;
% Apply a legend to the graph.
sOne = sprintf('53%c Ecoflex', char(176));
sTwo = sprintf('52%c Moldstar', char(176));
sThree = sprintf('56%c Oomoo', char(176));
legend(sOne,sTwo,sThree,'Location','NorthEast');
```

```
% Turn the box around the legend off
legend boxoff;
% Save the figure to use for the latex file document.
fileLocation = ['D:\MASc mechanical engineering\.MCG 7999'...
    ,' Thesis\written\images\graphs'];
nameForFile = 'instron_medium_angle_tight';
save_this_for_me(fileLocation,nameForFile,instronMediumAngleTight);
% ------------------------------------------------------------------------
% Instron experimental large braid angle with regular braid:
instronLargeAngleRegular = figure();
xAxisLimit = 2.15;
yAxisLimit = 70;
labelXAxis = 'Stretch ratio';
labelYAxis = 'Axial force (N)';
% Call the plot function to ensure consitency within graphing format
plot_this_for_me(instronLargeAngleRegular,xAxisLimit,yAxisLimit,...
    labelXAxis,labelYAxis)
% Plot the silicone tensile results
hold on;
plot(elongationR1c4a_61,axialForceR1c4a_61,'k-','Linewidth',1);
plot(elongationR1c4b_62,axialForceR1c4b_62,'k--','Linewidth',0.5);
plot(elongationR1c4c_64,axialForceR1c4c_64,'k-.','Linewidth',1.5);
hold off;
% Apply a legend to the graph.
sOne = sprintf('61%c Ecoflex', char(176));
sTwo = sprintf('62%c Moldstar', char(176));
sThree = sprintf('64%c Oomoo', char(176));
legend(sOne,sTwo,sThree,'Location','NorthWest');
% Turn the box around the legend off
legend boxoff;
% Save the figure to use for the latex file document.
fileLocation = ['D:\MASc mechanical engineering\.MCG 7999'...
    ,' Thesis\written\images\graphs'];
nameForFile = 'instron_large_angle_regular';
save_this_for_me(fileLocation,nameForFile,instronLargeAngleRegular);
% ------------------------------------------------------------------------
% Instron experimental large braid angle with tight braid:
instronLargeAngleTight = figure();
xAxisLimit = 1.95;
yAxisLimit = 70;
labelXAxis = 'Stretch ratio';
labelYAxis = 'Axial force (N)';
% Call the plot function to ensure consitency within graphing format
plot_this_for_me(instronLargeAngleTight,xAxisLimit,yAxisLimit,...
    labelXAxis,labelYAxis)
% Plot the silicone tensile results
hold on;
plot(elongationT1c4a_60,axialForceT1c4a_60,'k-','Linewidth',1);
plot(elongationT1c4b_63,axialForceT1c4b_63,'k--','Linewidth',0.5);
plot(elongationT1c4c_65,axialForceT1c4c_65,'k-.','Linewidth',1.5);
hold off;
% Apply a legend to the graph.
sOne = sprintf('60%c Ecoflex', char(176));
sTwo = sprintf('63%c Moldstar', char(176));
sThree = sprintf('65%c Oomoo', char(176));
legend(sOne,sTwo,sThree,'Location','SouthEast');
% Turn the box around the legend off
legend boxoff;
% Save the figure to use for the latex file document.
```

```
fileLocation = ['D:\MASc mechanical engineering\.MCG 7999'...
    ,' Thesis\written\images\graphs'];
nameForFile = 'instron_large_angle_tight';
save_this_for_me(fileLocation,nameForFile,instronLargeAngleTight);
% ------------------------------------------------------------------------
% Instron experimental testing until failure:
instronTestToFail = figure();
xAxisLimit = 2.2;
yAxisLimit = 225;
labelXAxis = 'Stretch ratio';
labelYAxis = 'Axial force (N)';
% Call the plot function to ensure consitency within graphing format
plot_this_for_me(instronTestToFail,xAxisLimit,yAxisLimit,...
    labelXAxis,labelYAxis)
% Plot the silicone tensile results
hold on;
plot(elongationT1a4a_40_fail,...
    axialForceT1a4a_40_fail,'k:','Linewidth',0.5);
plot(elongationT1a4b_43_fail,...
    axialForceT1a4b_43_fail,'k-','Linewidth',0.5);
plot(elongationT1a4c_45_fail,...
    axialForceT1a4c_45_fail,'k--','Linewidth',0.5);
plot(elongationT1b4c_50_fail,...
    axialForceT1b4c_50_fail,'k-','Linewidth',1);
plot(elongationR1a4c_47_fail,...
    axialForceR1a4c_47_fail,'k--','Linewidth',1);
plot(elongationR1a4b_49_fail,...
    axialForceR1a4b_49_fail,'k-','Linewidth',1.5);
plot(elongationR1b4b_53_fail,...
    axialForceR1b4b_53_fail,'k--','Linewidth',1.5);
plot(elongationR1b4c_50_fail,...
    axialForceR1b4c_50_fail,'k-','Linewidth',2);
plot(elongationR1c4c_64_fail,...
    axialForceR1c4c_64_fail,'k-.','Linewidth',1);
hold off;
% Apply a legend to the graph.
legend('T1A4A\_40','T1A4B\_43','T1A4C\_45','T1B4C\_50','R1A4C\_47',...
    'R1A4B\_49','R1B4B\_53','R1B4C\_50','R1C4C\_64',...
    'Location','NorthEast');
% Turn the box around the legend off
legend boxoff;
% Save the figure to use for the latex file document.
fileLocation = ['D:\MASc mechanical engineering\.MCG 7999'...
    ,' Thesis\written\images\graphs'];
nameForFile = 'instron_test_to_fail';
save_this_for_me(fileLocation,nameForFile,instronTestToFail);
% ------------------------------------------------------------------------
% Cellscale biaxial testing on pure silicone types:
biaxialTesting = figure();
xAxisLimit = 2.2;
yAxisLimit = 4500;
labelXAxis = 'Stretch ratio';
labelYAxis = 'Axial force (mN)';
% Call the plot function to ensure consitency within graphing format
plot_this_for_me(biaxialTesting,xAxisLimit,yAxisLimit,...
    labelXAxis,labelYAxis)
% Plot the silicone tensile results
hold on;
plot(elongationEcoflexX,axialForceEcoflexX,'k-','Linewidth',0.5);
```

```
plot(elongationEcoflexY,axialForceEcoflexY,'k--','Linewidth',0.5);
plot(elongationMoldstarX,axialForceMoldstarX,'k-','Linewidth',1);
plot(elongationMoldstarY,axialForceMoldstarY,'k--','Linewidth',1);
plot(elongationOomooX,axialForceOomooX,'k-','Linewidth',1.5);
plot(elongationOomooY,axialForceOomooY,'k--','Linewidth',1.5);
hold off;
% Apply a legend to the graph.
legend('Ecoflex X','Ecoflex Y','Moldstar X',...
    'Moldstar Y','Oomoo X','Oomoo Y','Location','NorthEast');
% Turn the box around the legend off
legend boxoff;
% Save the figure to use for the latex file document.
fileLocation = ['D:\MASc mechanical engineering\.MCG 7999'...
    ,' Thesis\written\images\graphs'];
nameForFile = 'biaxial_testing';
save_this_for_me(fileLocation,nameForFile,biaxialTesting);
% ------------------------------------------------------------------------
%  Stiffness plots large angle with regular braid:
disp('Plotting the stiffness now (regular)...');
instronStiffnessLargeAngleRegular = figure();
maxElongationRegular = max(instronElongationR1c4a_61);
for n = 1:1:3
    if maxElongationRegular < max(instronElongationR1c4b_62)
        maxElongationRegular = max(instronElongationR1c4b_62);
    elseif maxElongationRegular < max(instronElongationR1c4c_64)
        maxElongationRegular = max(instronElongationR1c4c_64);
    end
    maxStiffnessRegular = max(stiffnessR1c4a_61);
    if maxStiffnessRegular < max(stiffnessR1c4b_62)
        maxStiffnessRegular = max(stiffnessR1c4b_62);
    elseif maxStiffnessRegular < max(stiffnessR1c4c_64)
        maxStiffnessRegular = max(stiffnessR1c4c_64);
    end
end
xAxisLimit = maxElongationRegular + 20;
yAxisLimit = maxStiffnessRegular + 2;
labelXAxis = 'Elongation (mm)';
labelYAxis = 'Stiffness (N/mm)';
% Call the plot function to ensure consitency within graphing format
plot_this_for_me(instronStiffnessLargeAngleRegular,...
    xAxisLimit,yAxisLimit,labelXAxis,labelYAxis)
% Plot the silicone tensile results
hold on;
plot(instronElongationR1c4a_61(1:numel(stiffnessR1c4a_61),1)...
    ,stiffnessR1c4a_61,'k-','Linewidth',1);
plot(instronElongationR1c4b_62(1:numel(stiffnessR1c4b_62),1)...
    ,stiffnessR1c4b_62,'k--','Linewidth',1);
plot(instronElongationR1c4c_64(1:numel(stiffnessR1c4c_64),1)...
    ,stiffnessR1c4c_64,'k-.','Linewidth',1);
hold off;
% Apply a legend to the graph.
sOne = sprintf('61%c Ecoflex', char(176));
sTwo = sprintf('62%c Moldstar', char(176));
sThree = sprintf('64%c Oomoo', char(176));
legend(sOne,sTwo,sThree,'Location','NorthEast');
% Turn the box around the legend off
legend boxoff;
% Save the figure to use for the latex file document.
fileLocation = ['D:\MASc mechanical engineering\.MCG 7999'...
```

```
    ,' Thesis\written\images\graphs'];
nameForFile = 'instron_stiffness_large_angle_regular';
save_this_for_me(fileLocation,nameForFile,...
    instronStiffnessLargeAngleRegular);
% ------------------------------------------------------------------------
%  Stiffness plots large angle with tight braid:
disp('Plotting the stiffness now (tight)...');
instronStiffnessLargeAngleTight = figure();
maxElongationTight = max(instronElongationT1c4a_60);
for n = 1:1:3
    if maxElongationTight < max(instronElongationT1c4b_63)
        maxElongationTight = max(instronElongationT1c4b_63);
    elseif maxElongationTight < max(instronElongationT1c4c_65)
        maxElongationTight = max(instronElongationT1c4c_65);
    end
    maxStiffnessTight = max(stiffnessT1c4a_60);
    if maxStiffnessTight < max(stiffnessT1c4b_63)
        maxStiffnessTight = max(stiffnessT1c4b_63);
    elseif maxStiffnessTight < max(stiffnessT1c4c_65)
        maxStiffnessTight = max(stiffnessT1c4c_65);
    end
end
xAxisLimit = maxElongationTight + 20;
yAxisLimit = maxStiffnessTight + 2;
labelXAxis = 'Elongation (mm)';
labelYAxis = 'Stiffness (N/mm)';
% Call the plot function to ensure consitency within graphing format
plot_this_for_me(instronStiffnessLargeAngleTight,...
    xAxisLimit,yAxisLimit,labelXAxis,labelYAxis)
% Plot the silicone tensile results
hold on;
plot(instronElongationT1c4a_60(1:numel(stiffnessT1c4a_60),1)...
    ,stiffnessT1c4a_60,'k-','Linewidth',1);
plot(instronElongationT1c4b_63(1:numel(stiffnessT1c4b_63),1)...
    ,stiffnessT1c4b_63,'k--','Linewidth',1);
plot(instronElongationT1c4c_65(1:numel(stiffnessT1c4c_65),1)...
    ,stiffnessT1c4c_65,'k-.','Linewidth',1);
hold off;
% Apply a legend to the graph.
sOne = sprintf('60%c Ecoflex', char(176));
sTwo = sprintf('63%c Moldstar', char(176));
sThree = sprintf('65%c Oomoo', char(176));
legend(sOne,sTwo,sThree,'Location','NorthEast');
% Turn the box around the legend off
legend boxoff;
% Save the figure to use for the latex file document.
fileLocation = ['D:\MASc mechanical engineering\.MCG 7999'...
    ,' Thesis\written\images\graphs'];
nameForFile = 'instron_stiffness_large_angle_tight';
save_this_for_me(fileLocation,nameForFile,...
    instronStiffnessLargeAngleTight);
toc;
end
```

D.6 Plotting function for multiple step results

```
% ------------------------------------------------------------------------
```

```
% This code is used to graph experimental values from 1-2 discrete sets.
% Robert Shaheen (5273205)
% Summer 2016
% ------------------------------------------------------------------------

function graphing_discrete_data()
clc; % Clears command window each re-run
clear all; % Clears everything on re-run
format longg; % Sets the number of decimal places in the output
format compact; % Format for output window

% Number of specimens that will be graphed
numberGraphs = 2;
for k = 1:1:numberGraphs
    % ------------------------------------------------------------------------
    % Open the user-specified specimen raw data by requesting the user
    % input.
    % ------------------------------------------------------------------------
    flag = 0;
    while flag == 0
        prompt = ...
            'Please identify which specimen you would like to analyze:\n';
        containmentFolder = ['D:\MASc mechanical engineering'...
            ,'\.MCG 7999 Thesis\analysis\raw specimen data\'];
        specimenSelection = input(prompt, 's');
        if k == 1
            specimenSelectionOne = specimenSelection;
        elseif k == 2
            specimenSelectionTwo = specimenSelection;
        end
        baseFileName = '\raw_data.txt';
        fullFileName = sprintf('%s%s%s',containmentFolder,...
            specimenSelection,baseFileName); % Location of the raw_data
        % Make sure that the file exists, otherwise abort program
        if ~exist(fullFileName, 'file')
            % Check if the specified file exists
            warningMessage = ...
                sprintf('Error: the input file\n%s\nwas not found',...
                fullFileName);
            uiwait(warndlg(warningMessage));
        else
            flag = 1;
        end
    end
    tic;
    rawDataFile = fopen(fullFileName, 'rt'); % Open the chosen file
    baseFileNameOutput = '\output_data.txt';
    fullFileNameOutput = sprintf('%s%s%s',containmentFolder,...
        specimenSelection,baseFileNameOutput);
    % Create an output file
    outputDataFile = fopen(fullFileNameOutput,'w');
    % Assign the text file numbers to variable/variable arrays
    cellArray = textscan(rawDataFile, '%f %f %f %f %f %f', 1);
    % Scan the rest of the file and assign to variable, then close
    cellArray = textscan(rawDataFile, '%f %f %f %f');
    fclose(rawDataFile);
    % Import the data points for the raw data measurements
    pressureExpRaw = cellArray{1};  % Experimental pressure (MPa)
    radiusOutExpRaw = cellArray{2};
```

```
    % Experimental inner rad in current reference frame (mm)
    axialForceExpRaw = cellArray{3}; % Expermimental z-force (N)

    % ---------------------------------------------------------------------
    % Determine the axial stretch, lambda, using the image recogonition
    % software function and the 12 images taken during testing for the
    % selected specimen.
    % ---------------------------------------------------------------------
    pythagoreanDistance = zeros(numel(axialForceExpRaw),1);
    for i = 1:1:numel(pythagoreanDistance)
        baseFileName = sprintf('\\elongation_%d.JPG',i);
        % Location of the elongation image
        fullFileName = sprintf('%s%s%s',containmentFolder,...
            specimenSelection,baseFileName);
        pythagoreanDistance(i,1) = image_processing(fullFileName,...
            outputDataFile,i,numel(pythagoreanDistance));
    end
    % Determine the experimental stretch ratis from the returned values
    % from the image analysis function.
    lambdaExpRaw = pythagoreanDistance(:,1)./pythagoreanDistance(1,1);

    % ---------------------------------------------------------------------
    % pressureExpRaw,radiusInExpRaw,axialForceExpRaw,lambdaExpRaw, only
    % have about 12 data points.  They will be interpolated to yield about
    % 75 data points using a spline interpolation.
    % ---------------------------------------------------------------------
    [pressureExp radiusOutExp lambdaExp axialForceExp] = ...
        spline_interpolation(pressureExpRaw, radiusOutExpRaw,...
        lambdaExpRaw, axialForceExpRaw);
    % Make sure all of the arrays are column vectors
    pressureExp = pressureExp';
    lambdaExp = lambdaExp';
    % Set the data to correpsond with the respective graph number.
    if k == 1
        lambdaExpRawFirst = lambdaExpRaw;
        axialForceExpRawFirst = axialForceExpRaw;
        lambdaExpFirst = lambdaExp;
        axialForceExpFirst = axialForceExp;
    elseif k == 2
        lambdaExpRawSecond = lambdaExpRaw;
        axialForceExpRawSecond = axialForceExpRaw;
        lambdaExpSecond = lambdaExp;
        axialForceExpSecond = axialForceExp;
    end
end
theoForceElongation = figure();
xAxisLimit = 1.49;
yAxisLimit = 146;
labelXAxis = 'Stretch ratio';
labelYAxis = 'Axial force (N)';
% Call the plot function to ensure consitency
% within graphing format
plot_this_for_me(theoForceElongation,xAxisLimit,yAxisLimit,...
    labelXAxis,labelYAxis)
% Plot the results
% Graphing interpolated results and saving
% the files.  Stretch ratio vs. Axial force
hold on
plot(lambdaExpRawFirst,axialForceExpRawFirst,'k^:','Linewidth',0.5,...
```

```
    'markersize',5);
if numberGraphs == 2
    plot(lambdaExpRawSecond,...
        axialForceExpRawSecond,'kv:','Linewidth',0.5,'markersize',5);
end
hold off
% Insert a \ before _ in strings for the legend.
specimenSelectionOneLegend = horzcat(specimenSelectionOne(1:5),'\',...
    specimenSelectionOne(5+1:end));
specimenSelectionTwoLegend = horzcat(specimenSelectionTwo(1:5),'\',...
    specimenSelectionTwo(5+1:end));
legendEntryOne = sprintf('%s Experimental Data',...
    specimenSelectionOneLegend);
if numberGraphs == 2
    legendEntryThree = sprintf('%s Experimental Data',...
        specimenSelectionTwoLegend);
end
if numberGraphs == 1
    legend(legendEntryOne,legendEntryThree,'Location','NorthWest');
    % Turn the box around the legend off
    legend boxoff;
    % Save the figure to use for the latex file document.
    fileLocation = ['D:\MASc mechanical engineering\.MCG 7999'...
        ,' Thesis\written\images\graphs'];
    nameForFile = sprintf('%s_discrete_experimental_data',...
        specimenSelectionOne);
    save_this_for_me(fileLocation,nameForFile,theoForceElongation);
elseif numberGraphs == 2
    legend(legendEntryOne,legendEntryThree,...
        'Location','NorthWest');
    % Turn the box around the legend off
    legend boxoff;
    % Save the figure to use for the latex file document.
    fileLocation = ['D:\MASc mechanical engineering\.MCG 7999'...
        ,' Thesis\written\images\graphs'];
    nameForFile = sprintf('%s_%s_discrete_experimental_data',...
        specimenSelectionOne,specimenSelectionTwo);
    save_this_for_me(fileLocation,nameForFile,theoForceElongation);
end
% Close the output file
fclose(outputDataFile);
toc;
end
```

D.7 General plot function for formatted plots

```
% ------------------------------------------------------------------------
% Universal plot generator in the format that Dr. Doumit would like.
% ------------------------------------------------------------------------
function plot_this_for_me(figureName,xAxisLimit,yAxisLimit,labelXAxis,...
    labelYAxis)
% Set the default output font size and type for all figures and graphs.
set(gcf,'DefaultTextFontsize',10, ...
'DefaultTextFontname','Times New Roman', ...
'DefaultTextFontWeight','bold', ...
'DefaultAxesFontsize',10, ...
'DefaultAxesFontname','Times New Roman');
```

```
set(gcf,'visible','off')
% Sets the size and location of the figure.
set(figureName, 'PaperUnits', 'centimeters');
set(figureName, 'PaperPosition', [0 0 15 7]);
% Sets the axis limits of the figure in the format: [xmin xmax ymin ymax].
axis([1 xAxisLimit 0 yAxisLimit]);
% Chart labels.
xlabel(labelXAxis), ylabel(labelYAxis);
% Display the grid on the graph.
grid on;
end
```

D.8 General function to save figures

```
% ------------------------------------------------------------------------
% Universal figure saver.  Saves the figure as a png file.  Can be changed
% to another file format but for now this will suffice.
% ------------------------------------------------------------------------
function save_this_for_me(fileLocation,nameForFile,figureName)
% Save the graph to my graph images in the written folder
filePath = fileLocation;
fileName = nameForFile;
print(figureName,'-dpng','-r350',fullfile(filePath, fileName));
end
```